UNIVERSITÄT OSNABRÜCK

Fachbereich Biologie / Chemie
Institut für Chemie neuer Materialien

Dissertation
Zur Erlangung des Grades eines Doktors der Naturwissenschaften

(Dr. rer. nat)

Synthesis and Energy Storage Performance of Novel Redox-Active Polymers

vorgelegt von

Mahmood, Arsalan Mado Mahmood

Osnabrück 2022

This doctoral thesis was carried out at the Institut für Chemie neuer Materialien, Fachbereiche Biologe / Chemie, Universität Osnabrück, Germany, under the supervision of Prof. Dr. Lorenz Walder. The studies were performed in the period from Oct. 2015 to March. 2022, interrupted by the surgery for nine months from the 18th of January, 2019.

Hauptberichterstatter: Prof. Dr. Andreas Hennig, Universität Osnabrück

Zweitberichtestatter: Prof. Dr. Uwe Beginn, Universität Osnabrück

Weitere Mitglieder: Prof. Dr. Markus Haase, and Dr. Helmut Schäfer. Universität Osnabrück

This thesis is dedicated to my family

“Once you stop learning, you start dying”

- Albert Einstein -

Abstract

The lithium-ion battery is the most preferred choice for energy storage, for example, in electric vehicle batteries and electronic devices. These commonly utilized transition metal-based cathodes and graphite anodes. However, replacing the active materials with organic, redox-active materials is of great interest since these organic batteries are excelling in charging speed and cycling stability. Therefore, in the present thesis, the synthesis and characterization of potential organic electroactive materials, mainly polymers, are investigated. Concerning the structure of the polymers, linear polymers, three-dimensional / crosslinked polymers, as well as dendrimers, were chosen. The electroactive subunits include viologen, imide, triphenylamine, porphyrin, and ferrocene, either as homopolymer or copolymer, as well as active materials like graphene oxide (GO) or electrolytes. The characterization of the structures was performed by means of NMR, FTIR spectroscopy, and elemental analysis. The electrochemical properties of products were investigated by the cyclic voltammetry (CV) technique. Electrodes were prepared by drop-casting a solution of the polymers onto a current collector, and the (dis)charge performance was investigated. To enhance the conductivity of the layers, composites of the polymers with GO were prepared. Since the performance depends on the electrolyte composition, different types of solvents and salts were used and compared. The capacities in a thin film of pure polymers and dendrimers were much smaller than in the composite film with rGO. These performances are based on the molecular self-assembly of polymers and dendrimers on individual GO sheets yielding colloidal polymer/dendrimer@GO and efficient GO/rGO transformation electrocatalyzed by polymers and dendrimers. However, the stability and capacity of some polymers and dendrimers such as P2, P5, P6 and G_2 were not optimal in this type of composite film. Moreover, the peak potential in the positive charge range assigned to the nitrogen center of triphenylamine and porphyrin was found to decrease after the first scan, which is probably due to a dissolution of the film. Therefore different methods were used to composite polymer or dendrimer with GO such as reducing GO before mixing. As noticed that the redox behaviour of amine and ferrocene are reversible, but the stability of radical cation species is not stable in organic solvent after oxidation. Besides the preparation of electrodes by drop-casting, the layer-by-layer process was used by alternate dipping between cationic polymer solution and anionic GO or Poly(sodium p-styerenesulfonate) (PSS) solution. PSS acts as a counter ion for the polymer, which changes the moving species in the electrolyte from anion to cation. As noted that a large cation (TBA^+) shows

lower capacity compared to small cations (Li^+, K^+). Apart from the CV, quartz crystal microbalance (QCM) was used to monitor layer growth.

Acknowledgement

This dissertation could not have been completed without the great support that I have received from so many people over the years. I wish to offer my most heartfelt thanks to the following people.

Foremost, I would like to express my sincere gratitude to my advisor Prof. Dr. Lorenz Walder for the continuous support of my research. His patience, motivation and immense knowledge added considerably to my graduate experience. I appreciate all his contributions of his time and ideas to make my PhD experience productive and stimulating. I would also like to express my sincere gratitude to my advisor Prof. Dr. Andreas Hennig to continue my journey after my first supervisor retired, and to give me valuable feedback and expressions. I also thank Prof. Dr. Markus Haase for tolerating me completing the rest of the practical part in the lab after my first supervisor retired. Besides my advisors, I would like to thank the rest of my thesis committee: Prof. Dr. Uwe Beginn, Prof. Dr. Markus Haase, and Dr. Helmut Schäfer. I thank them for their availability and consent to evaluate my thesis.

I appreciate the whole faculty and colleagues of the "Institute für Chemie Neuer Materialien" for offering a friendly and comfortable environment to work at. My deepest gratitude goes to my research group members at the University of Osnabrück for their support and productive discussions. I have learned a lot by working with them all; Dr. Seyyed Mohsen Beladi Mousavi, Dr. Mohamed Nilam, Dr. Shamaila Sadaf, Dr. Marius Ciobanu, Jonas Klein, Alarslan Fatih, Wajiha Akram and Michael G. Garcia. In particular, I am grateful to Mrs. Simona Webersinn and Mrs. Christine Schulz-Kölbel for the friendly environment in the lab and their continued support regarding the laboratory and administrative works. Many thanks go to particular to Dr. Seyyed Mohsen Beladi Mousavi and Jonas Klein for giving information on the synthesis of several compounds which I used for my research project. I would like to express my thanks to our institute and department secretaries, Claudia Drieschner and Monika Dubiel for their kind help in administrative work. I would like to appreciate the support extended by Duhok University and my colleagues and friends in difficult times at the university. I would also like to appreciate the support extended by my colleagues and friends in difficult times in Germany.

Finally, but by no means least, thanks go to my family. My mother for her constant and countless prayers who always encouraged and supported me to achieve academic heights. I am deeply indebted to my siblings and the whole family for providing me with consistent support and incessant encouragement throughout my years of study. This accomplishment would not have been possible without them. Words cannot express how

grateful I am to my beloved wife Rezheen for her unflagging love, believing in me and being there for practical support in all those things of life beyond doing a PhD, and finally, my adored son Darian, for being a good baby and giving me all the power all the rocky path through.

Table of Contents

- ABSTRACT ..... **IX**

- ACKNOWLEDGEMENT ..... **XI**

- TABLE OF CONTENTS ..... **XIII**

- LIST OF PUBLICATIONS ..... **XV**

CHAPTER 1 ..... **2**

1.1 INTRODUCTION 2
1.2 ORGANIC REDOX SYSTEMS 5
1.3 ORGANIC BATTERIES 6
1.4 ADVANTAGES AND DISADVANTAGES OF ORGANIC ELECTRODE MATERIALS 7
1.5 GRAPHENE OXIDE (GO) 8
1.6 SCOPE OF THESIS 9

CHAPTER 2 LINEAR POLYMERS (LPS) **12**

2.1 INTRODUCTION 12
2.2 EXPERIMENTAL SECTION 14
2.2.1 Instrument *14*
2.2.2 Chemicals *14*
2.2.3 Synthesis *15*
2.2.3.1 Synthesis of Monomers 15
2.2.3.1.1 Organic Monomers 15
2.2.3.1.2 Organometallic Monomers 18
2.2.3.2 Synthesis of Linear Polymers 18
2.2.3.2.1 Organic LPs 18
2.2.3.2.2 Organometallic LP 22
2.2.4 Preparation of Electrochemical Solutions *22*
2.2.4.1 Solutions of LP@GO with Variable LP / GO Ratio 22
2.2.4.2 Solution of LP@rGO 23
2.2.5 Electrochemical Measurements and Preparation of Electrodes *23*
2.2.6 Electrochemical Transformation of $(LP@GO)_n$@CC to $(LP@rGO)_n$@CC *24*
2.3 RESULT AND DISCUSSION 24
2.3.1 Organic LPs *26*
2.3.1.1 Polymer 1 (P1) 26
2.3.1.2 Polymer 2 28
2.3.1.3 Polymer 3 30
2.3.1.4 Polymer 4 33
2.3.1.5 Polymer 5 35
2.3.2 Organometallic LPs (P6) *39*
2.4 SUMMARY 40

CHAPTER 3 DENDRIMERS & THREE-DIMENSIONAL (3D) / CROSSLINKED POLYMER **44**

3.1 INTRODUCTION 44
3.2 EXPERIMENTAL SECTION 47
3.2.1 Synthesis *47*
3.2.1.1 Synthesis of Dendrimers 47
3.2.1.1.1 Synthesis of Generation One (G_1) 48
3.2.1.1.2 Synthesis of Generation Two (G_2) 52
3.2.1.2 Synthesis of 3D Polymer and Crosslinked Polymer 56
3.2.2 Electrochemical Measurements *57*
3.3 RESULT AND DISCUSSION 58
3.3.1 Dendrimers *58*
3.3.1.1 Generation One (G_1) 58
3.3.1.2 Generation Two (G_2) 60

3.3.2 3D / Crosslinked Polymers *61*
3.3.2.1 3D Polymer (P7) 61
3.3.2.2 Crosslinked Polymer (P8) 64
3.4 SUMMARY 67

CHAPTER 4 DIP-COATING PROCESS 70

4.1 INTRODUCTION 70
4.2 EXPERIMENTAL SECTION 72
4.2.1 Instrument *72*
4.2.2 Chemicals *73*
4.2.3 Synthesis *73*
4.2.4 Dipping Solution Preparations *73*
4.2.4.1 Dipping Solution of P9, GO and P9/GO 73
4.2.4.2 Dipping Solution of PSS 74
4.2.5 LbL Formation Procedure *74*
4.2.6 Carbon Plate Electrode (CPE) Preparations *75*
4.2.7 Modification of the Gold Plated Quartz Crystal Microbalance (QCM) Measurements *75*
4.3 RESULT AND DISCUSSION 75
4.4 SUMMARY 80

CHAPTER 5 SUMMARY AND OUTLOOK 82

- REFERENCES 85

- ABBREVIATION 90

- CURRICULUM VITAE 92

- DECLARATION 94

List of Publications

1. S. M. Beladi-Mousavi, S. Sadaf, A.-K. Hennecke, J. Klein, **A. M. Mahmood**, C. Rüttiger, M. Gallei, F. Fu, E. Fouquet, J. Ruiz, D. Astruc, and L. Walder, *Angew. Chem. Int. Ed.* **2021**, 60, 13554 – 13558
2. S. M. Beladi-Mousavi, S. Sadaf, **A. M. Mahmood**, and L. Walder, *ACS Nano*, **2017**, 11, 8730 – 8740
3. Z. A. Jarjes, **A. M. Mahmood**, A. K. Sallo, H. A. Ibrahim, *Zanco J. Pure Appl. Sci.* **2016**, 28, 122 – 131
4. **A. M. Mahmood***, A. K. Sallo and M. A. Hasan, *J. Indian Chem. Soc.*, **2014**, 91, 2107 – 2111

Chapter 1
Introduction

Chapter 1

1.1 Introduction

Human always desire to search for a better life and our life is affected by climate change, and unfortunately, this change is mostly caused as results of the greenhouse gas emissions, like CO_2. On the other hand, a paradigm shift in the world's energy reliance from conventional fossil fuels to renewable energy has become necessary, such as green energy sources, solar radiation, wind power, and waves are renewable relating to living. That renewable energy sources require also parts that store the produced energy as batteries. Therefore, the aim of looking at battery research is to develop a long-term roadmap in future and that is through discover, develop, and design ultra-high-performance, durable, safer, sustainable, and low costs batteries for importance in the use of many applications and addressing climate change. The lithium-ion battery (LIB) is one of the sources that played an important role in the decarbonisation and reduction of greenhouse gases from nature and that is by using it in electric vehicle batteries and electronic devices[1]. Lithium-ion batteries can also be recycled, thus reducing the environmental impact[2].

Batteries, in contrast to fossil fuels, can change stored chemical energy to electrical energy with high efficiency and additionally do not produce gaseous exhaust. Since the 1990s, lithium-ion batteries, contained inorganic cathodes and graphite anodes, as well as polymers with suspended redox-active groups, have been employed in different organic electronic devices. The acceptable energy storages are associated with mobile electronic devices for many applications, start from small range energy storages such as smartwatches and computer devices to bigger measure such as electrical vehicles[3]. The battery cell contains an anode and cathode (some of the common inorganic cathode materials like TiS_2[4], $LiFePO_4$, $LiCoO_2$[5], etc.) separated by the electrolyte, ions and electrons move through the electrolyte and the external circuit, respectively as explained the process of charging and discharging in Figure 1.1. During the discharge of the cell, two reversible electrochemical reactions, occur in the anode and the cathode. The cations and electrons meet at the surface of the positive electrode (cathode), where they intercalate within the host material.

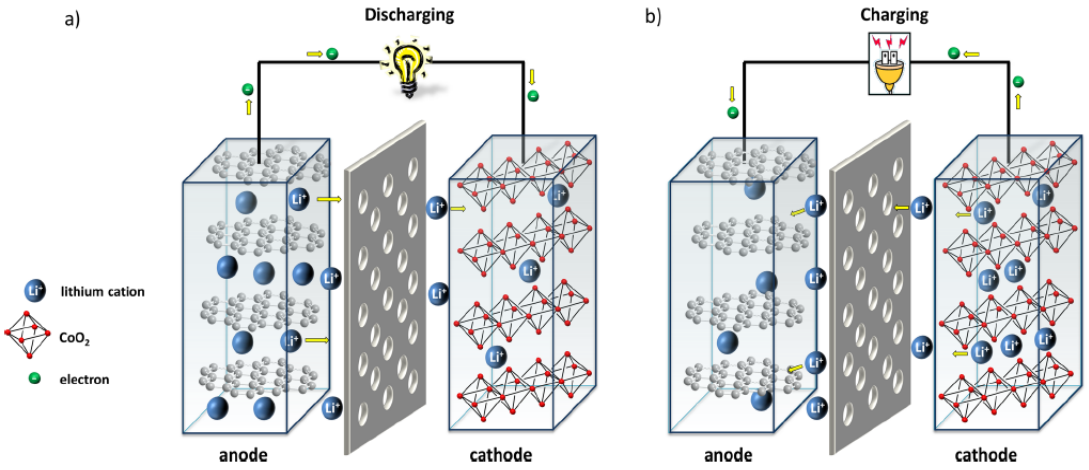

Figure 1.1 Schematic of principles of common Li-ion battery work a) discharging and b) charging process, adapted from ref[6]

For organic materials, the mechanism is different, for example, when a polymer is used as cathode material for rechargeable batteries. The mechanism depends on the structure of the polymer and its ability to transfer electrons like one example as polyimide explained in Scheme 1.1[7]. The mechanism process of discharging the organic battery and transferring electrons are shown in Figure 1.2.

Scheme 1.1 Electrochemical redox mechanism of polyimide-based on pyromellitic dianhydride (PMDA)

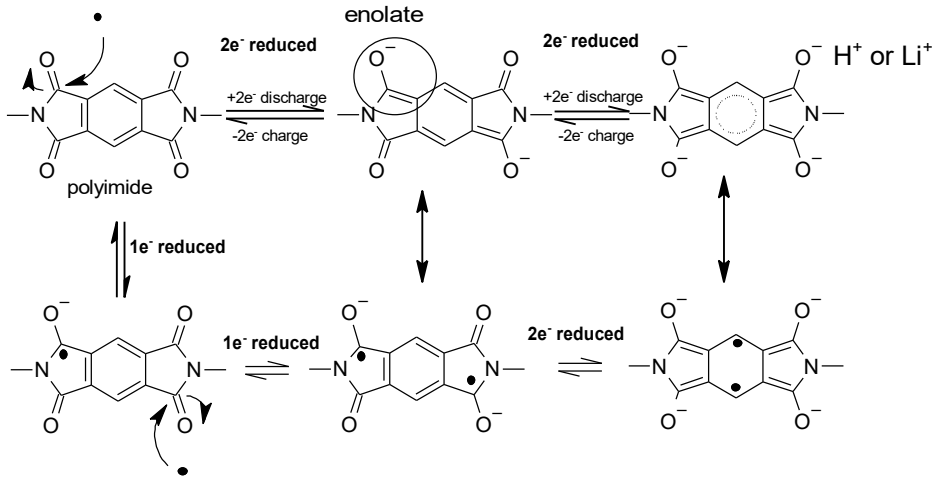

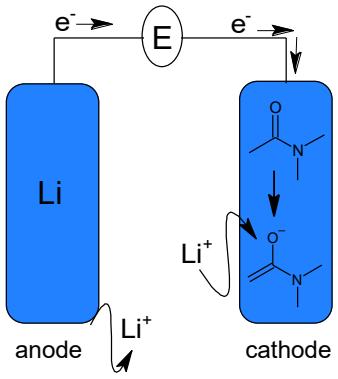

Figure 1.2 Mechanism of discharging an organic battery

Theoretical voltage (V [V]) is the difference between the potentials of the anode and the cathode of the battery. The theoretical capacity ($C_{theoretical}$, mAh g^{-1}) is one of the factors influencing the areal-capacity (mAh cm^{-2}) and the construction of excellent percolation paths for ions and electrons in the thick layers depending on the molecular weight (M_W) of the redox-active unit and the number of redox states (n) as calculated by Faraday law (eq. 1.1)[8]. The electrolyte window of the aqueous electrolyte is limited to max. 1.23 V due to possible decomposition into oxygen and hydrogen. Organic solvents on the other hand allow potentials > 3 V.[9]

$$C_{Theoretical} = \frac{n * F}{M_W} = \frac{n * 96485 \left(\frac{As}{mol}\right)}{M_W \left(\frac{g}{mol}\right)} = \frac{n * 26801}{M_W} \left(\frac{mAh}{g}\right) \qquad \text{Eq. 1.1}$$

Where n is the number of involved electrons, F is the Faraday constant, and M_w the molecular weight of the redox unit. Finally, the best batteries with a high energy density (Wh kg^{-1}) which care about standards safety, cost, biodegradability and recyclability, are also deciding factors, which should be esteemed in the developments of new battery materials[10].

Recently, there has been widespread interest in the use of metallocene and its derivatives in several applications including batteries. Given the exceptional properties of organometallic compounds including their tunable potential and ultrafast ET rate, such materials mainly in the monomeric state have been used as redox moieties in redox flow batteries. Among all well-known organometallics, ferrocene received the most attention in organic redox flow batteries mainly due to their redox potential which serves well as catholyte

(≈3.44 V vs. Li/Li^+)[11]. There has been a recent report on the fabrication of all organometallic redox flow batteries using ferrocene derivatives as cathode and cobaltocenium as an anode in aqueous and organic solutions. These systems allowed cell potential of up to 2 V after optimization of their functional groups. The main advantage of such a system is the fast ET rate of organometallic materials and the possibility of making large batteries to store energy in stationary places[11a, 12]. We have recently shown the possibility of using ferrocene and cobaltocene polymers as cathode and anode for conventional batteries. It is known that upon ion insertion during charging of an organic redox film, the volume of the film expands which could cause a short circuit with the opposite electrode. However, in our system, a reciprocal height change in cathode and anode upon ion de/insertion was built, which inhibited the development of any internal pressure or the short circuit and therefore the system was highly stable[13].

1.2 Organic Redox Systems

Despite organic redox reactions taking place in organic compounds, the oxidation and reduction for many reactions considered do not necessarily involve electron transfer in the electrochemical world. Thereby, the criterion for organic oxidation is gain of oxygen and/or loss of hydrogen, simple functional groups can be arranged in order of increasing oxidation state.

The redox reactions are important for several factors such as Coulombic repulsion of ionic reactants and ion solvation. This generates interest, in the relation between chemical structure and reactivity for chemically related compounds toward some are reagents [14]. Organic redox-active materials produce energy storage systems (ESSs), because they have considerable advantages in terms of a set of molecular structure, supreme chemical and physical properties, and excellent electrochemical storage performance compared with metal-based inorganic active materials. Therefore, organic redox-active materials can provide perfect solutions to further improve existing ESS technologies and a diverse basis from which to develop advanced ESSs. Redox-active polymers have been mainly applied for ESS applications rather than organic molecules due to the well-known advantages, such as good stability, excellent processability, and simple device fabrication[15].

Any electrode used for a reversible reaction generally contains those, elemental substances (e.g., Li, Na, C, O_2, S, Si, P, Sn), transition metals (e.g., Co, Mn, V, Fe, Ni). So,

organic materials (monomers, oligomers, dendrimers and polymers) are theoretically possible candidates for secondary batteries. Redox-active organic molecules normally contain a π-conjugated structure and atoms with lone pair electrons like O, N and S, the conjugated structure speeds up the charge delocalization of the redox product. These types of batteries care more about environmental issues[16].

1.3 Organic Batteries

Organic batteries (OBs) are more environmentally safe than traditional metal batteries and are considered to be a high-power alternative to the Li-ion battery. Typical cathode materials of Li-ion batteries suffer from a grave loss in specific capacity limiting their applications for the development of electronic medical devices, electric vehicles, and renewable energy storage. In addition, syntheses of conventional LIBs are often very costly. Furthermore, there are still serious safety concerns due to the unfavourable reaction between the electrode and the electrolyte (i) and the flammability of organic electrolyte (ii). Some other main factors that are still not easily feasible with normal LIBs, such as flexibility, diverting is redeeming research interest toward more progressive battery materials as Li-O_2, Li-S and Li-organic batteries. Interestingly, the research and industrial attention towards organic energy storage application when compared to inorganic electrodes are modest. This is historically due to the prompt developments of LIBs. However, the use of organic or organometallic redox compounds overbears many of the mentioned problems of the LIBs, and Figure 1.3 shows some of the known organic and organometallic redox compounds, which have their redox reaction potential[10b, 17].

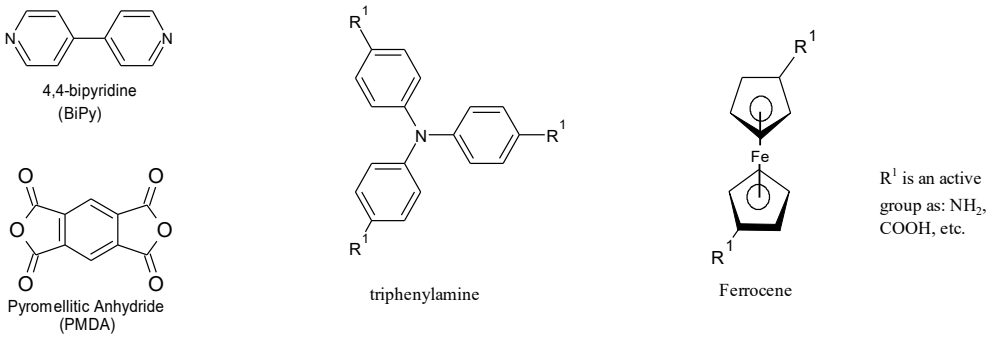

Figure 1.3 Some structures of redox-active materials.

The advanced new materials of organic chemistry, mixed with inorganic chemistry and other fields of chemistry, has been commonly developed to give big molecules polymers as examples of stable radicals in organic batteries came out by accurate polymerization techniques. The repeated subunit and sequences in the copolymers such as block or random copolymers are listed as the structural parameters to determine polymer structure. The polymers are affected by insert junctions in the polymer chains like the coordination, the number and types of junctions. The crosslinked or hyperbranched polymers have potential difficulty in designing as accurately, except for dendrimer and self-assembled polymeric structures are designed carefully by recurrent coupling reactions with systematic junctions[18]. More information about dendrimers is given in Chapter 3.

1.4 Advantages and Disadvantages of Organic Electrode Materials

Search for new organic materials has been the focus of researchers to derive a battery with high specifications. Organic electrode materials are very attractive for electrochemical energy storage devices because of their structural diversity, and they can be flexible, have surface functionalities and tenability, lightweight, low cost because organic materials can be produced from renewable natural resources[19], long-life requirements and safer. The functional rechargeable lithium batteries were not fully properties in spite of a large amount of research in this field because the increase in the request of highly functionalized applications always includes higher power density, energy density, excellent charge-discharge cycling performance, and more safety[20]. The made new organic redox polymers with optimized properties has more chance to achieve useful compounds because the synthetic variability is much greater than in the case of inorganic materials. Nevertheless, exciting progress has been synthetically, bringing organic electrodes to the attention of the energy storage community. Used the technique of addition of large amounts of the conductive carbon to raise the conductivity. However, this results in a lower specific capacity. Due to the low mass density and high surface area of the organic compounds, a larger amount of conductive carbon is necessary for organic redox materials compared to crystalline inorganic materials.

The polymers classes have all advantages of organic conjugated polymers but circumvent the disadvantages, like incomplete doping, the sloping voltage, and an inferior life cycle[6, 10b]. Finally, organic materials have intrinsic advantages, so it is possible to realize

commercial flexible energy storage devices and important consideration for the development of green energy storage devices and used in a variety of device architecture[19a, 21].

1.5 Graphene Oxide (GO)

The conductive additives have been used for the development of battery materials and to increasing the conductivity at addressed at the anode electrode like graphene oxide (GO). There are other conductive additives such as carbon nanotube, etc. The oxidized analogy of graphene can be regarded as one typical of two-dimensions various oxygen-containing functionalities as hydrophilic functional groups (-OH, epoxide, -COOH, carbonyl groups) as shown in Figure 1.4, depending on these properties modifying graphene sheets being dispersed in specific solvents. The interest in graphene oxide has exponentially risen two decades ago[22].

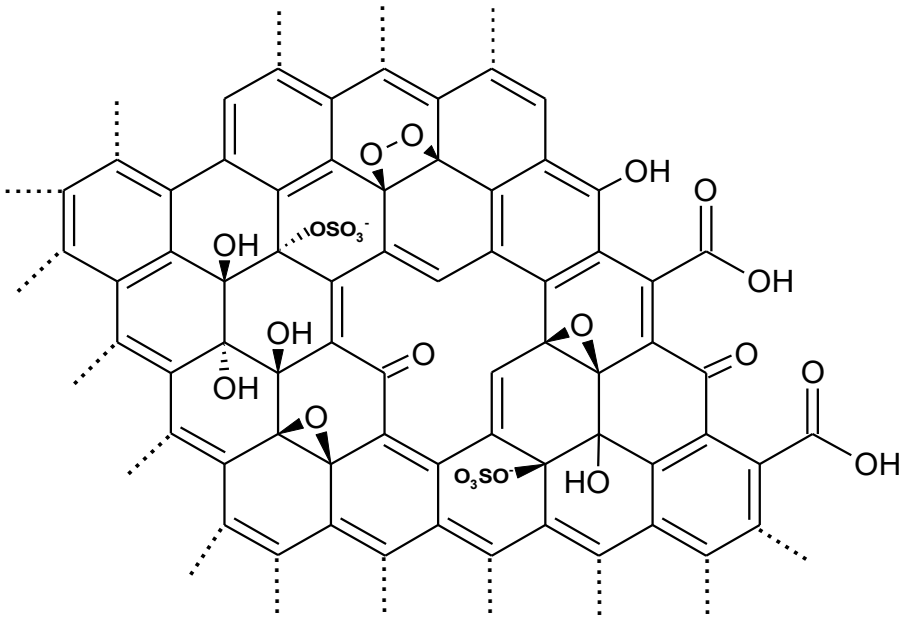

Figure 1.4 Structure of graphene oxide (GO)

The advantage of GO is that a small amount of polymer functionalized graphene has good specifications and safety properties as mechanical, electronic, optical, thermal and magnetic properties. GO is electrically insulating and is reduced with suitable processes getting conducting to result in reduced graphene oxide (rGO) contains residual oxygen and other heteroatoms[23]. Several methods have been used to reduce GO, electrochemically using cyclic voltammetry (CV) analyses[24], thermal annealing and chemical processing using strong

reductants like hydrazine[25]. Graphene is often composites with polymers, for ease of use in an aqueous electrolyte, depending on the method of reduction compatibility with the other components of the composite material. This thesis used a method of preparation as explained in Section (2.2.4.1) and then electrochemically reduced. While when it is not compatible with the other composite material in aqueous electrolyte, the thermal reduction method is used as described in Section (2.2.4.2).

GO and rGO are important applications that have been used in polymer composite materials, nanocomposite materials, energy storage, catalysis, biomedical[26], transparent conductors[27] and potential applications and as a surfactant with some overlaps between these fields[28]. Although possess unique physiochemical properties, they are limited in practical applications mostly due to difficulties in the formation of desired large-scale highly organized structures[29]. To achieve optimum physical and mechanical properties of graphene polymer nanocomposites, the solubility of graphene sheets should be maximized in a common solvent with that of the matrix polymer and the stress transfer should also be maximized through the interface due to the specific interaction between the sheet and polymer matrix[28].

1.6 Scope of Thesis

This thesis comprises work on organic materials, synthesis of novel redox-active polymers, their characterization, and evaluation of battery fabrication and performances. The known organic electroactive groups are converted to polymers able to undergo redox reactions. For this work, several types of polymer were prepared including linear polymers (LPs), dendrimers and three-dimensional (3D) / crosslinked polymers.

In Chapter 2 many different structures of LPs such as (poly viologen (PV), polyimide (PI) and Organometallic polymers) have been chosen to study the electrochemical characterization of polymers that have influenced the solubility and stability of polymer/GO complexes.

As for Chapter 3, a study was done on the solubility, stability of polymer/GO complexes and the electrochemical performance of dendrimers and three-dimensional (3D) / crosslinked polymers. In the previous chapters, I prepared the electrodes by drop-casting a solution containing the redox-active material and the conductive additive. In Chapter 4, the study was done on the dip-coating process (Layer-by-Layer) a linear polyviologen (redox-active material) was used as cationic species and GO as anionic species, with this system I prepared electrodes

and tested the electrochemical performance. Additionally, I used polymer / GO complex as cationic species and PSS as anionic species. Besides the electrochemical characterization, I used QCM to investigate layer growth. Finally, Chapter 5 included a summary and outlook of the thesis.

Chapter 2
Linear Polymers (LPs)

Chapter 2 **Linear Polymers (LPs)**

A part of this chapter is derived from the following Article:
Beladi-Mousavi, Seyyed Mohsen; Sadaf, Shamaila; **Mahmood, Arsalan Mado**; Walder, Lorenz, High Performance Poly(viologen)−Graphene Nanocomposite Battery Materials with Puff Paste Architecture. *ACS Nano*. **2017**, 11, 8730-8740.

2.1 Introduction

A polymer is a large molecule that found many applications. Both synthetic and natural polymers are an important part of our daily life. Polymers are produced by the polymerization of many small molecules namely monomers[16]. Historically, the linkage of repeating units by covalent chemical bonds has been the primary focus of polymer science. The properties of polymers are largely related to the structure of the monomer and the linkage between them[30]. Polymers containing redox-active units widely used in energy applications e.g. polymers are divided into three categories: i) Linear polymers (LP); consists of long and straight chains, for example, poly(butyl viologen), poly(vinyl chloride), etc. ii) Branched-chain polymers; these polymers contain linear chains having some branches. iii) Crosslinked or Network polymers; these are usually formed from bi-functional and tri-functional monomers such as melamine, etc[18].

Several redox polymers have been introduced as the active part of battery electrodes, including linear poly(viologens) (PVs). Generally, viologen derivatives were used as effective reducing agents for dioxygen, and the electrodes modified with the viologen were also useful in hydrogen evolution catalysis[18, 30].

Bipyridinium molecules are widely used to build supramolecular structures. They are used in molecular systems that exhibit controlled switching[31], rotational motion, and charge storage[32]. Many of these complexes provide controllable electrochemical properties which can be used in the context of electrochromic devices[33]. In such systems, the colour of cationic bipyridinium derivatives is highly dependent on the electronic ground state energy of the molecule, which can be finely tuned by varying the substituents. There have been many studies concerning the synthesis of oligomers and polymeric materials containing 4,4′-bipyridine (I)[34].

As a result of conjugation between pyridinium rings, which results in an increased electron delocalization, bipyridinium exhibits a more positive reduction potential than pyridinium, as shown in Scheme 2.1 [35].

Scheme 2.1 Redox process for pyridinium ion and bipyridinium ion

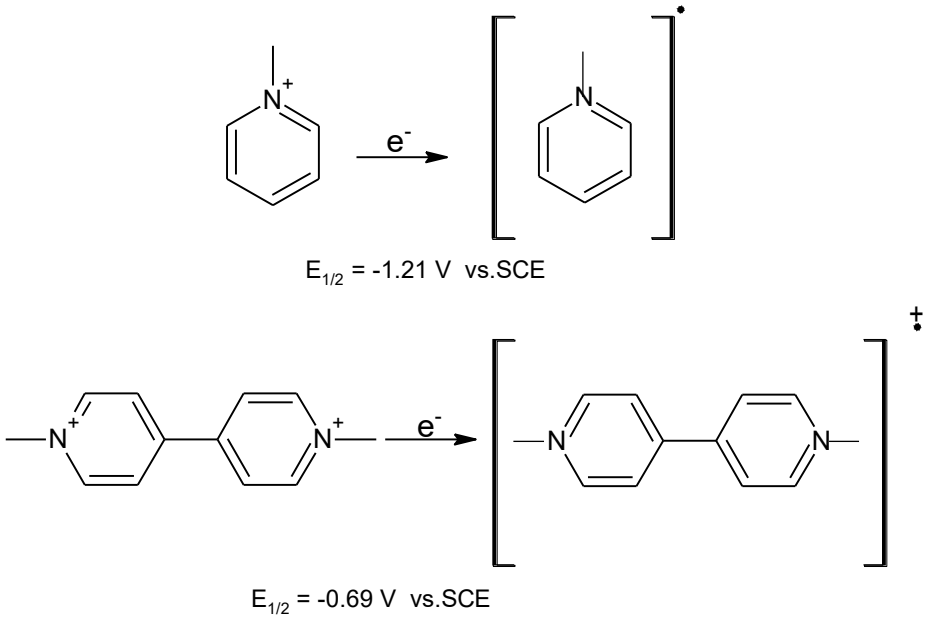

In recent years a wide range of metallocenes and their derivatives have been synthesized and used for different applications. Transition-metal organometallic compounds e.g., ferrocene and cobaltocene show exceptional redox properties mainly related to the oxidation/reduction of metallic center affecting their stable 18-electron state[36]. The redox potential of metallocenes can be as wide as 2V depending on the chosen transition metal ions and the functionalization of the cyclopentadienyl ligands[11a]. In the organometallic compounds, the redox orbital is extended to the Cp ligands as well as metal d orbitals. This allows a rapid reversible homogeneous and heterogeneous electron transfer (ET). Notably, it causes a very negligible dependence of the redox potential to the electrolyte solvent[13]. Hence, such types of polymers and dendrimers have been used for different applications including catalyst in bioelectrochemistry[37], batteries[10b, 13, 38], reference electrode[39], and for protection against overcharging in LIBs[38d].

Here in this chapter in addition to studying many different structures of polymers of active organic compounds such as (poly viologen (PV), polyimide (PI)), we propose using an

organometallic redox monomer i.e., ferrocene as cathode, and an organic redox monomer i.e., viologen as an anode in a single polymer. This allows to only prepare one single electrode which can be used as both cathode and anode, which is important regarding the scalability of these types of batteries. In general, the structures of polymers have influenced the solubility and stability of polymer/GO complexes.

2.2 Experimental Section

2.2.1 Instrument

The electrochemical properties were studied using cyclic voltammetry (CV) analyses using Autolab potentiostat (PGSTAT 20) interfaced to a computer with GPS software (version 4.9). The sonification was performed using an ultrasonic bath (VWR USC300TH, 80W). IR spectroscopy was performed on a Bruker VERTEX 70 FT-IR spectrometer. ^{1}H-NMR and ^{13}C NMR spectroscopy was performed on a Bruker Spectrospin Avance DPX-250 Spectrometer and 500 MHz respectively, using the solvent signal as an internal standard. Elemental analyses were performed on the "Elementar" instrument from Vario microcube instrument.

2.2.2 Chemicals

All the chemicals and solvents were from Sigma–Aldrich and used as received without further purification unless otherwise stated. Solvents and salts for the electrochemistry were of 99.9% purity. Graphene oxide (GO) was from "Graphenea" delivered as an aqueous solution (4 mg GO in 1 mL H_2O); The cellulose membrane for dialysis tubing was from "SPECTRUMLABS" with MWCO: 14 kDa.

2.2.3 Synthesis

2.2.3.1 Synthesis of Monomers

2.2.3.1.1 *Organic Monomers*

Scheme 2.2 Synthesis of conjugated 4,4′-bipyridinium oligomers II and III

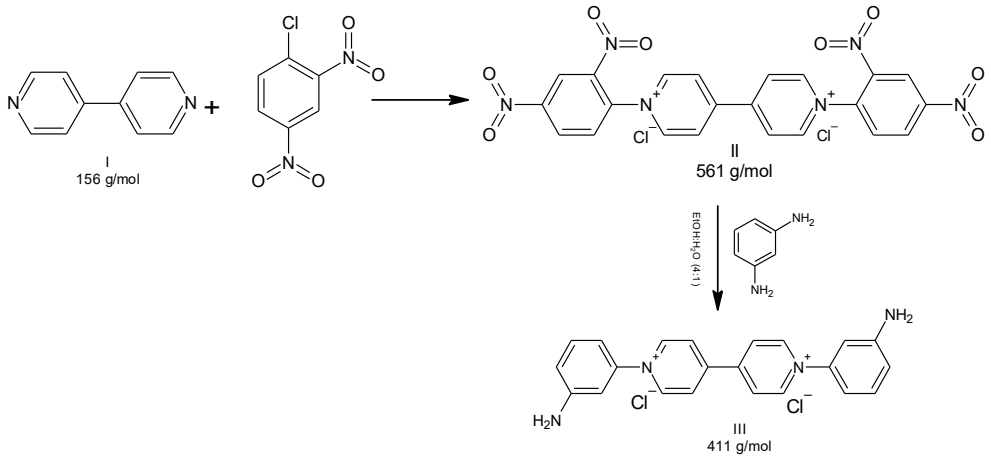

II and III were synthesized via Zincke reaction[40]. 1,1'-Bis-(2,4-dinitrophenyl)-4,4'-bipyridinium dichloride (II) was prepared based on a report by Nanasawa et. al.[40a] The I (6.4 g, 40 mmol) and 2,4-dinitrochlorobenzene (28.0 g, 140 mmol) were dissolved in dry MeCN 120 mL and refluxed for 72 h. The dense yellow precipitate was suspended with MeCN, filtered, and washed three times with MeCN. To remove monophenylated 1-(2,4-dinitrophenyl)-4-(4-pyridyl)-pyridinium chloride, the crude precipitate was washed several times with acetone. A pure (TLC: MeOH: HOAc: H_2O; 10/4/1) product was obtained **II** (74 % yield). ^{1}H NMR (D_2O, 250 MHz) δ: 9.41 (d, J= 7.5 Hz, 4H); 9.34 (d, J= 2.5 Hz, 2H); 8.89 (d, J=4 Hz, 4H); 8.87 (d, J=5 Hz, 2H); 8.25 (d, J= 10 Hz, 2H).

4,4'-Bipyridinium, 1,1'-bis(3-aminophenyl)-dichloride (III) was synthesized according to He et. al.[40b, 40c, 40e], using 1,1'-Bis(2,4-dinitrophenyl)-4,4'-bipyridinium dichloride with an excess amount of benzenamine derivative, with minor modification (using different solvent as EtOH:H_2O (4:1) with longer time of reflux and I used ether for re-precipitate). A solution of *m*-Phenylenediamine (0.578 g, 5.345 mmol) in 3 mL EtOH:H_2O (4:1) was added to a solution of II (1 g, 1.781 mmol) in 25 mL EtOH:H_2O (4:1), reflux 8 days at 90 °C, evaporate the solvent and the crude precipitate was washed several times with acetone, filtered and the precipitate was re-precipitate in EtOH (Ca. 200 mL)/ THF (Ca. 250 mL) and ether (Ca. 550 mL)), the

crude product was dried under high vacuum (HV) for 1 day. A pure (TLC: MeOH: HOAc: H_2O; 10/4/1) product was obtained **III** 600 mg (1.46 mmol, 82 % yield). ^{1}H NMR (250 MHz, CD_3OD) δ = 9.48 (d, 4H); 8.87 (d, 4H); 7.44 (t, 2H); 7.05 (t, 6H) ppm.

Scheme 2.3 Synthesis of triamine derivatives IV, V, VI, VII, and VIII

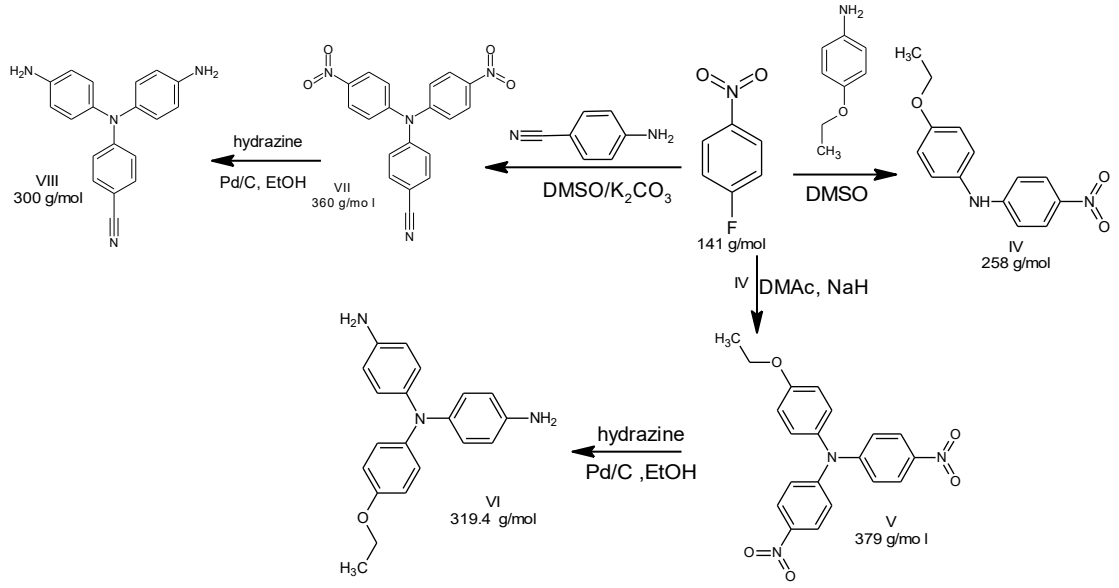

N-(4-nitrophenyl), *N*′-(4-ethoxyphenyl)phenylamine (IV) was synthesized according to the literature.[41] A suspension of 4-Ethoxyaniline (3.7 mL, 28.76 mmol) in anhydrous DMSO 25 mL and *p*-fluoronitrobenzene (1 mL, 9.43 mmol) was stirred for 1 day at 120 °C under argon gas and monitored by TLC (solvent: EtOAc). Then, the solution was poured into a 0.5 M hydrochloric acid (Ca. 80 mL). The precipitate was dissolved in ethyl acetate and the solution was then washed with 1 M hydrochloric acid solution, sodium hydrogen carbonate solution, and brine solution. The organic solution was dried over anhydrous magnesium sulfate, filtered, and evaporate the solvent from the organic layer. The crude product was purified by recrystallization from toluene and hexane, the product was dried under HV for 1 day to produce **IV** 1.94 g (7.52 mmol, 80 %) orange crystal. ^{1}H NMR: (250 MHz, $CDCl_3$), δ(ppm): 8.13-8.09 (s, 2H), 7.29 (s, 2H), 7.18-6.93 (s, 2H), 6.80 (s, 2H), 6.11 (s, N-H, 1H), 4.12 (q, 2H), 1.49 (t, 3H).

4-Ethoxy-4′,4″-dinitrotriphenylamine (V) and 4-ethoxy-4′,4″-diaminotriphenylamine (VI) was synthesized according to Lee et. al.[42] The compound IV (1 g, 3.87 mmol) was added

to a solution of sodium hydride (0.25 g, 10 mmol) in anhydrous DMAc 7 mL. The solution was stirred at room temperature (r.t) for 30 min and cooled to 0 °C. 4-Fluoronitrobenzene (0.798 g, 5.66 mmol) in anhydrous DMAc 3.5 mL was added dropwise to this mixture. After the addition was complete stirred at r.t for 10 min, then the mixture was stirred at 100 °C for 1 day and monitored by TLC (solvent: EtOAc). Then the mixture was cooled to r.t and poured into a 0.5 M hydrochloric acid solution (Ca. 40 mL). The crude product was collected by filtration and recrystallized from 2-propanol and water, dried under HV 1 day to gave dark orange crystals of **V** 1 g (2.638 mmol, 68 % yield). ^{1}H NMR (500 MHz, DMSO-d6, δ, ppm): 8.17 (d, 4H), 7.21-7.16 (m, 6H), 7.05 (m, 2H), 4.08 (q, 2H), 1.36 (t, 3H).

V (0.5 g, 1.319 mmol) and palladium on activated carbon (Pd/C) (0.02 g) were dissolved in ethanol 6.5 mL and the solution was refluxed. Hydrazine monohydrate 0.5 mL was added dropwise, and the mixture was stirred at this temperature for 1 day. The reaction solution was immediately filtered through Celite before cooling down to r.t due to the low solubility of VI in ethanol. The filtrate was concentrated and poured into water. The precipitate was collected by filtration and purified by recrystallization from ethanol to yield light brown crystals **VI** 0.3 g (0.94 mmol) in 71 % yield. ^{1}H NMR (500 MHz, DMSO-d6, δ, ppm): 6.72 (m, 8H), 6.50 (m, 4H), 4.78 (s, $ArNH_2$, 4H), 3.92 (q, 2H), 1.27 (t, 3H).

4-[Bis(4-nitrotriphenyl)amino]benzonitrile (VII) was synthesized according to the literature[43]. Dissolve 4-aminobenzonitrile (752 mg, 6.37 mmol) in anhydrous DMSO 0.5 mL and stirred under argon gas at r.t, add K_2CO_3 (440 mg, 3.18 mmol), stir at 120 °C for 20 min, add *p*-fluoronitrobenzene (1.35 mL, 12.73 mmol) and reflux at 150 °C under argon for 2 days. The reaction mixture was cooled to r.t and precipitated in 50 mL cold water. The solids were collected by filtration, washed with water and dried under HV at 45 °C for 1 day. The product was purified by filtering over a short silica column using dichloromethane and recrystallization using glacial acetic acid, the product was collected by filtration and dry under HV 1 day at 55 °C. Yield yellow precipitate **VII** 794 mg (2.2 mmol, 35 %; TLC (3:1 hexane:ethyl acetate)). ^{1}H NMR (500 MHz, DMSO-d6, δ, ppm): 8.24 (d, 4H); 7.89 (d, 2H); 7.38 (d, 2H); 7.32 (d, 4H).

4,4′-Diamino-4″-cyanotriphenylamine (VIII) was synthesized according to a similar procedure as VI. The yield white precipitate of **VIII** was 635 mg (2.11 mmol, 96 %; TLC (95% DCM, 4.5% MeOH, 0.5% NH_4OH)). ^{1}H NMR (500 MHz, DMSO-d6, δ, ppm): 7.42 (d, 2H), 6.92 (d, 4H), 6.60 (d, 4H), 6.53 (d, 2H).

2.2.3.1.2 ***Organometallic Monomers***

Scheme 2.4 The synthesis of 1,1'-Bis(chloromethyl)ferrocene (IX)

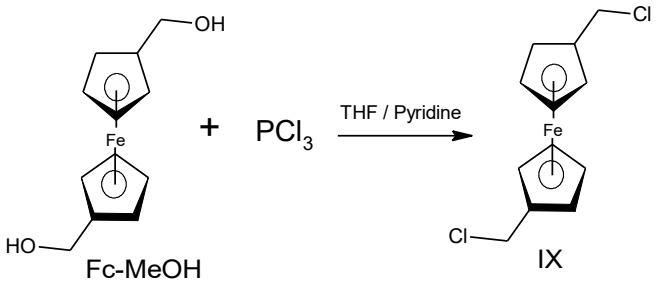

1,1'-Bis(chloromethyl)ferrocene (IX) was synthesized according to literatures[37a, 44]. A solution of PCl_3 (274 mg, 0.16 mL, 2 mmol) and 2.5 mL of dry THF has been added dropwise to a solution of 1,1'-Bis(hydroxymethyl)ferrocene (Fc-MeOH) (500 mg, 2.032 mmol) in mixture solvent (0.1 mL of dry pyridine and 12.5 mL of dry THF) with stirring under Ar gas at r.t. After the addition was over, stirring was continued for 3 h at r.t. Then, the solution was decanted and the residue was rinsed with 10 ml of THF. The combined solution was evaporated under reduced pressure, recrystallization from hexane **(IX)** was obtained as residual yellow crystals 245 mg (0.865 mmol, 43 %). ^{1}H NMR (500 MHz, CD_3CN, δ, ppm): 4.57 (d, 4H); 4.33 (d, 4H); 4.28 (d, 4H).

2.2.3.2 Synthesis of Linear Polymers

2.2.3.2.1 ***Organic LPs***

The polymer 1, 2, 3, 4, 5 and 6 were prepared by previously reported multiple Menshutkin reactions [35, 45] and Zincke reactions[37b, 40a, 40c, 40d, 46].

Scheme 2.5 Synthesis of Polymer 1

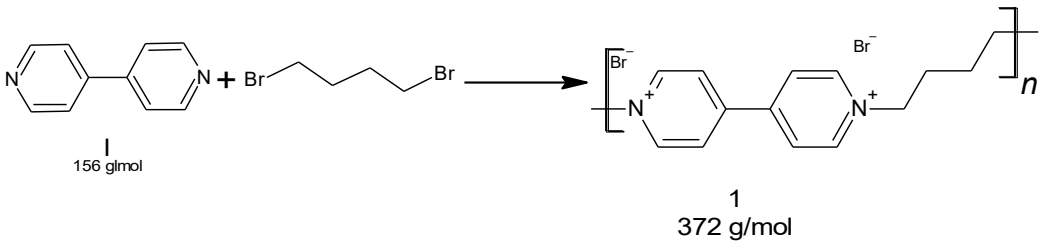

Polymer 1 was synthesized according to Lee et. al.,[45a] by mixing starting materials (I) with an alkyl halide. (0.78 g, 5 mmol) of (I) and 1,4-dibromobutane (1.08 g, 5 mmol) were dissolved in 15 mL MeCN and refluxed with a stirrer. After 1 day, 15 mL distilled water was added to dissolve the precipitates and transferred to a small pressure vessel (temperature: 110 °C, constant pressure: 3 bar). After 20 days, water was evaporated and the solid residue was washed with MeCN and ether and was dried under HV to obtain 1 (87.5 % yields) as yellow solid. In order to remove short oligomers, the crude product was separated by column chromatography on Sephadex LH-20 (ca. 100 mg) (length: 30 cm * surface 9.5 cm^2, mobile phase: H_2O). The final yield after removal of short oligomers was 73 % for **1**. ^1H NMR (250 MHz, D_2O, for Fraction 3) δ: 9.20 (d, 4H); 8.62 (d, 4H); 4.86 (s, 4H); 2.31 (s, 4H) ppm. IR: 3014 (Hetro ArH), 1634 (C=N), 1362 + 1385 (-CH_2-), 1178 (C-N) cm^{-1}. Anal. Calc. for $C_{14}H_{16}Br_2N_2$: C, 45.19; H, 4.33; N, 7.53; Br, 42.95. Found: C, 42.51; H, 5.26; N, 7.25; Br, 44.9.

Scheme 2.6 Synthesis of Polymer 2, 3 and 4

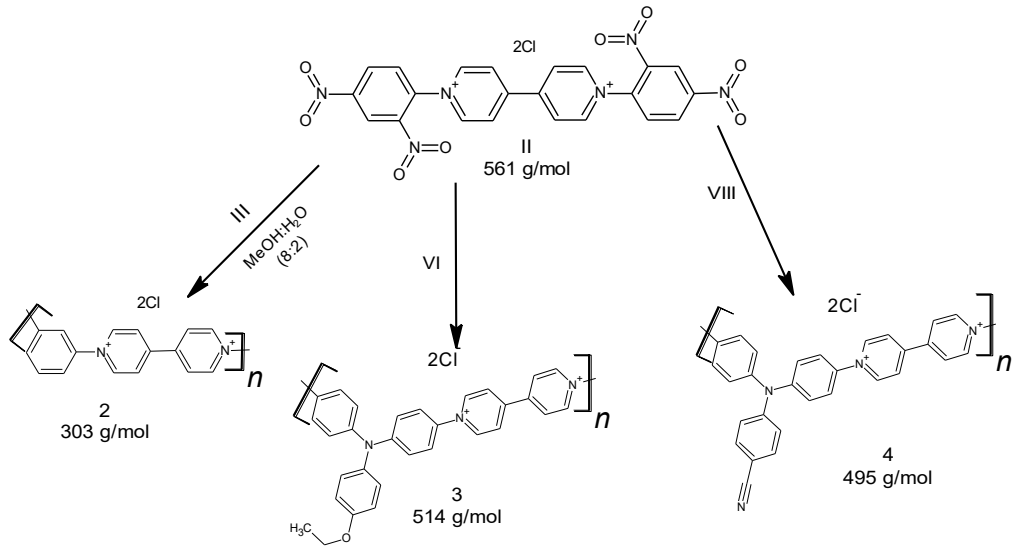

Polymer 2, 3, and 4 were prepared via Zincke reactions that have been reported in the literature[40a-d, 46], with minor modification. In one portion solution of II (683 mg, 1.216 mmol) in MeOH:H_2O (4:1) (5 mL) was added to a solution of III (500 mg, 1.216 mmol) in MeOH:H_2O (4:1) (20 mL), reflux at 100 °C for 2 weeks. Remove solvent the crude precipitate was washed several times with acetone, filtered and the crude precipitate was washed with EtOAc and re-precipitate in MeOH/EtOAc (three times). The precipitate was dissolved in MeOH:H_2O (4:1) (10 mL), the filtrate was isolated and centrifuged to remove the remaining precipitate and evaporate the solvent from the filtrate, the polymer 2 was obtained 270 mg (0.891 mmol, 73% yield). Purified by dialysis in water by using dialysis tubing of the aqueous phase, the crude product (Ca. 100 mg) was dissolved in MeOH:H_2O (4:1) (10 mL) (extracting compartment: agitated water for 1 week, daily exchanged). Separation of the phases and dialysis of the aqueous phase, yielded a dark-brown aqueous solution, evaporate water and the crude precipitate was washed with acetone and ether. The brown precipitate was dried under HV at 50 °C for 1 day. The final yield of **2** after removal of short oligomers was 71 mg (0.234 mmol, 19 %). ^{1}H NMR (250 MHz, CD_3OD) δ: 9.85 (d, 4H); 9.10 (d, 4H); 8.45 (d, 2H); 8.26 (d, 1H); 7.14 (q, 1H) ppm.

Polymer 3 and 4 were prepared via Zincke reactions according to a similar procedure as 2, with minor modification. In one portion under Ar gas a solution of II (685 mg, 1.22 mmol) in EtOH:H_2O (4:1) (10 mL) was added to a solution of VI (390 mg, 1.22 mmol) in EtOH:H_2O (4:1) (20 mL) for the synthesis 3 or solution of VIII (365 mg, 1.22 mmol) in MeOH:H_2O (4:1) (20 mL) for the synthesis 4, after 2 h remove Ar gas and continuous reflux at 100 °C for 1 week (TLC: 95% DCM, 4.5% MeOH, 0.5% NH_4OH). Remove solvent the crude precipitate was washed several times with acetone, filtered and the crude precipitate was washed with EtOAc and ether, the precipitate was dissolved in EtOH and reprecipitated in a mixture solvent of THF & Ether (three times). The product was dried under HV at 50 °C for 1 day to obtain 600 mg (1.167 mmol, 95.5 % yield) of 3. In order to remove short oligomers from 3, the crude product was separated by column chromatography using Sephadex LH-20 (ca. 100 mg) (length: 30 cm * surface 9.5 cm^2, mobile phase: MeOH:H_2O (4:1)). The final yield after removal of short oligomers of **3** was 253 mg (0.492 mmol, 40 %). ^{1}H NMR (500 MHz, CD_3OD) δ: 9.55 (d, 4H); 8.92 (d, 4H); 7.92 (d, 4H); 7.48 (d, 4H); 7.28 (d, 2H); 7.10 (d, 2H); 4.13 (q, 2H); 1.46 (t, 3H) ppm. Without more purification yield 500 mg (1 mmol, 82%) of **4** as a purple solid. ^{1}H NMR (500 MHz, DMSO-d6) δ: 9.78-9.56 (d, 4H); 9.17 (d, 4H); 8.13-7.93 (d, 4H); 7.58-7.43 (d, 4H); 7.27 (d, 2H), 7.06 (d, 2H) ppm.

Scheme 2.7 Synthesis of Polymer 5

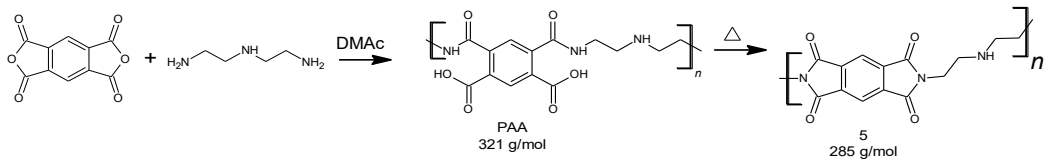

Polymer 5 was synthesized according to Chen et.al.[47]. To a solution of diethylenetriamine (100 mg, 1 mmol) in DMAc (5 mL), a solution of PMDA (0.22 g, 1 mmol) in DMAc (10 mL) was added in one portion. The mixture was stirred at r.t for 10 min to afford a viscous poly(amic acid) (PAA) solution. The mixture was refluxed for 3 days then cooled to r.t and the white solid was separated by filtration, washed with MeCN, acetone, EtOAc, and dried under HV at 50 °C for 1 day. In order to remove short oligomers, the crude product was separated by column chromatography using Sephadex LH-20 (ca. 150 mg) (length: 30 cm * surface 9.5 cm^2, mobile phase: H_2O). The final yield after removal of short oligomers was (53 %) for **PAA** as a white solid. ^1H NMR (500 MHz, D_2O) δ: 7.50 (s, 2H), 3.04 (s, 4H), 2.85 (s, 4H) ppm. IR: 2853 (O-H), 1537 (Amic C=O), 1356 (-CH_2-), 809 (C-N) cm^{-1}. Anal. Calc. for $C_{14}H_{15}O_6N_3$: C, 52.34; H, 4.71; N, 13.08; O, 29.88. Found: C, 44.56; H, 7.07; N, 16.53; O, 31.71.

The 50 mg of PAA was subsequently converted to polyimide film via a thermal imidization process (100 °C 1 h, 200 °C 1 h, and 250 °C 1 h) in a vacuum oven. Yield dark brown solid of **5** (42 %) IR: 1708 (Imid C=O), 1387 (-CH_2-), 724 (C-N) cm^{-1}. Anal. Calc. for $C_{14}H_{11}O_4N_3$: C, 58.95; H, 3.89; N, 14.73; O, 22.43. Found: C, 56.14; H, 3.65; N, 17.4; O, 22.67.

2.2.3.2.2 ***Organometallic LP***

Scheme 2.8 The synthesis of polymer 6

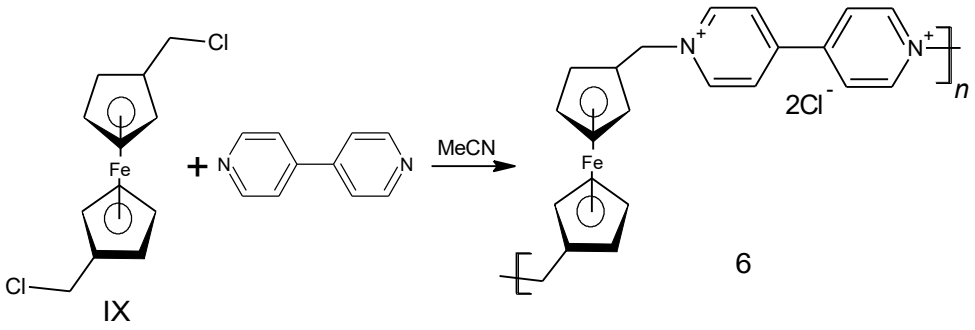

Polymer 6 was synthesized according to the literature[37b] with minor modification. In one portion the solution of IX (136 mg, 0.482 mmol) in 5 mL MeCN was added to the solution of I (75 mg, 0.482 mmol) in 5 mL MeCN (directly result in brown precipitate) and reflux at 90 °C under argon atmosphere after 4 days add 10 mL H_2O and continue reflux for another 2 days at 110 °C. The solvent was removed in a rotary evaporator; the residue was refluxed with 100 mL MeCN at 90 °C for 30 min, the black precipitate was separated by filtration and washed with MeCN (2*20 mL), acetone (20 mL), and diethyl ether (20 mL). The precipitate was reflux for 15 min in water and collect hot filtrate, evaporate water and refluxed with 50 mL MeCN separated by filtration, washed with MeCN (2*20 mL) and acetone (20 mL). The solid was dried overnight under HV to obtain 83 mg (0.189 mmol, 39 % yields) of 6 as black solid. In order to remove short oligomers, the crude product was separated in a column Sephadex LH-20 (ca. 75 mg) (length: 30 cm * surface 9.5 cm^2, mobile phase: H_2O). The final yield after removal of short oligomers was 47 mg (0.118 mmol, 24.5 %) for **6**. ^1H NMR (250 MHz, D_2O, for Fraction 5) δ: 8.99 (d, 4H); 8.40 (d, 4H); 5.74 (d, 4H); 4.79-4.68 (m, 4H); 4.54 (d, 4H) ppm.

2.2.4 Preparation of Electrochemical Solutions

2.2.4.1 Solutions of LP@GO with Variable LP / GO Ratio

An aqueous solution of commercial GO was diluted to 1 mg / 1 mL and sonicated for 30 minutes using an ultrasonic bath. a) Weight ratio 3:1 LP / GO: The GO solution (1 mL, containing 1 mg GO) was dropwise added to the P solution (3 mL, containing 3 mg of P) under sonification over 30 min. b) Other LP / GO ratios: The same procedure as in (a) using the same

amount of polymer solution, but varying the amount of GO solution for the desired ratio. c) Weight ratio 3:1 LP / GO in NMP solvent: The GO solution 4 mg/4 mL NMP (4 mL of NMP has been added to the aqueous solution of GO 4 mg/1 mL and evaporate water at high temperature) was dropwise added to the P solution under sonification over 30 min.

2.2.4.2 Solution of LP@rGO

An aqueous solution of commercial GO 4 mg / 1 mL was heated to 120 °C for 1 day to remove water, add NMP solvent and the solution was refluxed 2 days at 150 °C to reduce GO. Weight ratio 3:1 LP / rGO: The rGO solution (1 ml, containing 4 mg rGO) was dropwise added to the P solution (3 ml, containing 3 mg of P) under sonification over 30 min.

2.2.5 Electrochemical Measurements and Preparation of Electrodes

Using Ag/AgCl as a reference electrode, the electrochemical reduction of the composite was performed in the surface-confined state on glassy carbon (GC) electrode (surface: 0.071 cm^2, Metrohm, 6.0804.010) or carbon plate electrode (CPE, SGL Group, SIGRACELL TF6 and 0.8 mm thickness) with one side isolated using adhesive tape, thus exhibiting an open side surface of 0.9 cm^2 (CPE was cleaned with acetone, ether and dried in the oven at 50 °C) or on FTO or ITO (active surface: ca. 1 cm^2, "Aldrich"). GC was polished with alumina powder, then rinsed thoroughly with water, and dried in the oven at 50 °C. The electrodes were prepared by drop-casting of a polymer or LP@GO solution as a procedure (2.2.4.1) on the current collector followed by drying at (50 °C for 15 min or 100 °C for 1 h, 200 °C for 1 h and 250 °C for 1 h when using ITO or FTO) resulting in $(LP@GO)_n@CC$ (*$(LP@GO)_n@CC$*: composite material obtained from n-fold casting/drying on a current collector (CC)). Another type of CPE electrodes was prepared by drop-casting of LP@rGO solution (in 2.2.4.2) drying on the heater at (80-90 °C for 15 min and then in the oven at 60 °C for 1 h) resulting $(LP@rGO)_n@CC$, with n = number of layers with n > 2, bigger drops in the range between 5-20 µl is used of solution (2.2.4.1 and 2.2.4.2).

2.2.6 Electrochemical Transformation of $(LP@GO)_n@CC$ to $(LP@rGO)_n@CC$

In all of the electrochemical reduction experiments an aqueous solution of 0.1 M (KCl, $LiClO_4$, Na_2SO_4) and 1 M $LiN(CF_3SO_2)_2$) was used as the electrolyte/electrocatalyst. After electrochemical reduction of GO, the $(LP@rGO)_n@CC$ electrode was washed in distilled water (to remove salt) and organic solvent, then dried at 50 °C for 15 min. Then, the electrochemical properties were measured by using an organic solution of 0.1 M ($LiClO_4$, $TBAPF_6$, $TBABF_4$, $TBAClO_4$, $TEABF_4$ or LiTFSI) in MeCN, 0.1 M $TBAPF_6$/DCM, 0.1 M $LiClO_4$/propylene carbonate (PC), 1 M $LiN(CF_3SO_2)_2$/DMF and $LiClO_4$, LiTFSI/ethylene carbonate (EC):DCM (1:1).

2.3 Result and Discussion

We have selected six different structures of linear polymers (LPs) to investigate electrochemical properties. In general, the solubility and method forming linear polymer garaphene oxide complex (LP@GO) are independent of the polymer structure. Furthermore, some of these different structures comprised around garaphen oxide (GO) and provide stable LP@GO colloidal solutions, and some others are unstable. The physical and electrochemical properties concerning their energy storage performance of (linear polymer with garaphen oxide, linear polymer with reduced garaphen oxide) are presented in detail in this study and used as the electrodes material of the batteriesTable 2.1.

Table 2.1 The stability and yield percentage of linear polymer

P No.	Structure	Exp. Yield %	Stability LP@GO		Stability LP@rGO	Synth.
			Water	Organic solvent		
1	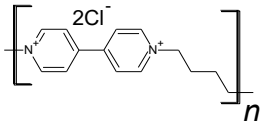	73	+	+		Our results were published[40d]
2	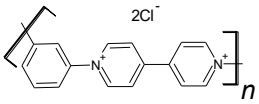	19	+	-	+	This work
3	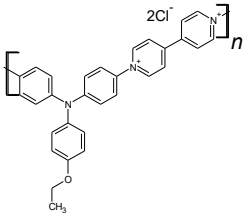	40	+	+	+	This work
4	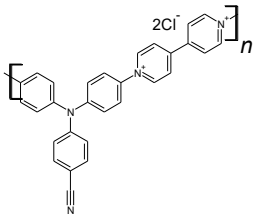	82	+	+	+	This work
PAA	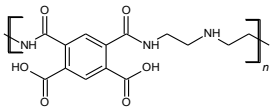	53	-	-		This work
5	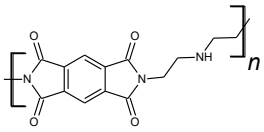	42	-	+		This work
6	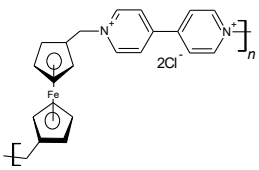	24.5	+	-		This work

2.3.1 Organic LPs

Redox active polymers were synthesized based on previous literature (see scheme 2.2, 2.3 and 2.4)[37a, 40-44]. In details, to prepare the redox polymers, the equivalent amounts of starting materials were refluxed with different solvent (see scheme 2.5-2.8). Additionaly for the purification of these polymers were carried out by Extraction, re-precipition and column separation. Also, synthesized redox polymers P2-P7 are novel material except P1 and dendrimers.

2.3.1.1 Polymer 1 (P1)

The solution of P1 & P1@GO in water as a procedure (section 2.2.4.1, a) and the electrodes were prepared using a drop-casting method as a procedure (section 2.2.5) and the electrolyte as a procedure (2.2.6 for experimental details). The P1 with and without GO were drop-casted on the GC electrode and then the film investigated the redox properties by CV method at different concentrations. Resulted, the peak currents of with and without GO were directly proportional to the concentration of a thickness film. For instance without GO, electric current increased upto 40 µg thickness of P1 on the electrode. However, further increses of thickness decrease the current Figure 2.1, part a). In addition of GO the current is increased upto 240 µg thickness and further increases decrease the current stability Figure 2.1, part b). Thus, this increase of current indicates the limitation arising from the kinetics of charge transfer and the role of GO in increasing the conductivity as shown in Figure 2.1, part c). Also reduced GO investigated, which shows identical current in the CV Figure 2.1, part d).

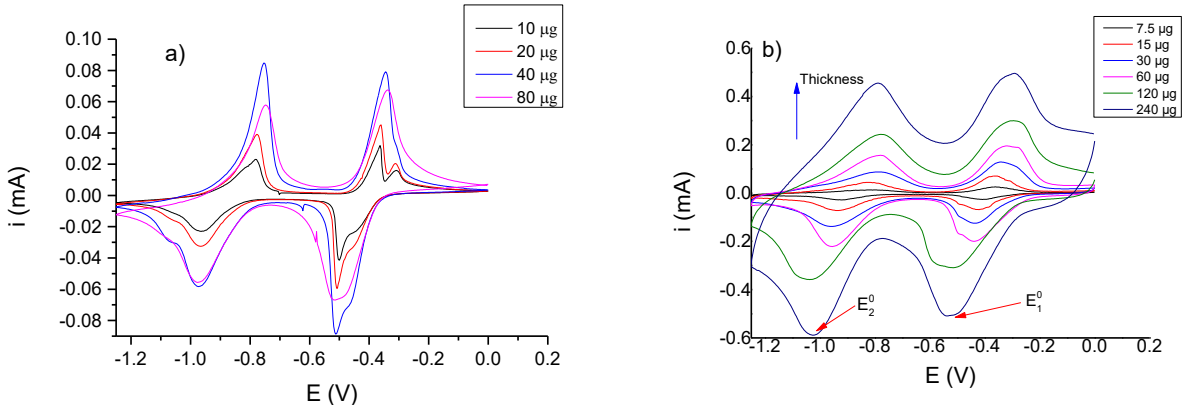

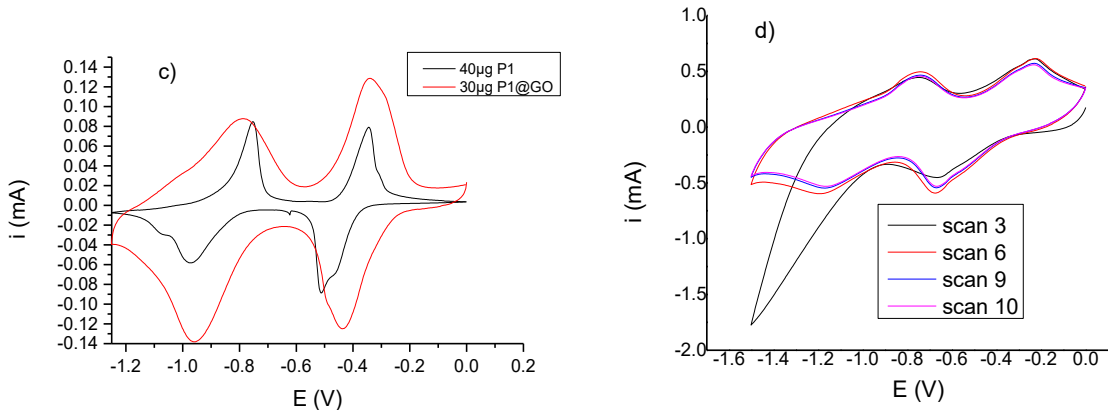

Figure 2.1 CVs, observed current vs. potential of P1 (F3), electrolyte 0.1 M $LiClO_4$ / MeCN, the GO was reduced in 0.1 M $LiClO_4$ / H_2O, at v = 10 mV s^{-1} on the GC electrode of a) pure P1 different concentration. b) P1@GO (3:1) different concentration. c) The comparison of P1 with P1@GO, different concentrations. d) reduced GO, different scan of P1@GO (3:1) 240 µg.

The theoretical capacity and specific capacity were expolored by Faraday's law, The analysis of the voltage-time curve from the galvanostatic cycling test afforded specific capacities P1 (252 mAh g^{-1}) and with reduced GO (216 mAh g^{-1}). Also, we have previously shown the effect of GO and reduced GO on the linear polymers,[40d] depending on the cycling rate used and also on the voltage range investigated (cut off voltage values) (see galvanostatic studies in Figure 2.2)[40d].

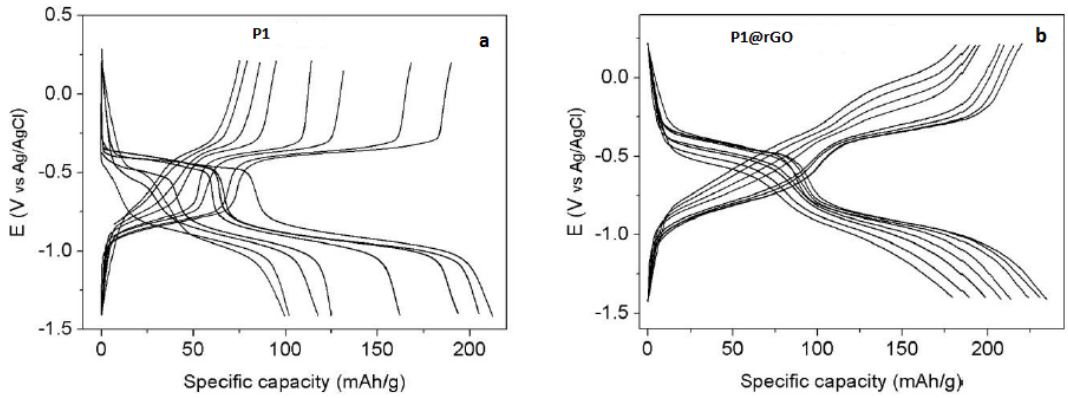

Figure 2.2 Galvanostatic response observed specific capacity vs. potential of P1 (F3), cutoff voltage = -1.5 – 0.5 V. Galvanostatic charging–discharging curves of polymer vs composites (a) P1@GC, (b)(P1@rGO)@GC ; observed capacity of 4.17 µAh cm^{-2}; charging-discharging rates 1, 3, 5, 10, 30, 50, 75, and 100 A g^{-1}, in 0.1 M $LiClO_4$/MeCN, obtained from b

2.3.1.2 Polymer 2

In the ^{1}H NMR spectrum of P2 Figure 2.3 all signals in the downfield are observed for arising from the (α&β)-protons of bipyridinium ion at (9.85 and 9.1 ppm, respectively) concerning the nitrogen atom. While the signal resonances for phenyl protons are observed at 8.4-7.1 ppm.

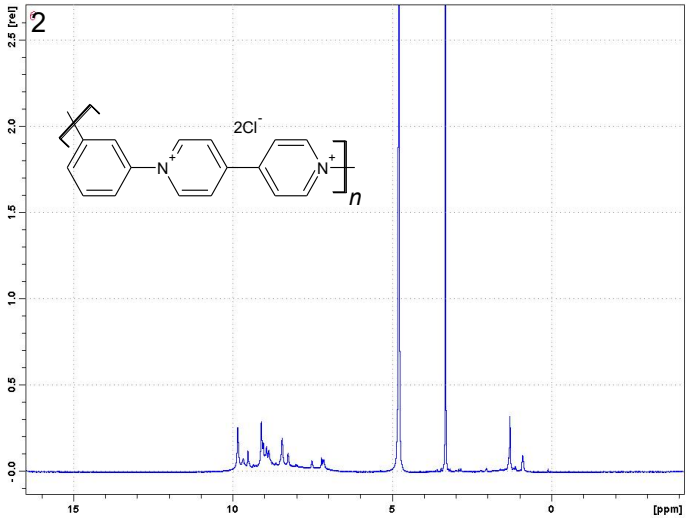

Figure 2.3 The ^{1}H NMR spectrum of P2

The electrochemical properties for P2, use without further refining collected cyclic voltammetric method by dissolving P2 in solvent H_2O:MeOH (4:1), the solution of P2@GO in different ratios were prepared as a procedure (2.2.4.1, a and b), the electrode and electrolyte as a procedure (2.2.5 and 2.2.6, respectively). The redox potentials of the P2@GO composite in $TBAPF_6$/MeCN is more positive than in $LiClO_4$/MeCN electrolyte and exhibits smaller coulombic efficiency reflecting the preferential of P2 by counter anion (ClO_4^-) compared to (PF_6^-), the coulombic efficiency little increasing at mixing with active materials such as GO as shown in Figure 2.4, part a) is around (13%). In addition, the P2 is not active and loses some of the materials at reducing GO in water. Therefore, I reduced GO before mixing as a procedure (2.2.4.2 in Experimental Suction) and became to higher coulombic efficiency (approximately 26 %) in the ratio of (P2@rGO) (1:1) comparison with other ratios as shown in Figure 2.4, part b).

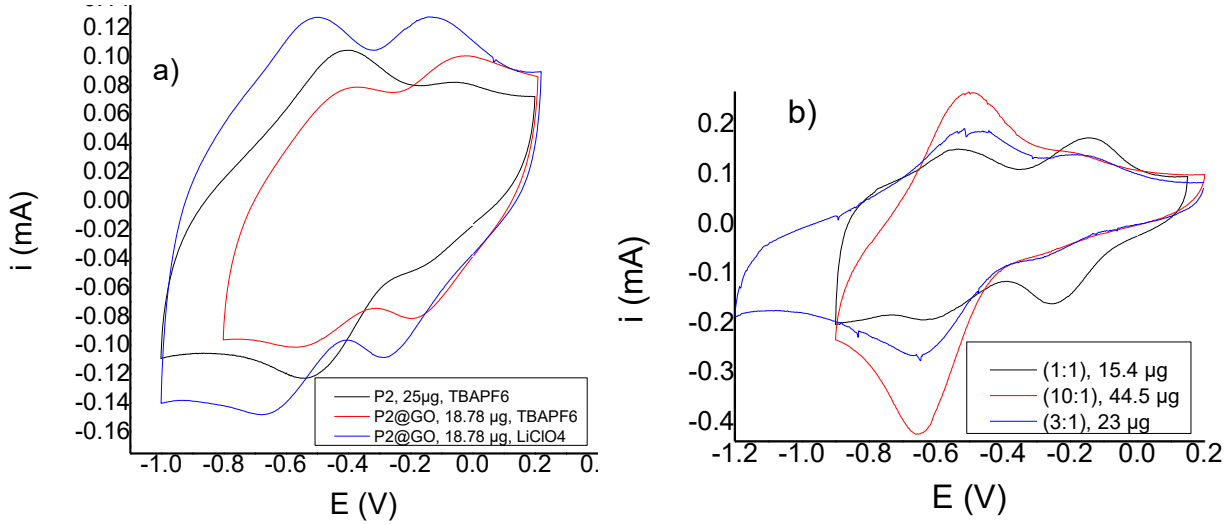

Figure 2.4 CVs measurements for P2 observed current vs. potential on the CPE. a) P2 (25 µg) and P2@GO (3:1) (18.78 µg), electrolyte 0.1 M different salt / MeCN at v = 20 mV s-1, after reduced GO in 0.1 M KCl / H_2O. b) P2@rGO in different ratios, electrolyte 0.1 M $LiClO_4$ / MeCN at v = 20 mV s^{-1}

2.3.1.3 Polymer 3

Eighteen chromatography-separated fractions from crude P3 Figure 2.5. The ^{1}H NMR resonances after fraction 18 are assigned to peripheral protons, resonances 5-17 are assigned to internal protons. With increasing chain length the peaks due to peripheral protons are fading out. A fraction represents the polycondensation reaction that can lead to aniline, nitro-or mixed end groups.

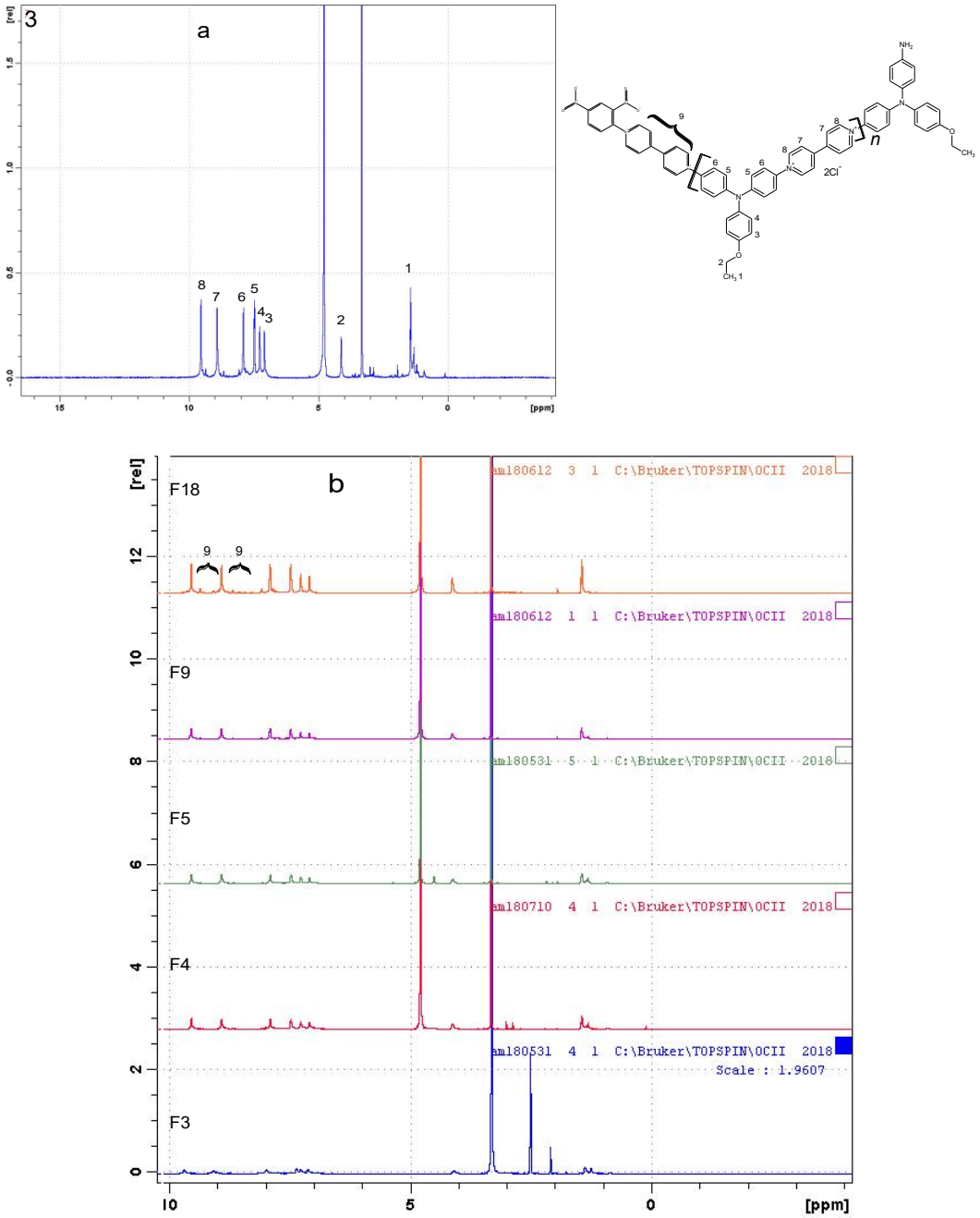

Figure 2.5 The ^{1}H NMR spectrum. a) P3 (mixture of F5-17) and b) Separation of crude P3 of fractions 3, 4, 5, 9 and 18

The below Figure 2.6 is a method for measuring cyclic voltammetric to determine the electrochemical properties of P3. The solution of P3@GO and P3@rGO was prepared as above procedure P2. Figure 2.6, part a) involved searching for the stability of P3@GO in $LiClO_4$/MeCN electrolyte, but it turned out that the nitrogen present in the triphenylamine center peak was unstable after the passage of several scans and with low coulombic efficiency. The instability and low coulombic efficiency (about 66 %) were found by changing salt and using the same solvent MeCN as shown in Figure 2.6, part b). In searching for the stability of nitrogen present in the triphenylamine center, electrolytes from several different salts and polar solvents were used as in Figure 2.6, part c) show the redox potential is shifted to positive in the $TBAPF_6$/MeCN electrolyte exhibits smaller reflecting the preferential of P3 by counter anion (ClO_4^-) compared to (PF_6^-). While through which it is evident that the stability is affected by the solvent and still is it low coulombic efficiency.

A non-polar solvent like DCM as shown in Figure 2.6, part d) was used to compare with polar solvents. It confirms that the nitrogen present in the triphenylamine center peak is more stable in a non-polar solvent and coulombic efficiency became higher around (86 %), but DCM solvent is not possible for battery applications. Otherwise, the coulombic efficiency becomes higher for the redox potential of viologen (approximately 90 % in $LiClO_4$/MeCN) in the polar solvent at reducing GO to rGO before mixing as (2.2.4.2 in Experimental Suction) as shown in Figure 2.6, part e). The

Table 2.2 explain the stability of P3 with different electrolyte.

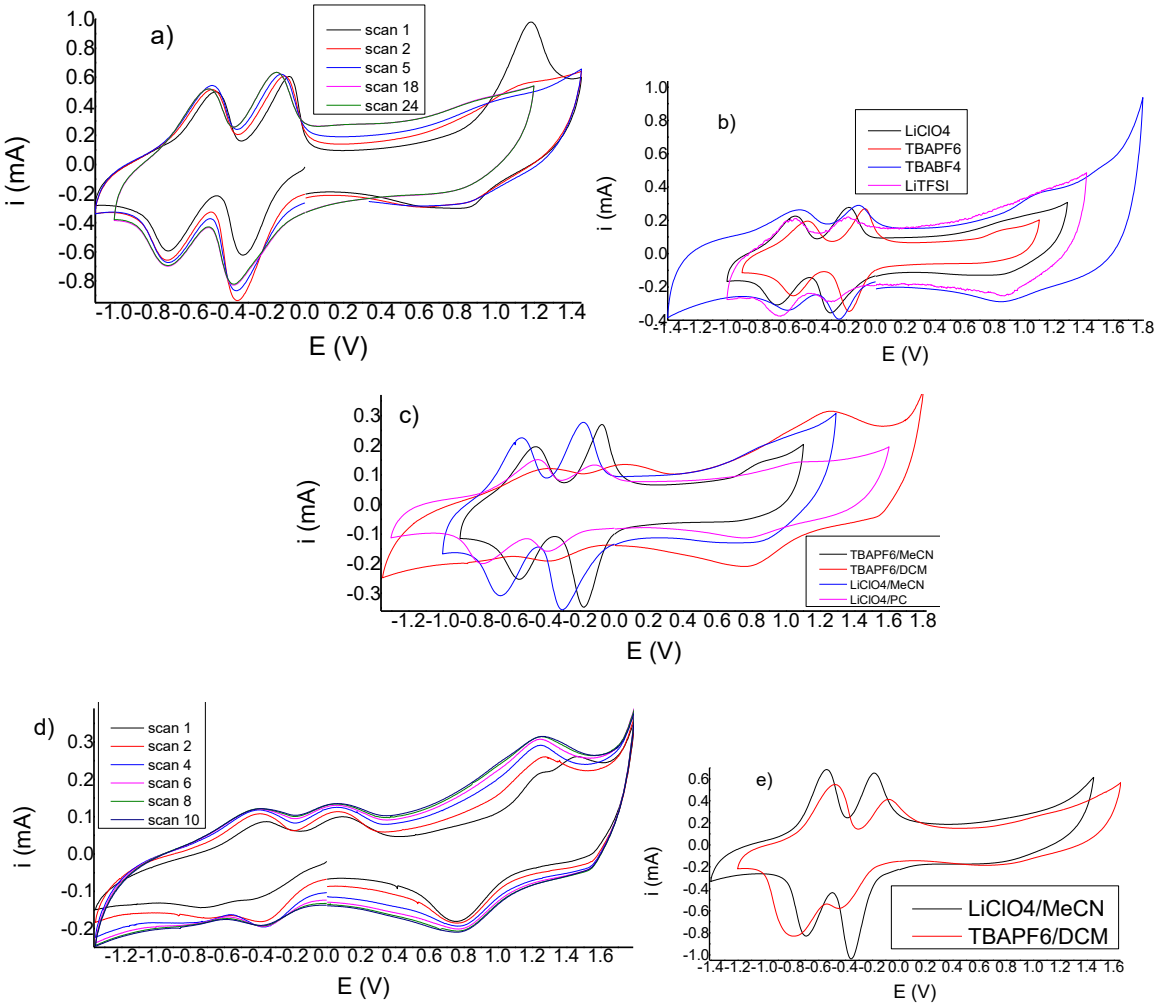

Figure 2.6 CVs measurements for P3 observed current vs. potential on the CPE. a) P3@GO (3:1), 19.3 µg, different scan number, electrolyte 0.1 M $LiClO_4$/MeCN, at v = 50 mV s^{-1}, after reduced GO in 0.1 M $LiClO_4$ / H_2O. b) P3@GO (3:1), 19.3 µg, 0.1 M electrolyte of different salt/MeCN at v = 20 mV s^{-1}, after reduced GO in 0.1 M $LiClO_4$ / H_2O. c) P3@GO (3:1), 19.3 µg, different electrolyte 0.1 M, at v = 20 mV s^{-1}, after reduced GO in 0.1 M $LiClO_4$ / H_2O. d) P3@GO (3:1), 19.3 µg, different scan number, electrolyte 0.1 M $TBAPF_6$/DCM, at v = 20 mV s^{-1}, after reduced GO in 0.1 M $LiClO_4$ / H_2O. e) P3@rGO (3:1) 39.5 µg, different electrolyte 0.1 M, at v = 20 mV s^{-1}.

Table 2.2 Stability of P3 with the CV electrolytes

Salt | Solvent	**MeCN**	**PC**	**DMC**	**EC:DCM(1:1)**
$LiClO_4$	+ve[a]	+ve[a] -ve[b]		-ve[b]
$TBAPF_6$	+ve[a] -ve[b]		+ve[a] +ve[b]	
$TBABF_4$	+ve[a]			
$TEABF_4$	-ve[b]			
LiTFSI	+ve[a]			-ve[b]

(a) means used P3@GO and (b) used P3@rGO

2.3.1.4 Polymer 4

The partial ^{1}H NMR spectrum of P4 Figure 2.7 shows that all signals are observed in downfield for arising from the (α&β)-protons of bipyridinium ion at 9.78 and 9.17 ppm (H6 and H5 respectively) with respect to the nitrogen atom, while the signal resonances for phenyl protons are observed at 8.1-7.06 ppm (H1, H2, H3, and H4).

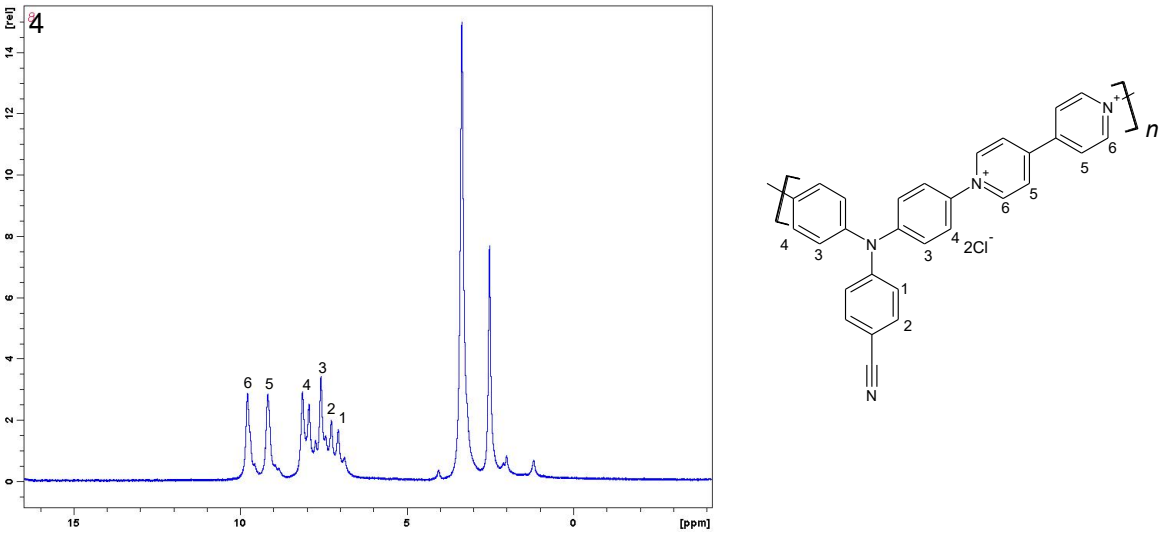

Figure 2.7 The ^{1}H NMR spectrum of P4

Figure 2.8 shows the cyclic voltammetric measurement of the electrochemical properties of P4. The mixture solution of P4@GO and P4@rGO was prepared according to procedure P2 method. As explained in Figure 2.8, part a) the viologen peak in the negative potential of P4 is reversible at oxidation and reduction, the rate of transferring of an electron is equal. Otherwise, peaks related to the nitrogen group with three phenyl groups in positive potential the down peak (reduction) is narrow and upper peak (oxidation) is broad. That means the transition of counterions in the losses of electron process in reduction is fast (higher) and in oxidation is slow (lower). Also, the oxidation peak is not stable decreasing by increasing number of the scan.

While the physical properties of nitrogen center of triphenylamine such as redox peaks are reversible and become higher capacity once composited with GO, the oxidizability of nitrogen center is not stable as when it is in an organic solvent after oxidation at positive potentials as shown in Figure 2.8, part b). The instability refers to a decrease of capacity with repeated cycling since the polymer dissolves in the electrolyte. To overcome this issue,

different ways were used such as different electrolytes, electrodes, and rGO. The electrochemical properties Figure 2.8, part c) using CPE and different salts show that the redox potential is shifted to positive at using $TBAClO_4$/MeCN electrolyte and exhibits the preferential of P4 by cation (TBA^+) compared to (Li^+). Moreover, the redox potential of both viologen and nitrogen center of triphenylamine became more stable at using rGO at CPE as shown in Figure 2.8, part d). In addition to all of that the coulombic efficiency of P4 was low. Therefore, still, we need new polymeric materials that have a high coulombic efficiency of active materials.

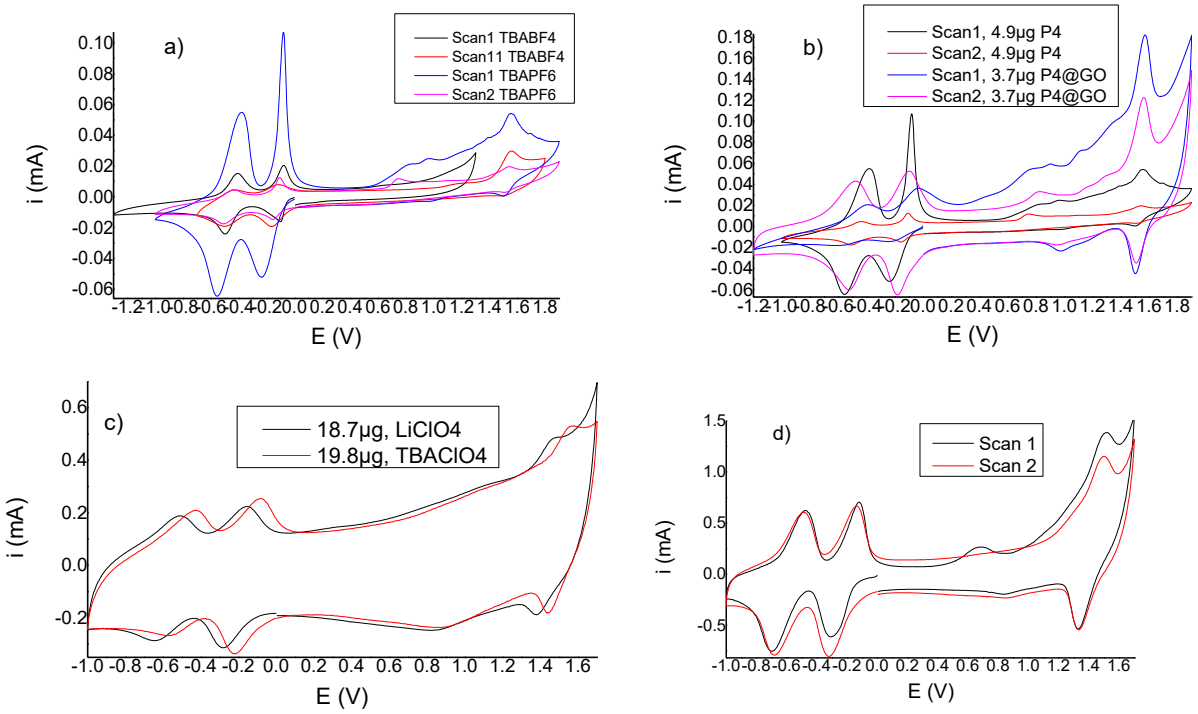

Figure 2.8 CVs measurements for P4 observed current vs. potential. a) P4, 4.9 µg on the GC electrode, electrolyte different salt/MeCN at v = 50 mV s^{-1}. b) Comparison (P4 & P4@GO 3:1)@GC, scan 1 and 2, electrolyte 0.1 M electrolyte 0.1M $TBAPF_6$/MeCN at v = 50 mV s^{-1}, after reduced GO in 0.1 M KCl/H_2O. c) P4@GO@CPE (3:1), electrolyte 0.1M different salt/MeCN at v = 20 mV s^{-1}, after reduced GO in 0.1 M KCl/H_2O. d) P4@rGO@CPE (3:1) 78 µg, electrolyte 0.1 M $LiClO_4$/MeCN at v = 20 mV s^{-1}

2.3.1.5 Polymer 5

During the synthesis, firstly, the open cycle PAA is produced and in high temperature, the cycle was closed and converts to P5. The molecular structure of PAA was detected by ^{1}H-NMR and FT-IR, while P5 was detected only by FT-IR spectra and not identified by ^{1}H-NMR as shown in Figure 2.9, part a) and b) because is insoluble in any solvent of ^{1}H-NMR and only is soluble in NMP as shown in Table 2.3. The ^{1}H-NMR of PAA resonance that the signal observed in downfield for aromatic protons at 7.50 ppm. In addition to it the signal resonances for aliphatic protons -CH_2- are observed upfield at 3.04-2.85 ppm. The FT-IR spectra was used as a comparison between P5 and PAA, the OH of the acid group was found in PAA at 2853 cm^{-1} but is removed in P5, the distinct absorption peaks at 1537 cm^{-1} confirm the existence of C=O acid group and is changed to 1708 cm^{-1} for C=O imide in P5. There are peaks at 1356 and 1387 cm^{-1} owing to aliphatic -CH_2- groups of (PAA and P5, respectively), and peaks at 809 and 725 cm^{-1} owing to the C-N stretching of (PAA and P5, respectively).

Table 2.3 The solubility of PAA and P5

	Solvent				
	H_2O	**H_2O&HCl PH=4**	**DMF**	**DMSO**	**NMP**
PAA	+	+	+		
P5	-	-+t	-+t	-	+t

-+: meaning partial soluble, t meaning at high temperature

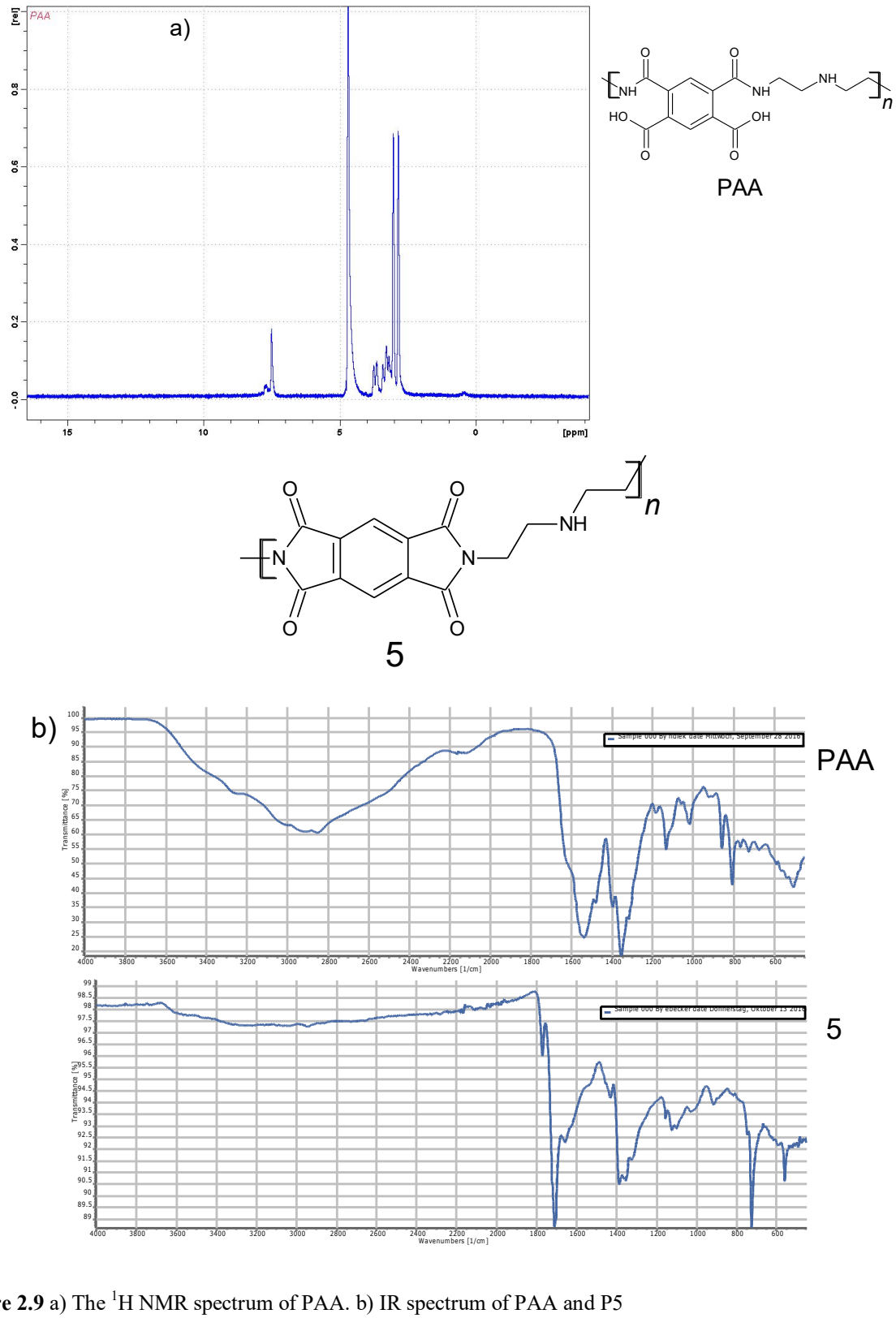

Figure 2.9 a) The ^{1}H NMR spectrum of PAA. b) IR spectrum of PAA and P5

Cyclic voltammetry was used for measuring the electrochemical properties of P5. Firstly, the poly(amic acid) (PAA) was converted to polyimide film via a thermal imidization process whereby the cycle was closed and converts to P5 on the surface of the electrode. The best temperature is 300 °C as explained in Figure 2.10, part a). This process is suitable with polymer 5 only because the solution of PAA is unstable with GO/H_2O and results in a colloid solution. Therefore, the solvent of GO was replaced from water to NMP as a procedure (2.2.4.1, c in Experimental Suction) to produce a suitable solution, but the CV measurement was not good in both aqueous and organic electrolytes as shown in Figure 2.10, part b).

Hence, the CV was measured for P5 after dissolving in NMP. Figure 2.10, part c) shows that the redox reaction is reversible but unstable and that the capacity was decreasing by increasing scan number. Figure 2.10, part d) shows the effect of cation on the electrochemical properties because P5 does not have a counter ion so changing the cation of electrolyte affected the capacity by using different cation such as Na^+ ion. In addition to this, the electrochemical properties of composite P5@GO (the GO was prepared as (2.2.4.1, c in Experimental Suction)) is shown in Figure 2.10, part e) explained that the P5@GO composite is unstable in aqueous electrolyte but is a reversible redox reaction in organic electrolyte.

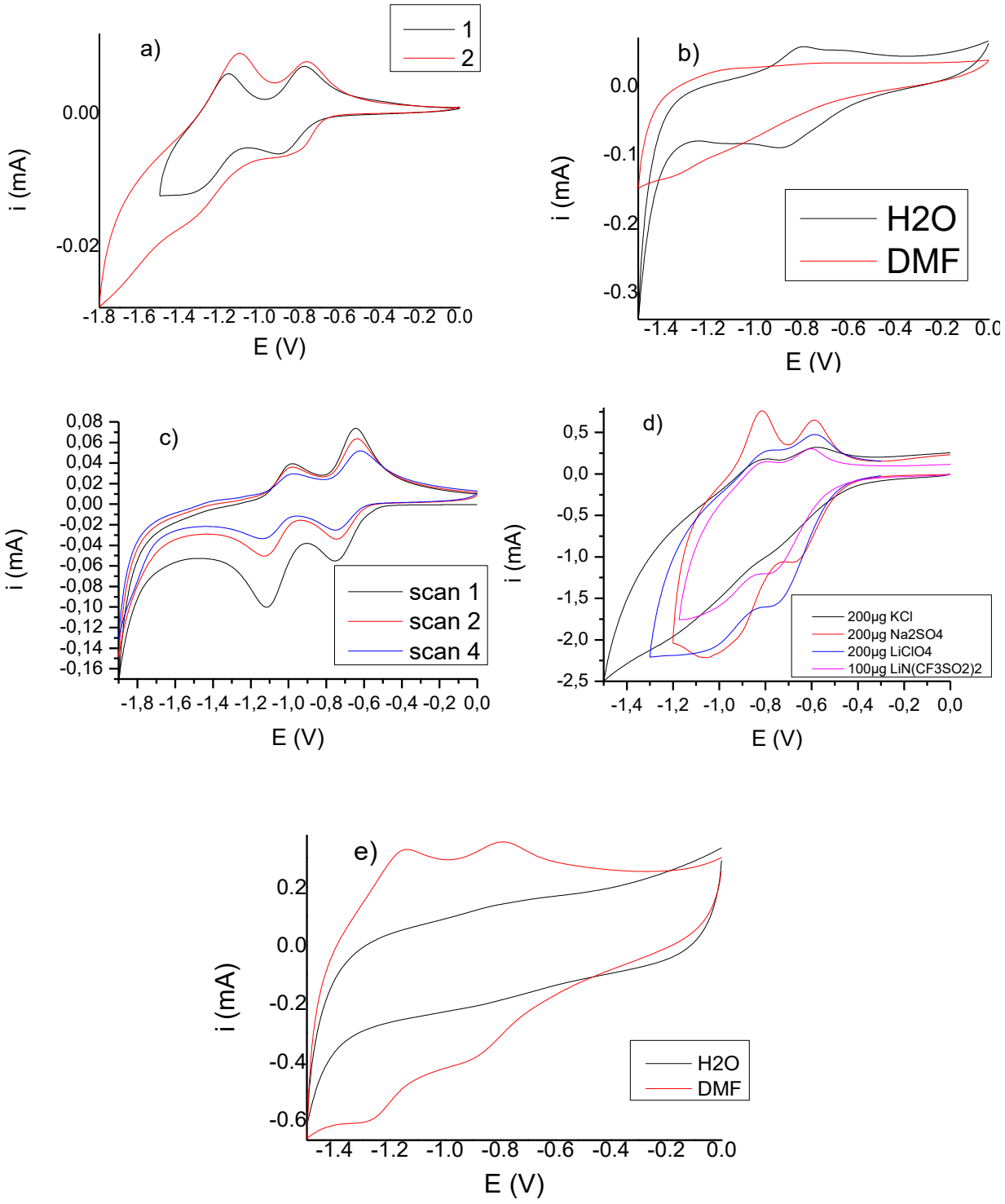

Figure 2.10 CVs measurements observed current vs. potential. a) PAA@FTO, 100 µg, electrolyte 1M $LiN(CF_3SO_2)_2$/DMF at v = 30 mV s^{-1}. (1: PAA is heating at 100 °C 1h and 200 °C 1h. 2: PAA is heating at 100 °C 1h, 200 °C 1h and 300 °C 1h.). b) PAA@GO@FTO, 70 µg at 300 °C, electrolyte 1 M $LiN(CF_3SO_2)_2$ in different solvent at v = 30 mV s^{-1}. c) P5@ITO, 5 µg, electrolyte 1 M $LiN(CF_3SO_2)_2$/DMF at v = 30 mV s^{-1}. d) P5@CPE, different concentration, 0.1 M electrolyte different salt /H_2O at v = 30 mV s^{-1}. e) P5@GO@CPE, 35 µg at 300 °C, electrolyte 1 M $LiN(CF_3SO_2)_2$ in different solvent at v = 30 mV s^{-1}

2.3.2 Organometallic LPs (P6)

The organometallic molecule (IX) was used as a monomer to synthesize an organometallic polymer. This is a known compound being synthesized according to literature as shown in the above Scheme 2.4 (page 18) and characterized by ^{1}H NMR and FT-IR spectroscopy. The partial ^{1}H NMR spectroscopic data for the P6 (F5) is shown in Figure 2.11. All signals observed in downfield for arising to the bipyridinium protons at 8.99 & 8.40 ppm, while the signal for the ferrocene protons observed at 4.79-4.54 ppm. In addition, the signal resonances for aliphatic protons $–CH_2–$ are observed at 5.74 ppm.

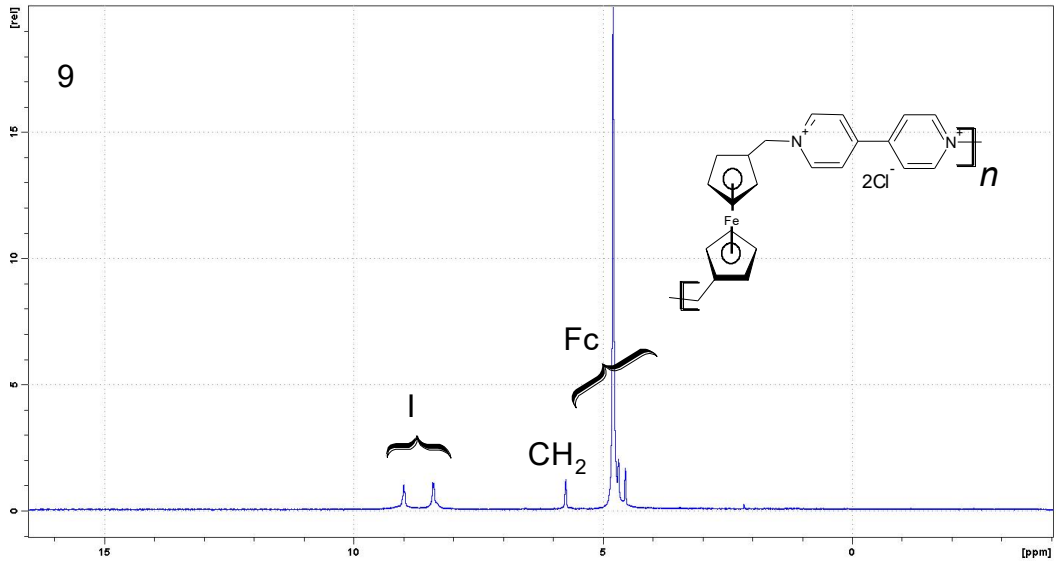

Figure 2.11 ^{1}H NMR spectrum of P6

The electrochemical properties prepared as in Chapter 2 (2.2.4.1.a, 2.2.5, and 2.2.6) in Figure 2.12, part a) explain that the P6 is stable and has two reversible peaks in negative charge for viologen and one reversible peak in positive charge for ferrocene, but the capacity of ferrocene decreases by increasing number of the scan. The film of composite P6 with GO is unstable in the organic solvent, and Figure 2.12, part b) shows that the redox reaction is reversible when composites with GO are in an aqueous electrolyte. The coulombic efficiency in water is approximately 33 %, otherwise, the film is unstable by using an organic solvent.

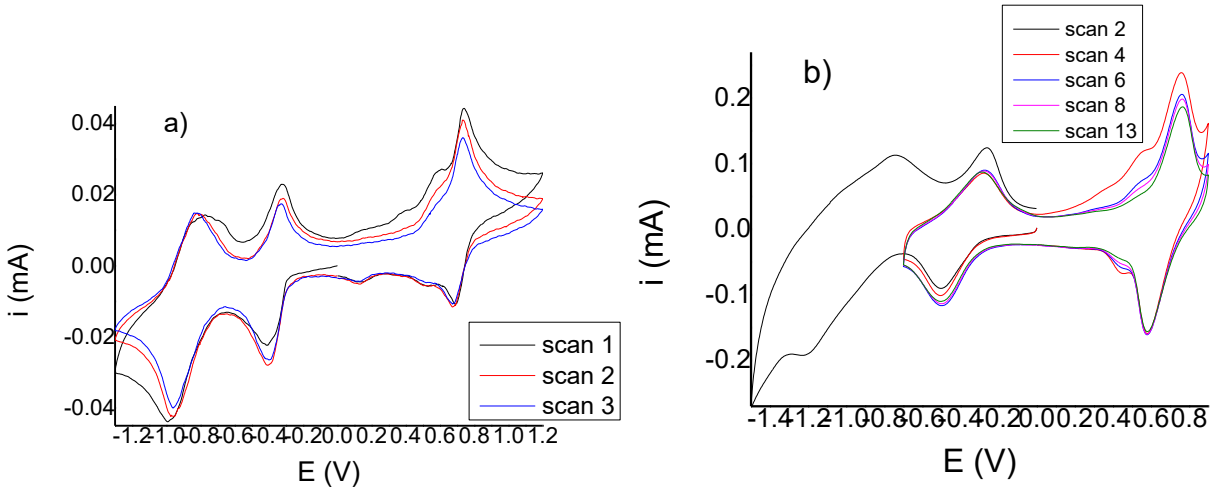

Figure 2.12 CVs measurements for P6 observed current vs. potential. a) P6@GC, 5 µg, different scan, electrolyte 0.1 M LiClO4/MeCN at v = 50 mV s-1. b) P6@GO@GC (3:1), 7.5 µg, electrolyte 0.1 M $LiClO_4/H_2O$ at v = 50 mV s-1

2.4 Summary

It is well-known that polymers have advantages in chargeable batteries such as lightweight, small size, high energy storage capacity, lower assembly costs[15, 19]. In this chapter, the electrochemical behaviour of LPs-rGO composite was studied. It was shown, that the injectable charge, as well as the kinetics in a thin film of pure polymer, were much smaller than in the composite film with rGO. Also in this type of LPs it was found that the electrochemical performance of these polymers was not optimal in terms of stability, capacity, and conductivity. This disparity arises because of the different speeds of electrons move in the redox process, which is dependent on the type of polymer or electrolyte. As demonstrated in Figure 2.1, part b), the capacity is directly proportional to the concentration of P1@GO and becomes higher current at increasing thickness film nearly to 240 µg, while the theoretical capacity is it 252 mAh g^{-1} is higher than the observed capacity of P1@rGO 216 mAh g^{-1} as shown in Figure 2.2. Due to the loss of some materials at reducing GO in water and less solvational changes during the redox process in organic solvents as compared to H_2O, the reduced GO (GO→rGO) method was used before mixing as a procedure (2.2.4.2 in Experimental Suction). The coulombic efficiency became better and get a stable electrode, this is caused to the covalent functionalization properties on graphene surface related to the transport of electrons and their connection with the type of polymer. Interestingly in this chapter, the physical properties of an amine such as redox potential are reversible,

transportability of positive charge via the radical cation species is not stable in organic solvent after oxidation nitrogen of the triphenylamine center comparison with viologen. The besides those recent advances and related literature, there is still a need for new polymeric materials to go beyond the efficiency of actual materials.

The use of supramolecular chemistry has opened a new way for the preparation of active organometallic polymers and exhibit rich redox chemistry. That is because of one-electron increase or decrease from their 18-electron stable state, which also was studied in this chapter. The reversible peak in redox reaction and increasing capacity of composites with GO in the aqueous electrolyte as shown in Figure 2.12 indicates that P6 supports already battery applications in aqueous electrolyte, but does not work in organic solvents as (MeCN and DMF). Otherwise, the ferrocene was unstable during the cycles, and it is decreasing by increasing the number of the scan.

Chapter 3
Dendrimers & Three-Dimensional (3D) / Crosslinked Polymers

Chapter 3 **Dendrimers & Three-Dimensional (3D) / Crosslinked Polymer**

3.1 Introduction

So far I have presented only LP. They showed different yields, stability with GO as battery applications. Redox polymerization electrodes were discussed in the former section, involve cleavage of the main chain and encounter low capacity retention (as a result of dissolution) and recombination efficiency (because of fragment diffusion)[21]. Lately, after synthesizing LPs the chemists started synthesizing star homopolymers[48] and dendrimers[49].

Dendrimers and network polymers / crosslinked polymers differ from linear polymers by their intrinsically three-dimensional structure and they have a lot of reactive functional groups. Dendrimers are nearly perfect mono-disperse macromolecules with a regular and highly branched architecture that resembles a tree branch. Typically, symmetric dendrimers surround the core and often adopts a spherical three-dimensional morphology that belongs to a unique class of highly branched, synthetic polymers. Increasing the number of molecules attached to the core will increase the size of the dendrimer, which is known by the term 'generation' of the dendrimer. Each generation has different properties, which is advantageous for some applications. Therefore, the tuning of their properties became a major priority of researches[49-50]. Two methods are used to synthesize dendrimers, divergent or convergent approach as shown in Figure 3.1, part a) and b). The divergent approach was used in this thesis.

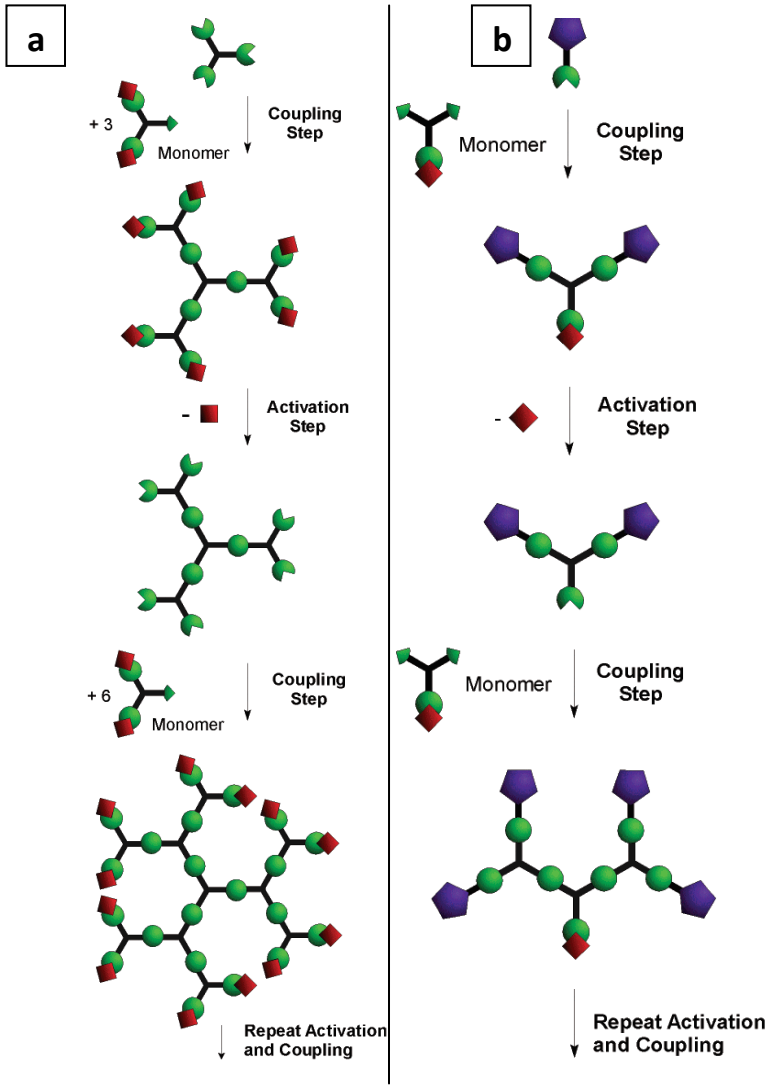

Figure 3.1 General example for a) Divergent approach. b) Convergent approach, adapted from ref[51].

The main study of dendrimers was made in biomedicine and was applied in various fields like drug delivery systems[52] and oncological applications[53]. In recent decades they have been used in different applications such as molecular recognition, electrochromic molecular batteries, solar cells and liquid crystals[54]. Many potential applications for dendrimers have been studied and reviewed in the past. P. Bhattacharya and coworkers were the first ones to use dendrimer as catalysts in lithium-oxygen (Li-O_2) batteries[55], recently, applied for lithium-ion batteries such as lithium-sulfur batteries because widely used for electronics and consumer products[56] the kind of dendrimers was used in battery application is it ionic dendrimers[57]. Also, dendrimer has been used for industrial sensors for detection of bacterial contamination in water supplies[58]. The advantages of dendrimers are commercially available and that by

synthetic control, numerous modifications can be conducted, either on the surface or within their molecular infrastructure, thus taking benefit of their unimolecular properties[59].

Dendrimers and hyper-branched polymers are inherently different from each other. Hyper-branched polymers are highly branched and three-dimensional structures. Many types of hyperbranched polymers function as novel dendritic macromolecules. Hyperbranched polymers are less structurally controlled when compared to synthetic dendrimers. This significantly limits their applications in materials science. Hyperbranched polymers attracted significant attention because of their specific structure which had unique physical properties compared with those of other polymers like intramolecular cavities[60], good solubility, multi-functionality, lower intrinsic viscosity[61], and low glass transition temperature. Therefore, used in many applications such as coatings, drug-delivery vehicles, and catalysts[62].

Since it is difficult to control their structure such as the number of branching points, branching density, its use in the field of industry is limited compared to linear polymers. However, the compounds containing triphenylamin (TPA) are excellent star molecules and possess redox activity due to the high oxidizability of nitrogen center. They are studied widely and used as various optoelectronic materials like organic light-emitting diodes, non-linear optical materials, dye-sensitized solar cells[63], sensors, organic field-effect transistors[43a], memory devices[64] and electrochromic devices [65]. The design of the 3D polymer and the suitable crosslinked structures was also used for aqueous-based redox flow batteries[66]. Over the years, new low-bandgap polymers have been synthesized and used in advanced industries such as solar spectrum, especially at the potential 1.4–1.9 V region[67]. The sulfur-rich is a kind of hyperbranched polymers that were utilized as the cathode materials in Li-S cells[60, 68] and in lithium-ion batteries as a solid-state polymer electrolyte[69]. Moreover, a novel hyperbranched poly(triphenylamine) was used for the battery performance test[70]. Many types of linear polymers have been used in battery applications. The goal of this chapter is to explore, if the dendrimers and hyperbranched polymers offer a pathway to be used in battery applications in the future. Therefore, this chapter involved the synthesis a dendrimer based on viologen with two different generations (G_1 and G_2), synthesis of a 3D polymer containing viologen with triphenylamine and synthesis of porphyrin polymer as a crosslinked polymer containing viologen. With all materials I investigated the redox response with and without GO for battery applications.

3.2 Experimental Section

As explained above (Chapter 2) the same instruments were used. In addition to it, differential scanning calorimetry (DSC) was performed using power-compensated differential scanning calorimeter Perkin Elmer 8500 equipped with Intracooler 3 cooling unit. Sample was analyzed using aluminium pans. Data was acquired using Pyris Manager software. Thermogravimetric analysis (TGA) was performed with a SDT Q600 (TA Instruments). MUA/TEG-AuNP samples (2 – 5 mg) were prepared by drying and the temperature range between 20 °C and 500 °C was scanned at a rate of 5 °C/min under a nitrogen flow of 100 ml/min. All chemicals and solvents from Sigma–Aldrich as received without further purification, except TAA (Tris(4-aminophenyl)amine), which was purchased from *Alfa Asear* (99.0 % purity) and porphyrin (5,10,15,20-Tetrakis(4-aminophenyl)porphyrin), which was purchased from Tokyo chemical industry TCI CO (> 95.0% purity). Solvents and salts for the electrochemistry were of 99.9% purity.

3.2.1 Synthesis

3.2.1.1 Synthesis of Dendrimers

The intermediates A, $P_0.3PF_6$, $P_1.6PF_6$, $P_2.18PF_6$, $G1.18PF_6$, and G_2 are known compounds that have been reported and synthesized according to Heinen[71]. $B.PF_6$ and $C.PF_6$ have been synthesized according to the literature [71-72]. In order to guarantee the quality, their spectra and elemental analysis are reported here, modified procedures are given in full detail.

3.2.1.1.1 *Synthesis of Generation One (G_1)*

Scheme 3.1 Synthesis of G_1

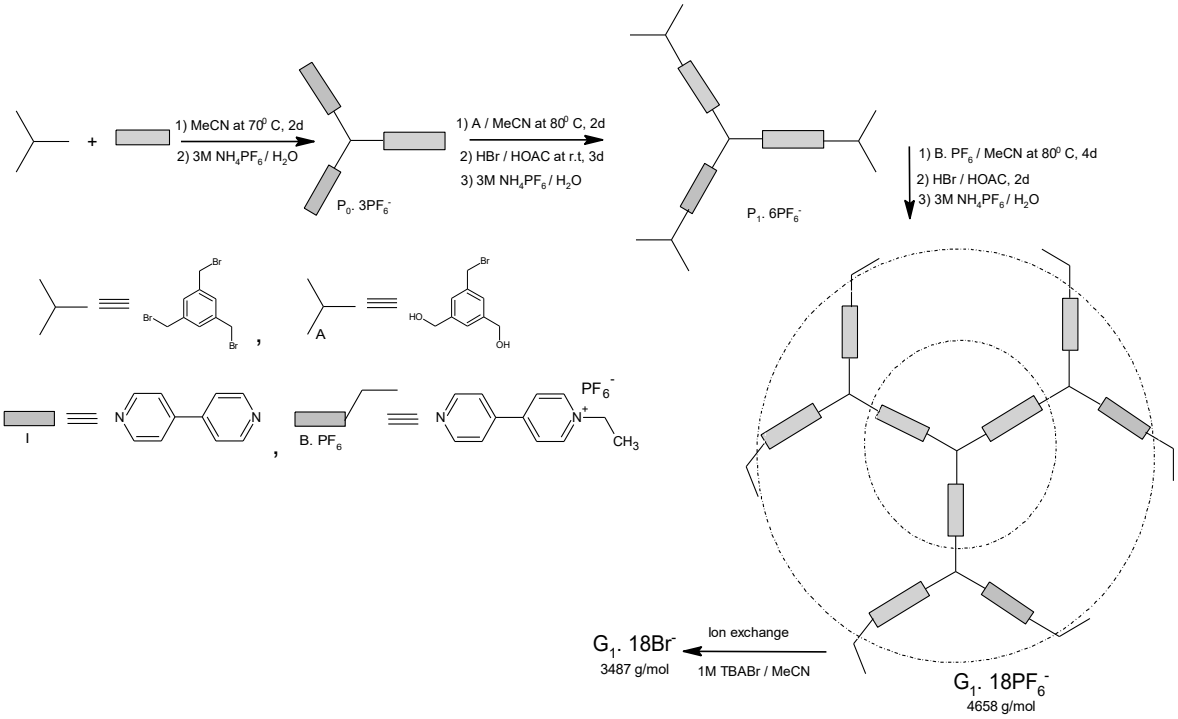

Synthesis of 1-ethyl-4-(pyridin-4-yl)pyridinium hexafluorophosphate ($B.PF_6$)

The ($B.PF_6$) was synthesized according to the literature [71-72], with minor modification. 3 mL (40 mmol) of ethyl bromide was added to a solution of I 0.5 g (3.2 mmol) in 3 mL DCM and stirred at 35 °C under reflux. After 1 h, a further portion of 1.6 mL ethyl bromide was added dropwise and continues reflux for 1 day. Evaporate of solvent gave a precipitate thoroughly washed with dry diethyl ether and toluene. Recrystallization of the product from ethanol / ether-toluene slowly precipitates (2 days at 4 °C). The resulting yellowish powder of (**B.Br**) was dried for 1 day in HV 350 mg (1.3 mmol, 41% yield). The salt was dissolved in water, and re-precipitated in 3 M NH_4PF_6 aqueous solution. The resulting white solid (**$B.PF_6$**) was filtered off, washed with cold water, and dried for 1 day in HV 325 mg (1.015 mmol, 78 %

yield). ^{1}H-NMR: (500 MHz, MeCN) δ: 8.88 (d, 2H); 8.81 (d, 2H), 8.34 (d, 2H), 7.81 (d, 2H), 4.65 (q, 2H), 1.67 (t, 3H) ppm.

Synthesis of 1,3,5-Tris((4,4′-Bipyridinium)methyl)benzene-tris-hexafluorophosphate ($P_0.3PF_6$)

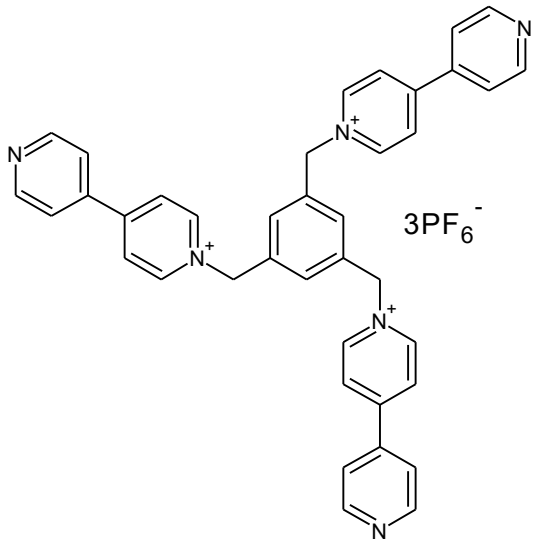

$P_0.3PF_6$ was synthesized according to the literature [71-72]. (1.347 g, 8.63 mmol) of I was dissolved in warm MeCN (8 mL), and (0.2 g, 0.56 mmol) of 1,3,5-tris(bromomethyl)benzene in 5 mL MeCN was added within 40 min (1 mL/8,5 minute). The mixture was stirred at 70 °C for 2 days under reflux. The cold mixture was filtered and washed three times with DCM. The solid was dissolved in water and extracted five times with DCM to remove excess viologen. The aqueous layer was evaporated. Re-precipitate, the solid was dissolved in MeOH and precipitated again in ether, the precipitation was dried under HV obtained yellow powder ($P_0.3Br$) 400 mg (0.484 mmol, 86.5 %).

The bromide -salt (200 mg, 0.242 mmol) was dissolved in 5 mL of water and an aqueous solution of 3 M NH_4PF_6 was added dropwise. The precipitate was filtered and washed with cold water. A white powder was dried for 1 day under HV and obtained 202 mg (0.198 mmol, 82 %) of (**$P_0.3PF_6$**). ^{1}H-NMR: (500 MHz, CD_3CN), δ: 8.89 (d, 6H); 8.79 (d, 6H); 8.36 (d, 6H); 7.80 (d, 6H); 7.57 (s, 3H); 5.77 (s, 6H) ppm.

Synthesis of ($P_1.6PF_6$)

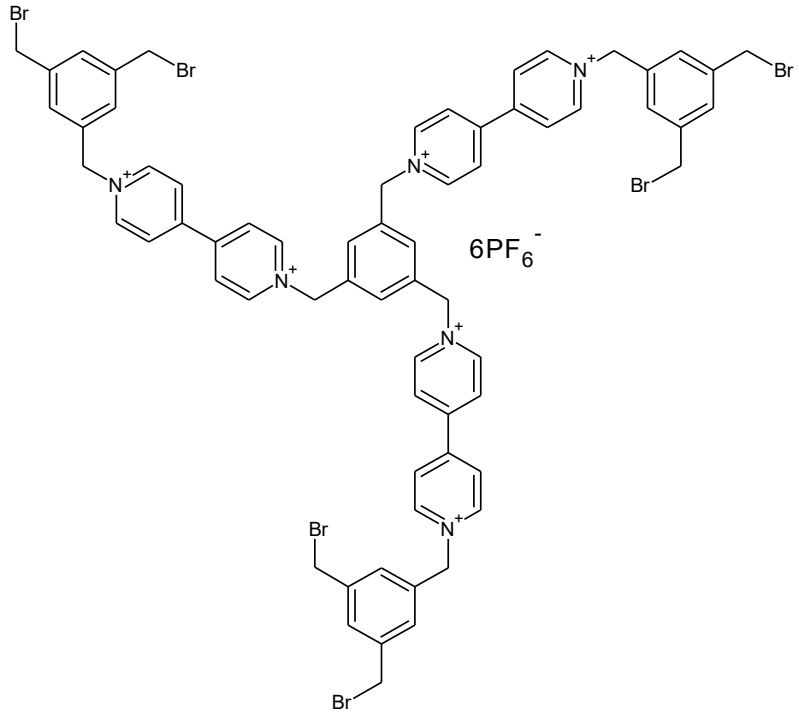

$P_1.6PF_6$ was synthesized according to Heinen[71], (175 mg, 0.757 mmol) of 3,5-bis(hydroxymethyl)benzyl bromide (A) was added to a solution of ($P_0.3PF_6$) (195 mg, 0.191 mmol) in 11 mL MeCN and reflux mixture at 80 °C for 2 days. The cold mixture was filtered, then 10 mL of ether was added to the filtrate and re-filtered. Wash all precipitate from either filtration process by ether. The solid was dried under HV. Add 52 mL HBr (5.7 M bromine in acetic acid) to the solid. The mixture was stirring at r.t for 3 days. Filtration (to remove insoluble materials) and evaporating under reduced pressure gave ($P_0.3Br.3PF_6$) as a yellow oil. An aqueous solution of 3 M NH_4PF_6 was added dropwise to it. The precipitate was filtered and washed with cold water and ether. A white powder was dried for 1 day under HV and obtained 194 mg (0.113 mmol, 59 %) of (**$P_1.6PF_6$**). ^{1}H-NMR: (500 MHz, CD_3CN), δ: 9.03 (d, 6H); 9.00 (d, 6H); 8.44 (d, 12H); 7.74 (s, 3H); 7.64 (s, 3H); 7.51 (s, 6H); 5.89 (s, 6H); 5.84 (s, 6H); 4.61 (s, 12H) ppm.

Synthesis of (G_1.18Br)

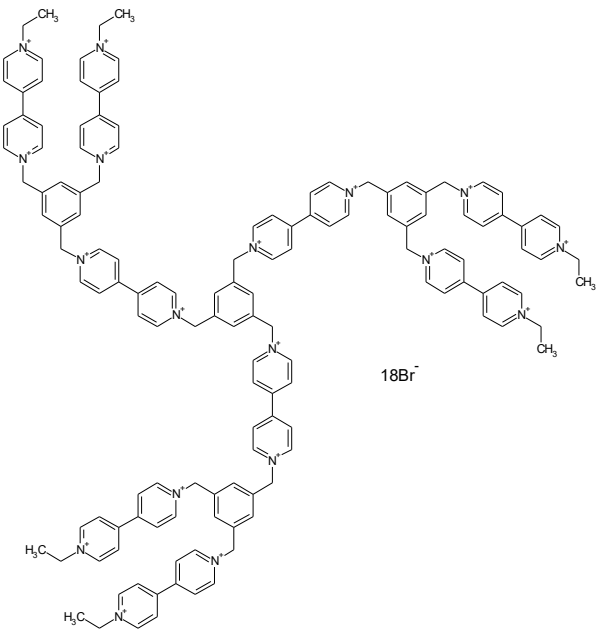

The (G_1) was synthesized according to Heinen[71], with minor modification. $P_1.6PF_6$ (50 mg, 0.0218 mmol) and $B.PF_6$ (55 mg, 0.166 mmol) were dissolved in 4.2 mL MeCN, stirred at 70 °C for 5 days. Evaporate solvent, the solid was dissolved in $MeNO_2$ and extract with 1 mL (3 M NH_4PF_6) one time and with water 2 times. Evaporate solvent of organic phase under reduced pressure, the precipitate was washed with water and dried under HV to yield ($G_1.18PF_6$) dendrimer (53 mg, 0.011 mmol, 54%). In order to remove starting material, the crude product (ca. 50 mg) was separated on a Sephadex LH-20 column (length: 30 cm * surface 9.5 cm^2, mobile phase: MeCN). The final yield after purification was light brown solid (**$G_1.18PF_6$**) (30 %) for the first four fractions. ^{1}H-NMR for (F1-F4) (500 MHz, CD_3CN) δ: 8.98 (unresolved coupling, combined integral, 36H); 8.44 (unresolved coupling, combined integral, 36H); 7.71 (unresolved coupling, combined integral, 12H); 5.87 (s, 24H); 4.72 (q, 12H); 1.68 (unresolved coupling, combined integral, 18H) ppm.

Ion exchange: the final salt of $G_1.18PF_6$ (25 mg, 0.0064 mmol) was dissolved in MeCN and treated with (1 M) TBABr / MeCN solution. The precipitated (**G_1.18Br**) was filtrated and washed with MeCN, dried under HV for 1 day. Yield 20 mg (0.0057 mmol, 26 %). ^{1}H-NMR (500 MHz, D_2O) δ: 9.17 (unresolved coupling, combined integral, 36H); 8.57 (unresolved coupling, combined integral, 36H); 7.81 (unresolved coupling, combined integral, 12H); 6.02 (s, 24H); 1.69 (unresolved coupling, combined integral, 18H) ppm.

3.2.1.1.2 *Synthesis of Generation Two (G_2)*

Scheme 3.2 Synthesis of G_2

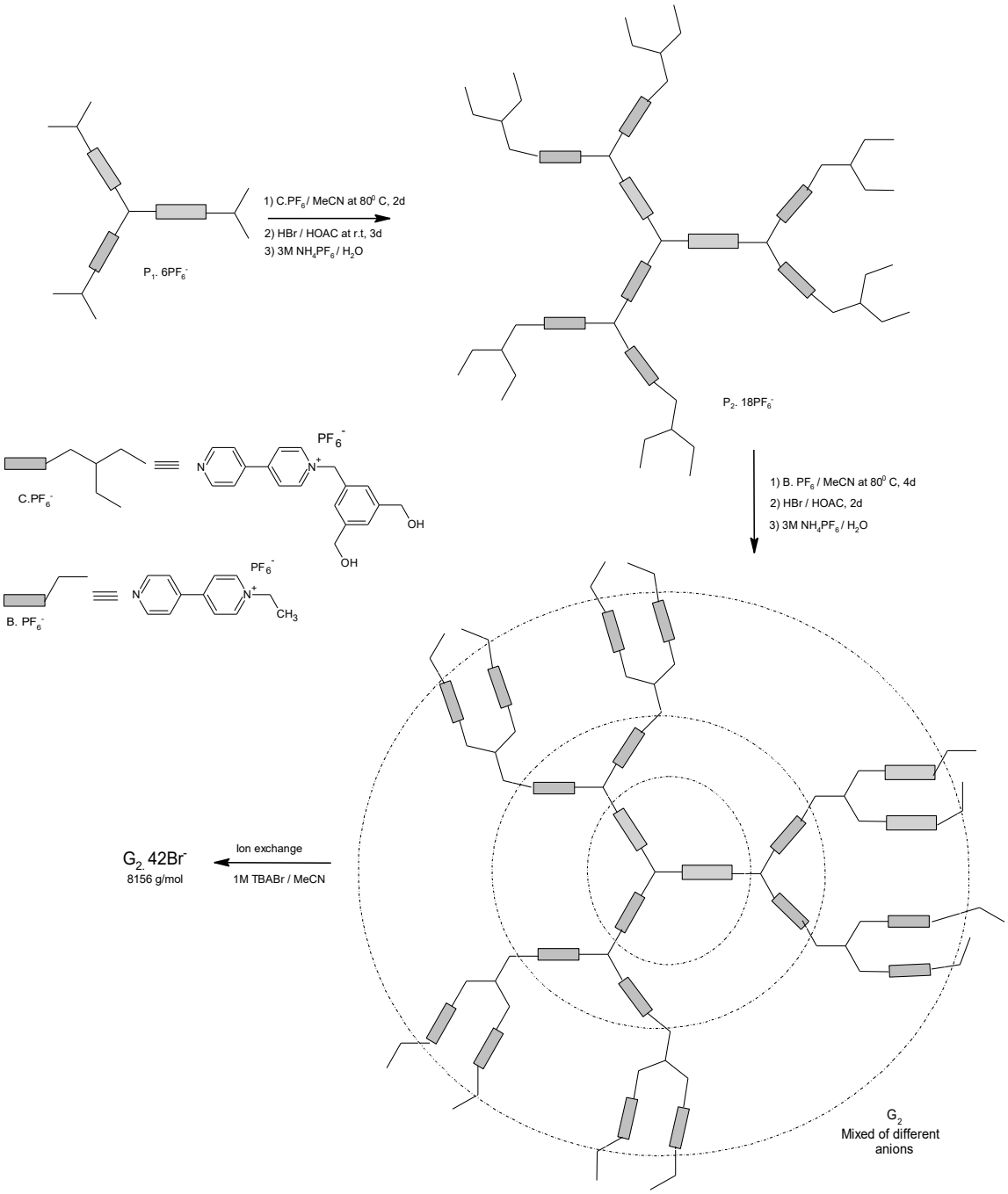

Synthesis of N-(3,5-di(hydroxymethyl)-benzyl)-4,4'-bipyridinium hexafluorophosphate ($C.PF_6$)

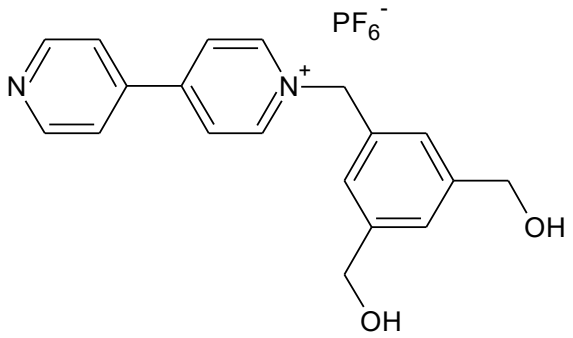

The synthesis of ($C.PF_6$) was performed according to the literature [71-72]. 246 mg (1.067 mmol) of I and 164 mg (0.711 mmol) 3,5-di (hydroxymethyl)-benzylbromide (A) were dissolved in 15 mL of anhydrous THF. The reaction mixture was then refluxed at 60 °C for 1 day under Ar gas. During that time the product precipitated as a pale yellow solid which was filtered, washed with DCM 2 times, and dried under HV to yield 250 mg (0.645 mmol, 91 %) of bromide salt (C.Br). The bromide salt (250 mg, 0.645 mmol) was dissolved in water, and 12 mL of (3 M) aq. NH_4PF_6 solution was added dropwise. Filtered, washed with cold water, and dried for 1 day under HV gave a white powder (**$C.PF_6$**) 209 mg (0.462 mmol, 71.5 %). ^{1}H-NMR (250 MHz, CD_3CN), δ: 8.89-8.85 (m, 4H); 8.35 (d, 2H); 7.81 (d, 2H); 7.43 (s, 1H); 7.38 (s, 2H); 5.77 (s, 2H); 4.65 (d, 4H), 3.31 (b, 2H) ppm.

Synthesis of (P_2.18PF_6)

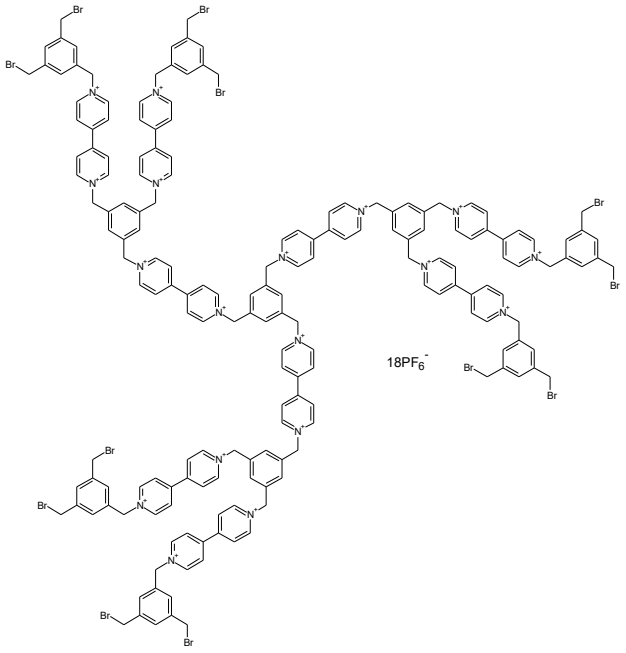

(P_2.18PF_6) was synthesized according to literatures[49, 71], with minor modification. P_1.6PF_6 (72 mg, 0.0316 mmol) and C.PF_6 (100 mg, 0.221 mmol) were dissolved in 5 mL MeCN, refluxed at 70 °C for 4 days. The solution was cooled, filtrated and ether was added to the mother filtrate and all precipitate was collected by filtration process and washed with ether. The collected precipitate was dried under HV for 1 day.

Ion exchange: the final salt (92 mg) was dissolved in water (10 mL) and treated with (3 M) aq. solution NH_4PF_6. The precipitate was filtrated and washed with water, dried under HV for 1 day.

Brominated: The salt (91 mg) was stirred with (22 mL, 5.7 M) HBr / HOAc at r.t for 3 days. After filtration, the acid was removed under reduced pressure, add 1 mL of aq. solution 3 M NH_4PF_6 to the residue, filtered, washed with excess water and dried under HV for 1 day to yield (**P_2.18PF_6**) as a pale brown powder 63.5 mg (0.01 mmol, 32.7 %); ^{1}H-NMR (250 MHz, CD_3CN) δ ppm: 9.023 (m, 36H); 8.45 (m, 36H); 7.73 (s, 12H); 7.65 (s, 6H); 7.52 (s, 12H); 5.88 (s, 36H); 4.61 (s, 24H).

Synthesis of (G_2.42Br)

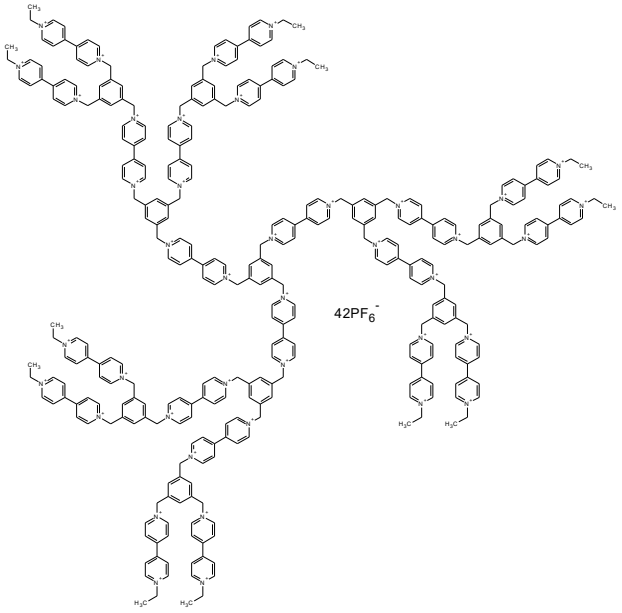

The (G_2.42Br) was synthesized according to the literature [49, 71] with minor modification. In a dry two-neck flask, add slowly solution of (P_2.18PF_6) (62 mg, 0.01 mmol) in 5 mL MeCN to the solution of (B.PF_6) (46.6 mg, 0.141 mmol) in 1.5 mL MeCN and reflux at 70 °C for 7 days. The solution was cooled and filtrated to result (bromide salt) fraction 1. The solvent was evaporated from the mother filtrate, the residue was mixed with water and separated by filtration to gave (PF_6-salt) fraction 2. Dry both fractions under HV for 1 day.

Ion exchange: Fraction 2 was dissolved in MeCN and treated with (1 M) TBABr / MeCN solution. The precipitate was filtrated, washed with MeCN and mixed with fraction 1, dried under HV for 1 day. Yield (**G_2.42Br**) 35.5 mg (0.0043 mmol, 43.5 %); ^{1}H-NMR (250 MHz, D_2O); δ ppm: 9.21-9.13 (m, 84H); 8.63-8.58 (m, 84H); 7.85 (m, 30H); 6.04 (s, 60H); 4.82 (s, 24H); 1.74 (t, 36H). ^{13}C-NMR (63 MHz, D_2O); δ ppm: 150.2, 145.8, 145.3, 140.1, 135.1, 131.8, 127.6, 127.5, 127.1, 63.6, 57.7, 15.6, 2.7. Anal. Calc. for $C_{324}H_{318}N_{42}Br_{42}$: C, 47.71; H, 3.93; N, 7.21; Br, 41.15. Found C, 26.98; H, 2.64; N, 3.93; Br, 66.44.

3.2.1.2 Synthesis of 3D Polymer and Crosslinked Polymer

Scheme 3.3 Synthesis of 3D Polymer 7 (P7)

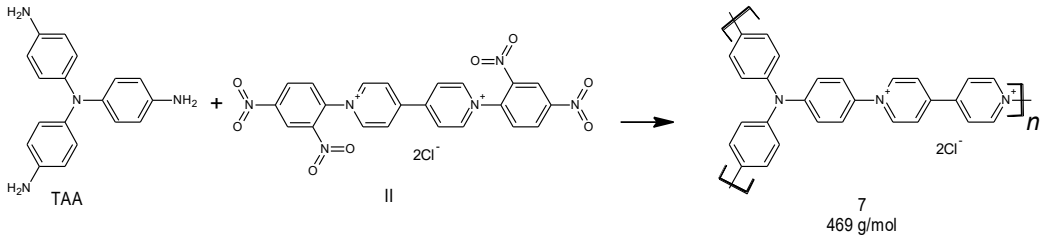

:

The polymer 7 was prepared via Zincke reactions depending on the literature[40d]. In a 100 mL three-necked round bottom flask was dissolved (100 mg, 0.344 mmol) of tris(4-aminophenyl)amine (TAA) in 30 mL of EtOH:H_2O (4:1), and (193 mg, 0.344 mmol) of II in 25 mL EtOH:H_2O (4:1) was added in one portion to the TAA solution at 100 °C for 4 h. Then continued reflux at 130 °C for 2 days and monitored by TLC (solvent: MeOH:HOAc:H_2O (10:4:1)). The solvent was removed with a rotary evaporator, the residue was washed in 100 mL acetone and reflux at 100 °C for 2 h (two times). The solid (purple-black) was refluxed with ethyl acetate 100 mL at 100 °C for 1 day to remove excess of TAA. The precipitate was separated in a centrifuge and washed with 30 mL acetone and 30 mL of diethyl ether, dried overnight under HV. The product **7** was obtained as black-violet powder 127 mg (0.27 mmol, 79 %); ^{1}H-NMR (500 MHz, MeOD); δ ppm: 9.54 (d, 4H); 8.91 (d, 4H); 7.89 (s, 4H); 7.48 (s, 4H); 7.09 (s, 4H). Anal. Calc. for $C_{28}H_{20}N_3Cl_2$: C, 71.65; H, 4.29; N, 8.95; Cl, 15.11. Found C, 55.32; H, 4.51; N, 9.64; Cl, 29.73.

Scheme 3.4 Synthesis of crosslinked polymer 8 (P8)

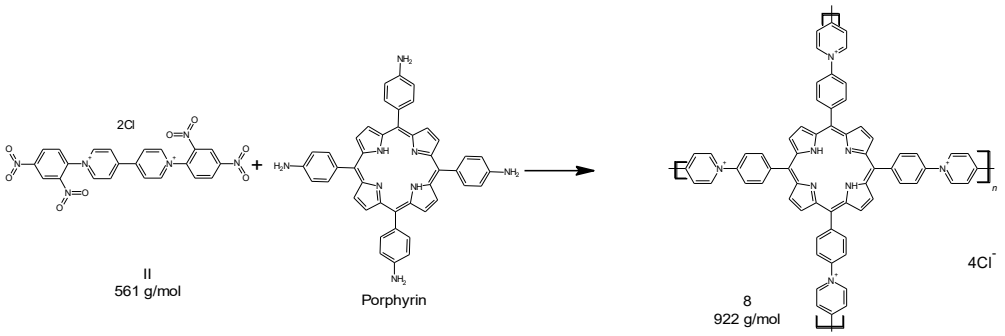

The polymer 8 was prepared via Zincke reactions according to the literature[73] as a similar procedure of synthesis P3 in Chapter 2. In one portion under Ar gas, a solution of II (685 mg, 1.22 mmol) in EtOH:H_2O (4:1) (10 mL) was added to a solution of porphyrin (50 mg, 0.0741 mmol, 2 eq. of II) in EtOH:H_2O (4:1) (15 mL). After 2 h remove Ar gas and continuous reflux at 100 °C for 1 week (TLC: 95% DCM, 4.5% MeOH, 0.5% NH_4OH). Remove solvent, and the crude precipitate was washed several times with acetone, filtered and the crude precipitate was washed with EtOAc and ether, re-precipitate three times by dissolving salt in EtOH and precipitate in solvent THF & Ether (1:1). The product was dried under HV at 50 °C for 1 day to obtain 8. Without more purification, a dark brown solid of **8** was obtained 53.5 mg (0.058 mmol, 78 %). ^{1}H-NMR (250 MHz, MeOD); δ ppm: 10.06-8.97 (d, 32H); 8.92-8.45 (m, 24H).

3.2.2 Electrochemical Measurements

As received in Chapter 2 (2.2.4, 2.2.5, and 2.2.6) the same procedure was used for the preparation of the electrochemical solution, electrodes, and electrolytes.

3.3 Result and Discussion

The dendrimers were synthesized and their redox properties investigated. All organic compounds were synthesized and used as an intermediate material to generation dendrimers is knowing compound and prepared according to literature as shown in above Scheme 3.1, Scheme 3.2 and characterized by ^{1}H NMR spectroscopy.

The starting material of 3D / crosslinked polymers, II was synthesized as explained in Chapter 2, Scheme 2.2 to form P7 (Scheme 3.3) and P8 (Scheme 3.4), respectively.

3.3.1 Dendrimers

3.3.1.1 Generation One (G_1)

The solution of G_1 & G_1@GO as a procedure (2.2.4.1, a) and the electrodes were prepared using a drop-casting method as explained in chapter 2 (2.2.5). The dendrimers with and without GO were drop-casted on the GC electrode and then the film redox properties were investigated by CV with different solvents as electrolytes. Figure 3.2, parts a) and b) show the CVs measured in MeCN and water, respectively, and show sharper peaks in water-electrolyte. In Figure 3.2, part c), electrodes measured with water show higher capacity, because G_1 is more stable in water compared with MeCN, and the coulomb efficiency in water became higher than in acetonitrile solvent. Then the electrochemical properties were measured by adding GO to enhance the conductivity. Figure 3.2, part d) is a comparison of G_1 and G_1@GO and show higher capacity with GO and better conductivity. The efficiency with and without GO is around 46 and 14 %, respectively. To investigate the performance for different mass loadings of G_1@GO composite Figure 3.2, part e) shows increasing the mass loading increases the capacity, but only up to 7.5 µg.

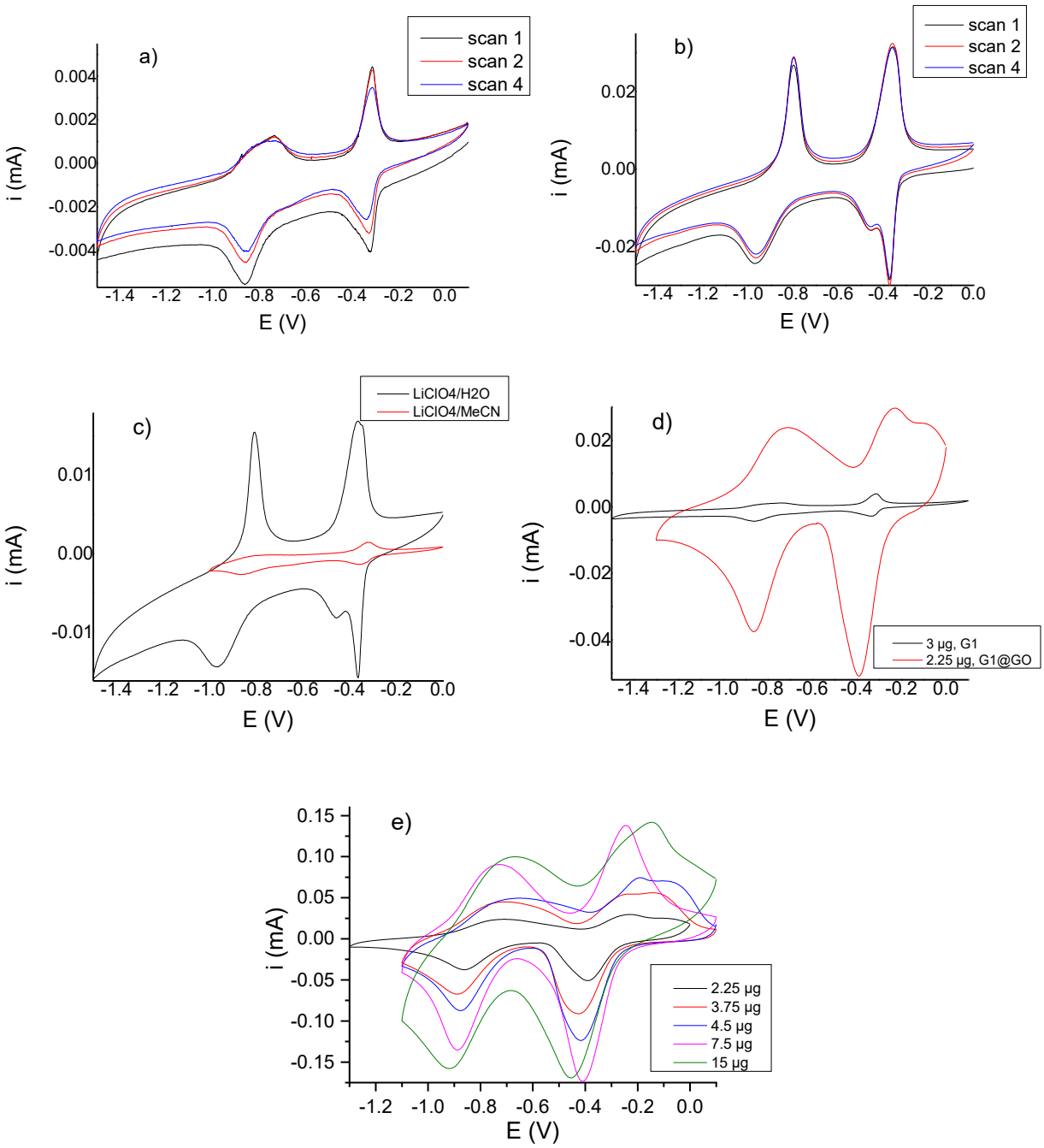

Figure 3.2 CVs measurements observed current vs. potential. a) G_1@GC 3 µg, different scan number, electrolyte 0.1 M $LiClO_4$/MeCN at v = 50 mV s^{-1}. b) G_1@GC 3 µg, different scan number, electrolyte 0.1 M $LiClO_4/H_2O$ at v = 50 mV s^{-1}. c) G_1@GC 3 µg, electrolyte 0.1 M $LiClO_4$ in different solvents at v = 30 mV s^{-1}. d) (G_1 & G_1@GO)@GC (3:1) different concentration, electrolyte 0.1 M $LiClO_4$/MeCN at v = 50 mV s^{-1}, after reduced GO (GO→rGO) in 0.1 M $LiClO_4/H_2O$. e) G_1@GO@GC (3:1) different concentration, electrolyte 0.1 M $LiClO_4$/MeCN at v = 50 mV s^{-1}, after reduced GO (GO→rGO) in 0.1 M $LiClO_4/H_2O$

3.3.1.2 Generation Two (G_2)

At the next step, another generation was added to the dendrimer as described in the literature[71] to explore the effect of the size of generation on the electrochemical properties. The electrode film was prepared as explained above in G_1. The CV was measured of pure G_2 Figure 3.3, part a) and shows nice peaks of viologen and G_2 stable in water. Then, also added GO and compared it with pure G_2. Figure 3.3, part b) show a lot more capacity with GO in water-electrolyte (instable in organic solvent). The efficiency with and without GO is around 71 and 18 %, respectively. Then the comparing performance of different mass loadings in Figure 3.3, part c) shows better performance than G_1. More mass loading is possible, which is due to the large size of molecules of G_2. Figure 3.3, part d) is a comparison between G_1@GO and G_2@GO. A potential shift of the G_2 wave to more positive values as compared to G_1 is observed and efficiency is becoming higher for G_2@GO in comparison with G_1@GO (71 and 68, respectively, in water-electrolyte). Otherwise, G_1@GO is more stable in organic electrolytes.

Finally, the peak currents of both generations were directly proportional to the concentration of a thickness film of nearly 7.5 µg for G_1@GO. While the G_2@GO shows a higher current and is more stable in water to a thickness film nearly to 30 µg, this increase of current indicates the limitation arising from the kinetics of charge transfer.

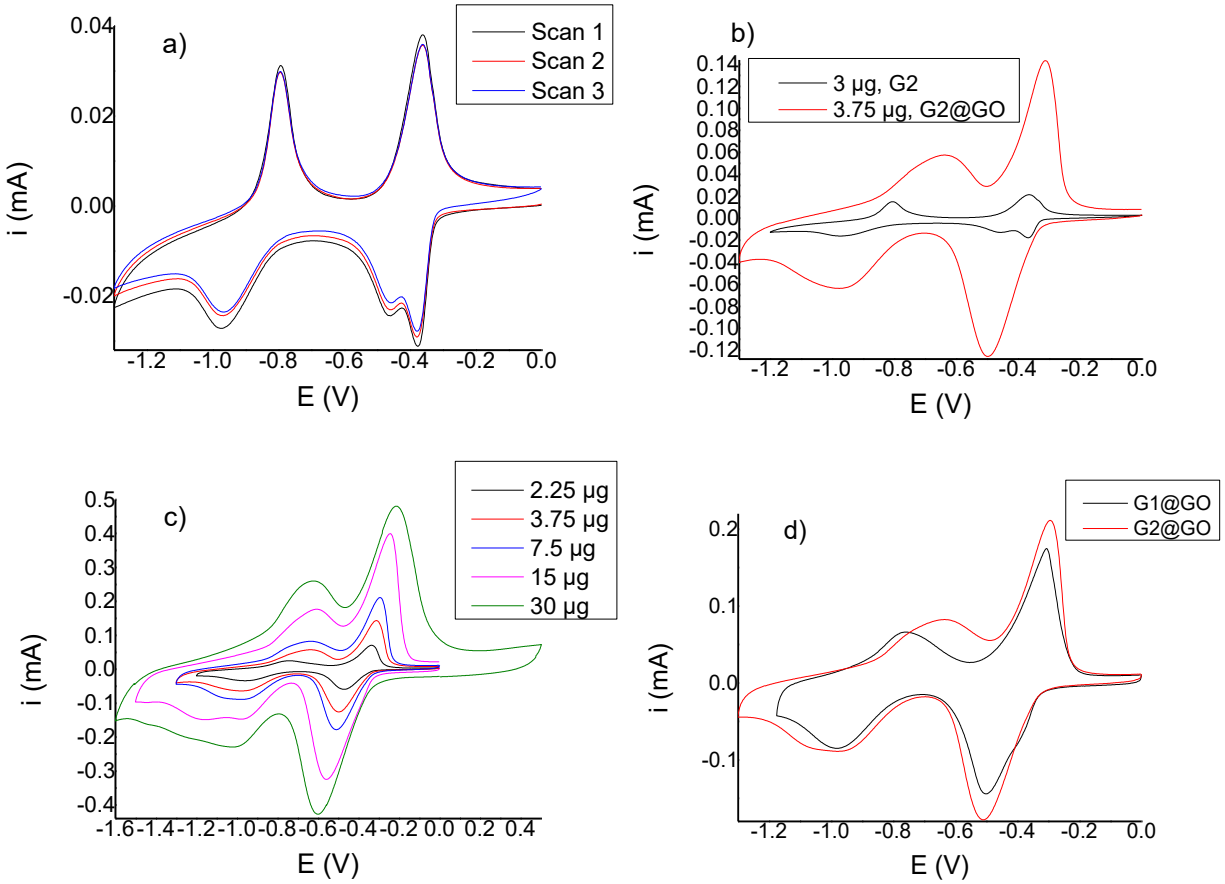

Figure 3.3 CVs measurements observed current vs. potential. a) G_2@GC 3 µg, different scan number, electrolyte 0.1 M $LiClO_4/H_2O$ at v = 50 mV s^{-1}. b) (G_2 & G_2@GO)@GC (3:1) different concentration, electrolyte 0.1 M $LiClO_4/H_2O$ at v = 30 mV s^{-1}. c) G_2@GO@GC (3:1) different concentration, electrolyte 0.1 M $LiClO_4/H_2O$ at v = 30 mV s^{-1}. d) (G_1 & G_2)@GO@GC (3:1) 7.5 µg, electrolyte 0.1 M $LiClO_4/H_2O$ at v = 30 mV s^{-1}

3.3.2 3D / Crosslinked Polymers

3.3.2.1 3D Polymer (P7)

The partial ^1H NMR spectroscopic data of P7 is shown in Figure 3.4. All signals observed in the downfield are assigned to the bipyridinium protons at 9.54 & 8.91 ppm, while the signal for the phenylene protons was observed at 7.89-7.09 ppm. These changes in chemical shifts are characteristic of the subunit of P7 inclusion three phenyl groups.

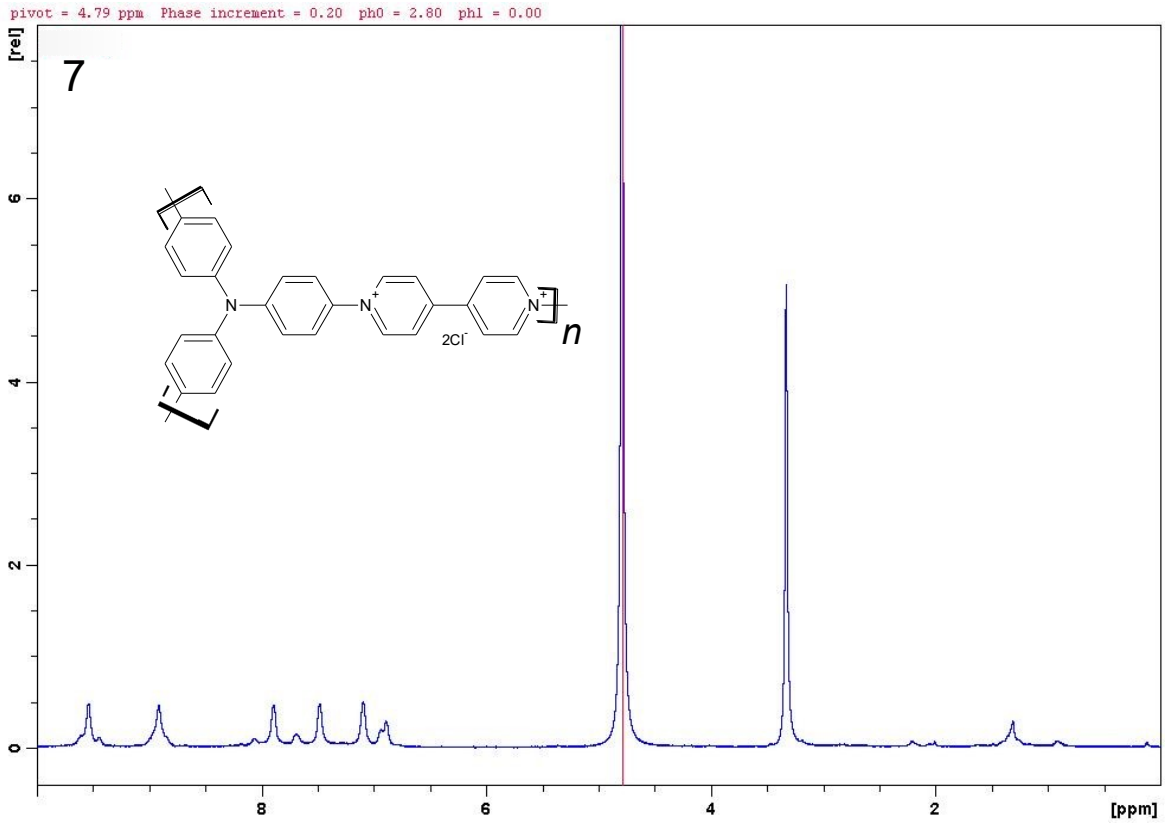

Figure 3.4 ^{1}H NMR spectrum of P7

The electrochemical properties of P7 were measured by cyclic voltammetry. The solution of P7 was prepared by dissolving a polymer in MeOH:H_2O (1:1), and P7@GO solution was prepared by mixing the polymer with GO as a ratio (3:1). The electrodes were prepared using a drop-casting method as explained in Chapter 2 (2.2.5). The P7 with and without GO were drop-casted on the GC electrode and then the film investigated the redox properties by CV with different electrolytes. In the beginning, CV was measured of pure P7 in MeCN and Figure 3.5, part a) show nice reversible viologen peaks, but peak related to the nitrogen of triphenylamine in positive charges were unstable. The transition of counterions in the losses of an electron is not stable as explain in P3 and P4. Then comparing polymer with GO in Figure 3.5, part b) shows that the viologen peaks in negative potential are reversible at oxidation and reduction. When P7 is composite with GO it also shows capacity at positive potentials but is still not stable and the coulombic efficiency has become 44 %.

To find the stability of nitrogen present in the triphenylamine center, specific electrolytes, as shown in Table 3.1, were utilized. However, as demonstrated in Figure 3.5, part c), the nitrogen center remains unstable in each electrolyte system as the viologen peaks are

constantly shifting. Figure 3.5, part d) shows a comparison of DCM and DCM/$MeNO_2$ solvents, and based on the graph, the non-polar solvent is as stable as DCM and DCM:$MeNO_2$ (1:1). DCM/$MeNO_2$ shows slightly more reversible behaviour than triphenylamine. Figure 3.5, part e) comparison of DCM and water show higher capacity in water but cannot go to positive potentials. Based on these results the polymer is needless for battery applications, but this approach demonstrates a novel molecular design principle for utilizing poly(triphenylamine-viologen) based polymers in battery applications.

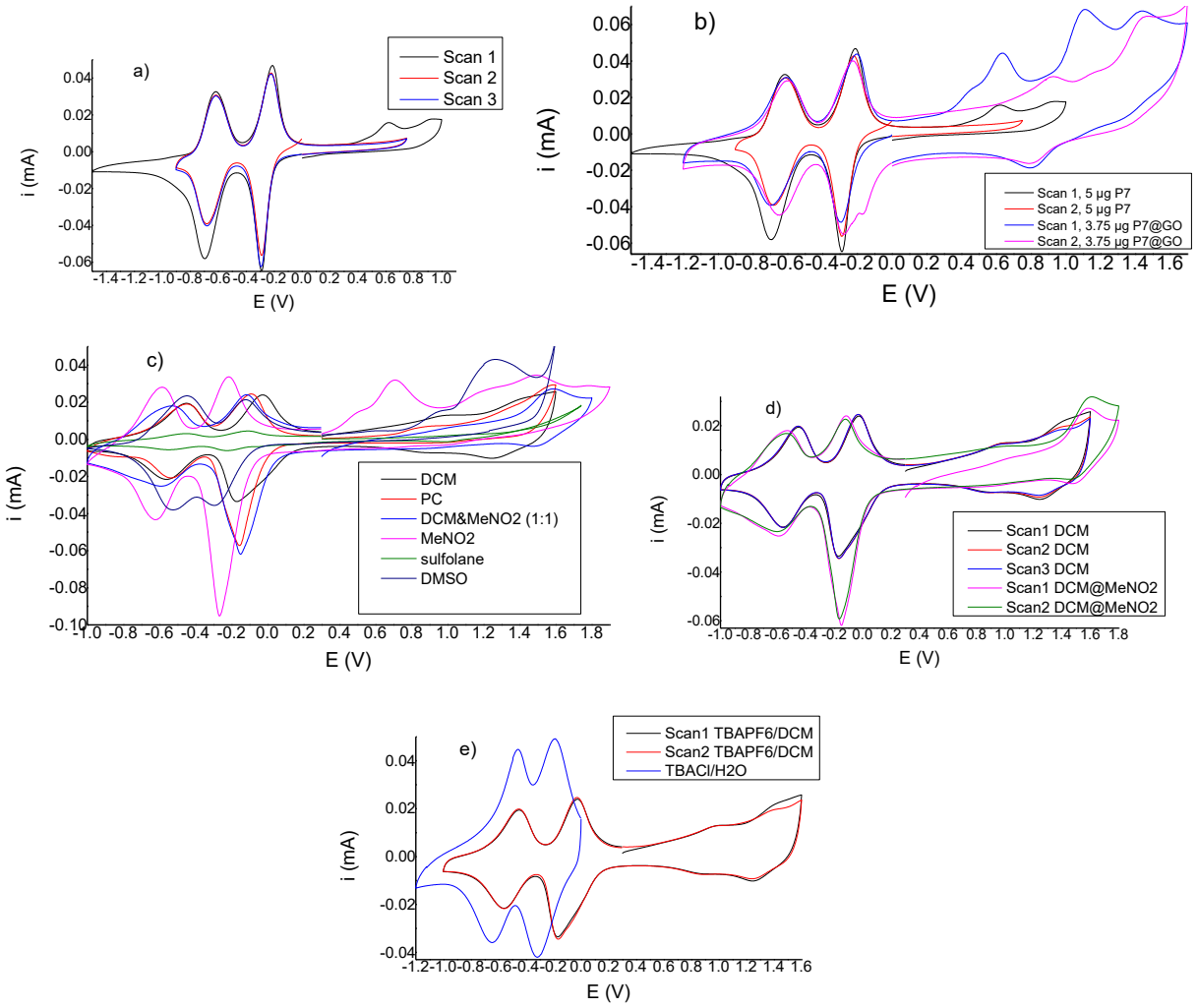

Figure 3.5 CVs measurements observed current vs. potential using GC electrode. a) P7, 5 µg, different scan number, electrolyte 0.2 M $LiClO_4$/MeCN at v = 20 mV s^{-1}. b) P7 and P7@GO (3:1) at different concentration, electrolyte 0.2 M $LiClO_4$/MeCN at v = 20 mV s^{-1}, after reduced GO (GO→rGO) in 0.1 M $LiClO_4/H_2O$. c) P7@GO (3:1), 7.5 µg, scan number one, electrolyte 0.1 M $TBAPF_6$ in different solvents at v = 20 mV s^{-1} after reduced GO (GO→rGO) in 0.1 M $LiClO_4/H_2O$. d) The stability of P7@GO (3:1), 7.5 µg, electrolyte 0.1 M $TBAPF_6$ in different solvents at v = 20 mV s^{-1}, after reduced GO (GO→rGO) in 0.1 M $LiClO_4/H_2O$. e) The stability in aqueous and organic electrolyte P7@GO (3:1), 7.5 µg, different electrolyte 0.1 M at v = 20 mV s^{-1}, after reduced GO (GO→rGO) in 0.1 M $LiClO_4/H_2O$

Table 3.1: Stability of P7 with the CV electrolytes

Salt | *Solvent*	H_2O	MeCN	DMC	DMC:$MeNO_2$ (1:1)	$MeNO_2$	PC	Sulfolane	DMSO
$LiClO_4$	+	-				-		
KCl	+-							
$TBAPF_6$			+-	+-	-	-	-	-
TBACl	+-							

(+-) means partial stable

3.3.2.2 Crosslinked Polymer (P8)

The partial ^{1}H NMR spectrum of P8 is shown in Figure 3.6 and all signals are observed in the downfield for arising from the (α&β)-protons of bipyridinium ion at 10.06-8.97 ppm with respect to the nitrogen atom, while the signal resonances for phenyl and pyridine protons are observed at 8.92-8.45 ppm.

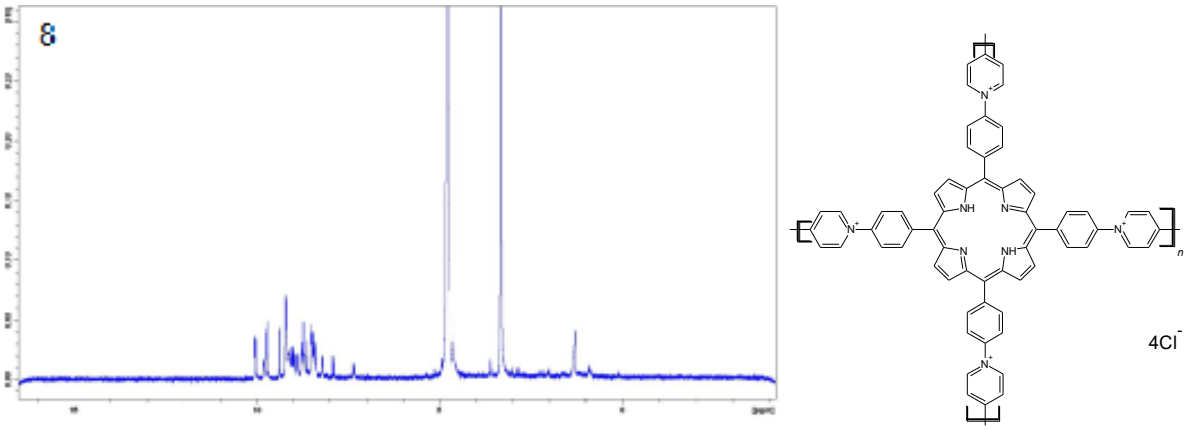

Figure 3.6 The ^{1}H NMR spectrum of P8

The electrochemical properties of P8 were measured by the cyclic voltammetric method, the solution of P8@GO and P8@rGO was prepared as procedure P2 in Chapter 2. As explained in Figure 3.7, part a) using CPE the viologen peak in the negative potential of P8 is reversible at oxidation and reduction. Otherwise, peaks related to the nitrogen of porphyrin in positive potential are unstable in both $LiClO_4$ and LiTFSI salts. With $TBAPF_6$ the redox potential is shifted to positive and nitrogen peaks of porphyrin are reversible because they exhibit lower capacity reflecting the preferential capacity of P7 by counter anions, ClO_4^- or $TFSI^-$, compared

to the higher capacity of PF_6^-. Nonetheless, the overall capacity is lower than the capacity of viologen. Searching for the stability of nitrogen peaks of porphyrin different ways were used like different electrolytes, electrodes, and rGO. In Figure 3.7, part b), the electrochemical properties using the GC electrode show that the redox potential of the viologen peak is reversible and stable in a few scans, but still nitrogen peak of porphyrin is unstable. Moreover, the redox potential of both viologen and nitrogen of porphyrin became less stable at using rGO at CPE in the different electrolytes as shown in Figure 3.7, part c). In addition to all of that the coulombic efficiency of P8 was low. Therefore, still, we need new polymeric materials that have a high coulombic efficiency of active materials.

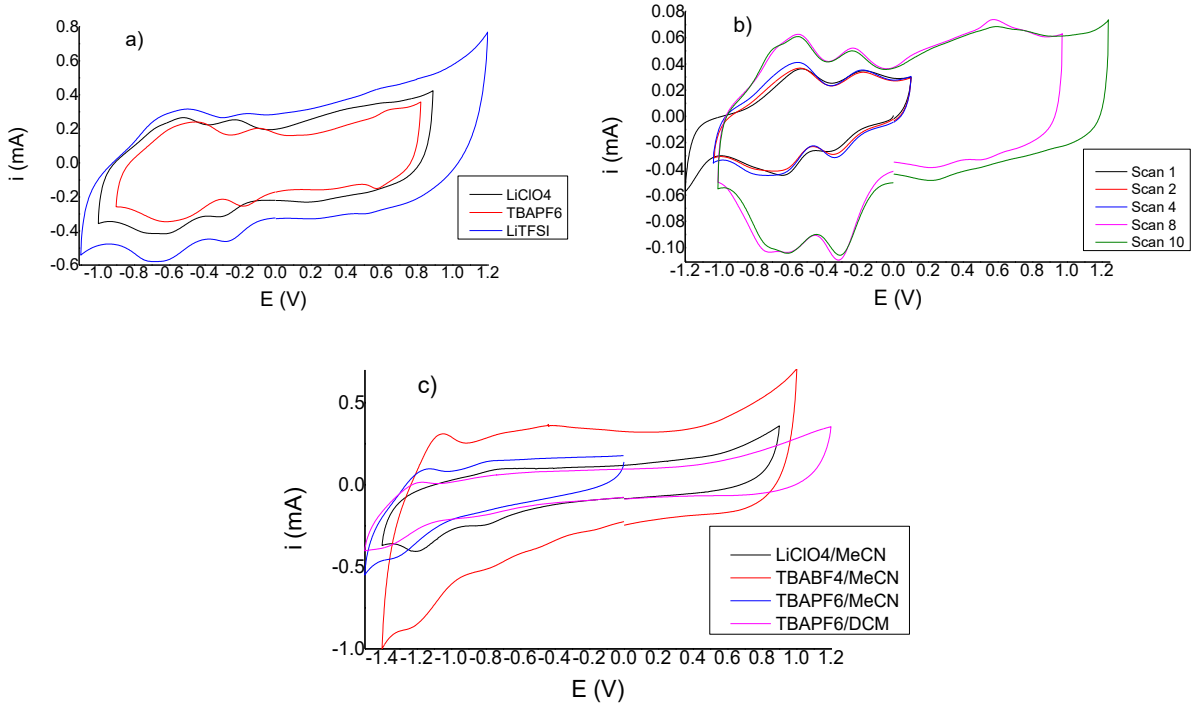

Figure 3.7 CVs measurements for P8 observed current vs. potential. a) P8@GO@CPE (3:1), 18.75 µg, electrolyte different salt (0.1M)/MeCN at v = 50 mV s^{-1}, after reduced GO in 0.1 M $LiClO_4/H_2O$. b) P8@GO@GC (3:1), 7.5 µg, electrolyte 0.1 M $LiClO_4$/MeCN at v = 50 mV s^{-1}, after reduced GO in 0.1 M $LiClO_4/H_2O$. c) P8@rGO@CPE (3:1) 18.75 µg, different electrolyte at v = 50 mV s^{-1}

The anodic charge storing properties of the polymers are investigated Table 3.2, It should be noted that the pyridinium or imide have a lone pair electron. Also these polymers contains different stiffness and conjugations. Reduction potential is shifted to negative value accordingly substitute of functional groups namely imide, pyridinium of homopolymer, dendrimers and copolymer.

Thermal stability of the polymers were investigated through TGA and DSC and P1 shows excellent stability upto 340 °C. Also polymer P7 and P8 stable upto 500 °C (see in Figure 3.8 a). Unfortanately, DSC is unable to perform P7 and P8 due to limitation of the maximum temperature of the instrument. Thus, we have carried out DSC with P1, and found heat capacity (ΔCp) 0.50 J/g °C, and glass transition temperature (Tg) 196.7 °C (Figure 3.8, b).

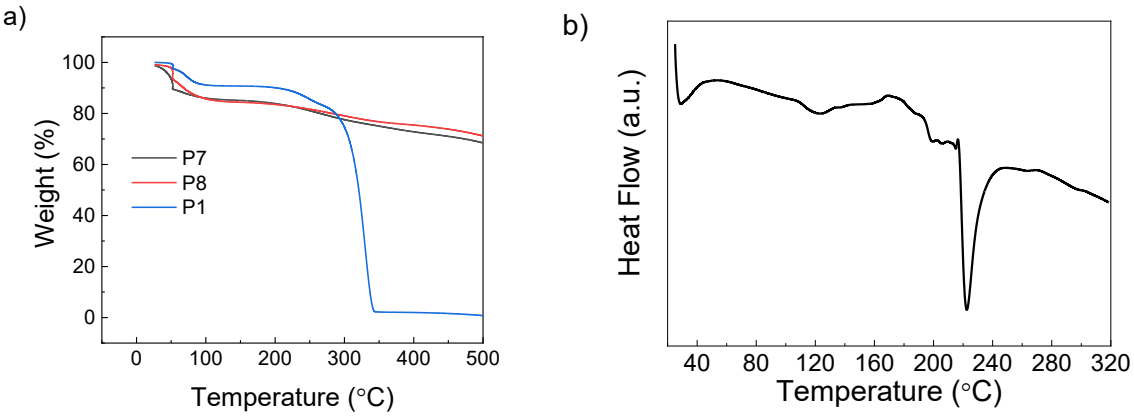

Figure 3.8 a) Thermogravimetric analysis (TGA) of different polymer. b) Differential scanning calorimetry (DSC) of P1.

Table 3.2 Properties of polymers and reduction potentials

P No. & Dendrimers	Purity (%)	Solubility (mg/mL)	E_1^0, E_2^0 (V)
1	92	20 / H_2O	-0.48, -0.95
2	78	15.2 / H_2O:MeOH (4:1)	-0.31, -0.68
3	91.6	8 / H_2O:MeOH (4:1)	-0.30, -0.61
4	78.2	3 / H_2O:MeOH (4:1)	-0.25, -0.60
5	-[a]	0.5 / NMP	-0.70, -1.11
6	85.5	30 / H_2O	-0.38, -0.94
7	91.8	5 / H_2O:MeOH (1:1)	-0.24, -0.62
8	70	1.8 / H_2O:MeOH (4:1)	-0.29, -0.68
G_1	89	17 / H_2O	-0.31, -0.81
G_2	84	14 / H_2O	-0.4, -0.85

[a] Not soluble in common NMR solvents.

3.4 Summary

This chapter involves the synthesis of a dendrimer containing viologen units, the ongoing research in our lab has shown better redox properties in aqueous electrolyte compared to MeCN. The performance of the dendrimers is enhanced when combine with GO, but its coloumbic efficiency remains below 100%, Figure 3.2, part d). Dendrimers with GO produce a thick film with high coloumbic efficiency, Figure 3.2, part e). Adding another generation to the dendrimer resulted in better performance when the mass loading of the electrodes has increased the efficiency of G_2 compared to G_1 and the potential of G_2 shifted to more positive compared to G_1 as explained in Figure 3.3, part d). It was noted during the results and discussion that the dendrimer generations affect electrochemical properties. For instance, G_2 showed higher coulombic efficieny than the G_1. On the other hand, G_2 showed inferior stability, as dissolves in the electrolyte. Therefore, more investigations have to be performed in order to find dendrimers with suitable electrochemical performance.

A synthetic 3D polymer containing viologen and triphenylamine units was prepared. This polymer displays separate peaks for viologen. The redox response of the triphenylamine unit only shows one irreversible oxidation peak. Two large viologen peaks are observed in the negative potential range with a cathodic electrocatalytic contribution. The nitrogen of the triphenylamine center peak of 3D polymer with GO is smaller than the viologen peak, due to the instability of nitrogen present in the triphenylamine center in the electrolyte. Coulombic efficiency increased when composited with GO (44 %). Then the chapter has involved the synthesis of P8 as a crosslinked polymer containing viologen and porphyrin, but also found that the nitrogen peak of porphyrin is not stable as in P7. Use of method reduced GO (rGO) (Procedure 2.2.4.2 in Experimental Section) as it has been applied to some of the polymers in Chapter 2 due to the instability of the P8 in the aqueous electrolyte when reduced by the CV method, did not succeed. As a result deterioration of the covalent functionalization properties on the graphene surface is related to the transport of electrons in the P8. The oxidation/reduction of nitrogen present in the triphenylamine center could be slightly improved with non-polar solvents as electrolytes, these however are not suitable for battery applications. Table 3.2 moderately anodic charge storing components (two electrons per pyridinium or imide, Chapter 2 and Chapter 3) show all two consecutive one-electron reductions shifting negative with the type of substitution in the sequence: imide, and pyridinium of homopolymers, dendrimers, and copolymers.

Chapter 4
Dip-Coating Process

Chapter 4 **Dip-Coating Process**

4.1 Introduction

In the previous chapters, the electrodes were prepared by drop-casting a solution containing the redox-active materials and the conductive additive. This chapter considers the preparation of multilayer thin films and coatings. The layer-by-layer (LbL) assembly method has attracted much interest because they allow the surface structure and thickness of a film to be precisely controlled. The alternate dipping forms polyion complexes on the surface to create ultrathin polymeric films.

The LbL assembly method is used for a lot of materials and the researchers used the successful LbL assembly fabrication for synthetic linear polymers[74], block copolymers[75], dendritic molecules, organic components, and polyelectrolytes, and complexes of these species to help to bring in some functional groups[76]. There are many different techniques Figure 4.1 used to prepare operating LbL assemblies such as dipping LbL assembly, spin-assisted LbL assembly, spray-assisted LbL assembly, and others[77].

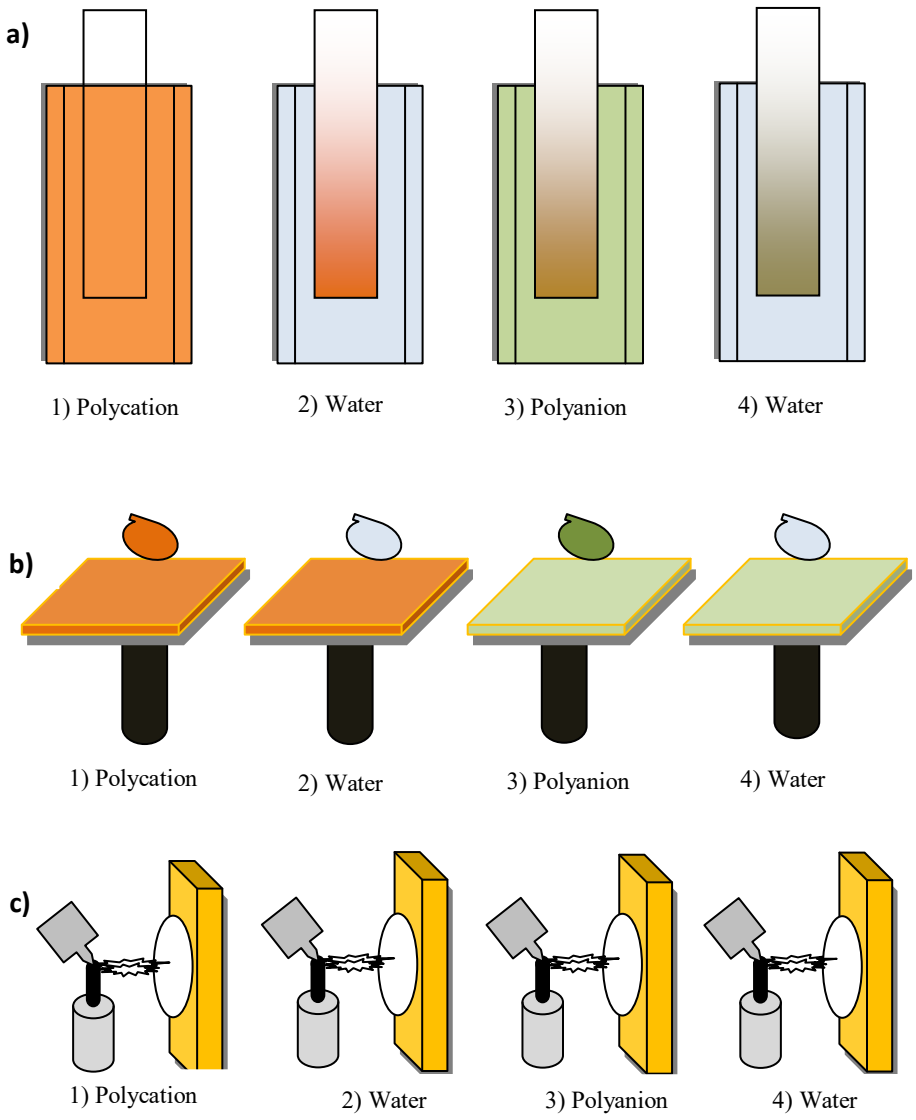

Figure 4.1 General scheme of the processes used to fabricate multilayer films by LbL assembly. (a) Dip coating: CPE and beakers are used in this method. Steps 1) and 3) represent the exposure of a polycation and GO or polycation@GO and polyanion (PSS) respectively, and steps 2) and 4) are rinsing steps, the four procedures would be repeated many times. (b) Spin-assisted LbL assembly. (c) Spray-assisted LbL assembly

LbL assembly is an easy, eco-friendly method to control the physical properties of the obtained film, but also there is some downside. The swelling behaviour of the film during work can ruin the mechanical properties of the material and the fabrication time is too long for many industrial applications[78]. nonetheless, versatile functionality of LbL assembly was shown, such as anti-reflective and superhydrophobic coatings, dye release, and drug delivery systems. Lately, the LbL technique has been proven by the researcher's field and has had great concern over the last two decades[79]. In this chapter, the film was produced by the dipping method through the LbL assembly method. A linear polyviologen (redox-active material) was used as

cationic species (P9 Figure 4.2) and as anionic species, GO was used. With this system, electrodes were prepared and the electrochemical performance were tested. Then, polymer/GO complex as cationic species and Poly(sodium p-styerenesulfonate) (PSS) as anionic species are additionally utilized as the original material and the electrochemical properties was studied of the films. Besides electrochemical characterization the layer growth was followed using quartz crystal microbalance (QCM).

Characterizations of LbL films are typically done by optical polarizing microscopy, scanning electron microscopy (SEM)[80], atomic force microscopy (AFM), or ellipsometry, and the mechanical properties are often measured by techniques like QCM[81]. The QCM technique is used as an experimental method for measuring mass adsorption by the conversion of frequency to mass. The mass changes due to film deposition and composite on the gold surface of oscillating quartz crystal cause a change in the resonance frequency as explained by the Sauerbrey equation:

$\Delta f = - C_f * \Delta m$ eq. 4.1

$\Delta f = - f^2/K * \Delta m$ eq. 4.2 $K = A\sqrt{Pq\ \mu q}\ /2$ put K in eq. 4.2

$\Delta f = - 2f^2/ A\sqrt{Pq\ \mu q} * \Delta m$ eq. 4.3

where Δf is the change of the frequency in Hz, C_f is the calibration constant (the calibration constant for a 5 MHz At-cut quartz crystal in the air is 56.6 Hz μg^{-1} cm^2, C_f for electrode 8 MHz = 56.6 $(1.6)^2$ = 144 Hz $\mu g^{-1} cm^2$ (8/5 = 1.6)), and Δm is the mass change (g cm^{-2}), f is a resonant frequency of the fundamental mode (Hz), A is piezoelectrically active crystal area (Area between electrodes, cm^2), Pq is the density of quartz (Pq = 2.648 g cm^{-3}), and μq is the shear modulus of quartz for AT-cut crystal (μq = 2.947 * 10^{11} g cm^{-1} s^{-2}.[82]

4.2 Experimental Section

4.2.1 Instrument

The electrochemical properties were studied using cyclic voltammetry (CV) analyses (as explained in chapter 2). The QCM experiments were conducted in a three-electrode cell from ALS Co., Ltd, Japan (QCM Flow cell kit) under potential scanning conditions using gold plated 8 MHz AT-cut crystal (KVG Quartz Crystal Technology, GmbH). The potential was controlled by a potentiostat (Gamry, Interface 1000) and a frequency analyzer (Gamry, QCM 10M).

4.2.2 Chemicals

All the chemicals and solvents for the electrochemistry (99.9 % purity) were from Sigma–Aldrich and used as received without further purification, unless otherwise stated. Graphene oxide (GO) was from "Graphenea" and delivered as an aqueous solution (4 mg GO in 1 mL H_2O).

4.2.3 Synthesis

The P9 was synthesized according to the described method[40d], the structure of P9 and poly(sodium p-styerenesulfonate) (PSS) were shown in Figure 4.2 below.

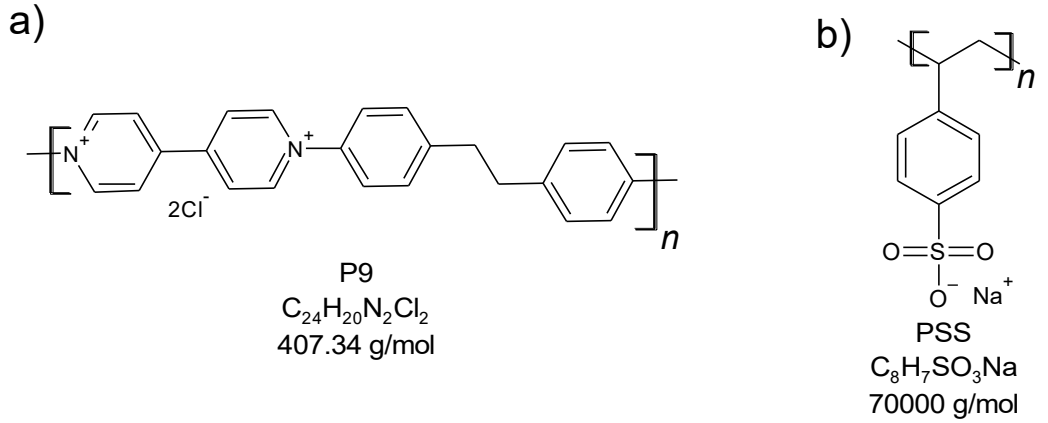

Figure 4.2 The structure of polymers. a) Polycation (P9) and b) polyanion poly(sodium p-styerenesulfonate) (PSS)

4.2.4 Dipping Solution Preparations

4.2.4.1 Dipping Solution of P9, GO and P9/GO

a) As explained above (2.2.4.1, a), 40 mg P9 (0.098 mmol) were dissolved in a mixture of 1.5 mL MeOH and 1.5 mL deionized water (DIW). A solution of GO (3.33 mL of the commercial GO solution (4 mg GO/mL H_2O) was diluted with 3.7 mL DIW).

b) The above two solutions were mixed and stirred for 30 min to yield a P9@GO solution with a P9:GO weight ratio of ca. 3:1 consisting of colloidal particles with a net positive charge.

4.2.4.2 Dipping Solution of PSS

40 mg (0.19 mmol) PSS poly(sodium p-styerenesulfonate) (ACROS Organic; average M.W= 70000 g/mol) was dissolved in 10 mL DIW and directly used as PSS dipping solution.

4.2.5 LbL Formation Procedure

The films were prepared on a carbon plate electrode (CPE) with one side isolated using adhesive tape, thus exhibiting an open side surface of 0.9 cm^2. Using a homemade dip coater, the electrode was sequentially dipped in the coating and cleaning solutions according to the scheme below.

Modification version a:

1) P9
2) DIW washing step
3) GO
4) DIW washing step

Modification version b:

1) P9@GO (positive surface charge).
2) DIW washing step.
3) PSS (negative surface charge).
4) DIW washing step.

One cycle is comprised of dipping into solutions 1 – 4 of one of the above-mentioned methods (version a or b). The electrode was vertically exposed into the solutions for 1 min each. Electrodes with different numbers of cycles were prepared.

4.2.6 Carbon Plate Electrode (CPE) Preparations

The CPE films were prepared according to three methods with one side isolated using adhesive tape, thus exhibiting an open side surface of 1.05 cm^2:

1) 100 µL of diluted GO (1 mg / 1 mL H_2O) was drop-casted on the electrode and reduced in an aqueous electrolyte / electrocatalyst solution of 0.5 M LiCl / 4 mM 1,1′-diethyl-4,4′-bipyridinium dichloride (MV^{2+}). After reduction, the electrode was washed in distilled water to remove all MV^{2+} and dried at 50 °C for 15 min.
2) 100 µL of diluted GO (1 mg / 1 mL H_2O) was drop-casted on the electrode and used without reducing.
3) The clear electrode was used without GO.

Using a homemade dip coater, the dip-coating sequence was then performed according to the 4 step method as explained above (4.2.5, b).

4.2.7 Modification of the Gold Plated Quartz Crystal Microbalance (QCM) Measurements

The gold-plated 8 MHz quartz was exposed shortly to a piranha solution, rinsed with water and ethanol, and further treated with plasma under HV (Used plasma to remove O_2 on the surface of gold electrode). The electrode was then submerged in a solution of (1 mM) 3-mercaptopropan sulfonate for 24 h. The dip-coating sequence was then performed according to the 4 step method as explained above (4.2.5, b).

4.3 Result and Discussion

The LbL method was used to prepare electrodes with polyviologen as cationic species and GO as anionic species. The CV properties were measured of an electrode prepared according to LbL procedure (Modification Version a). Figure 4.3, part a) shows the GO reduction in first cycles and viologen peaks, which are not nicely separated. Then, performance was compared in different dip-coating cycles. Figure 4.3, part b) shows more cycles increase capacity but after 15 cycles capacity does not increase anymore. This increase of current indicates the limitation arising from the kinetics of charge transfer.

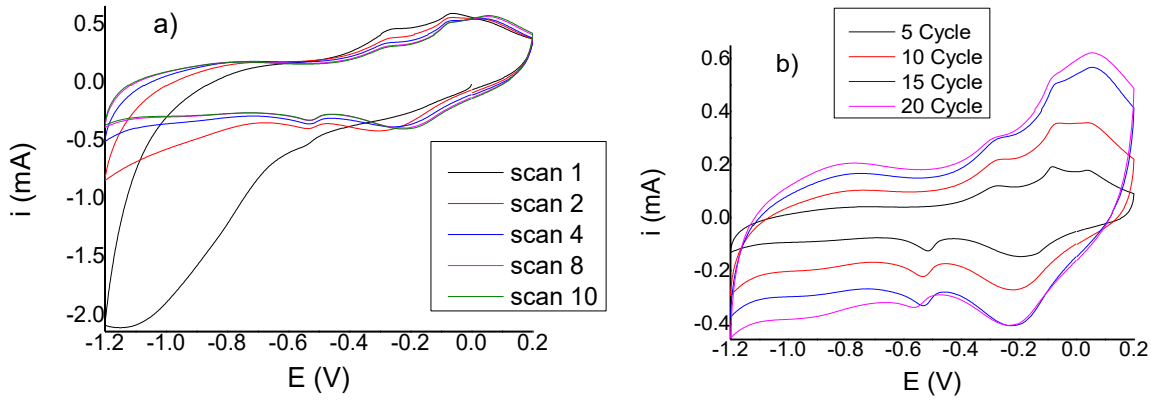

Figure 4.3 CV measurements of the LbL modified electrode (CPE) at a scan rate of 20 mV/s and increasing modification numbers using LbL Modification Version a. The electrolyte 1 M KCl/H_2O, the surface of electrode 0.9 cm^2. a) different scan at 15 cycles. b) different cycles at scan number 10

The CV properties were measured using a P9@GO complex as cationic species and PSS as negative species because is a strong polyelectrolyte[83]. The thickness of P9:PSS thin films was experimentally optimized to maximize the enhancement of carrier mobility via a layer-by-layer process because is it electrically conductive[84]. With a modified electrode prepared by LbL procedure (Modification Version b), CV was measured. Figure 4.4, part a) show that with only a few scans the peaks are well separated and the GO is reduced (GO→rGO) in scans 2 – 4. Then again compare performance different dipping cycles. Figure 4.4, part b) show with increasing dip-coating cycles the peaks are not well separated anymore after 100 cycles. However, the capacity of electrodes increases even further after 100 dip-coating cycles. Figure 4.4, part c), displays the dependence of capacity on the scan rate for the different numbers of dip coating cycles. With increased layer thickness, lower scan rates yield higher capacities. This behaviour can be assigned to either limited electron transfer or ion movement. Due to the increase in layer thickness the ion pathways are longer which decreases the capacity with increasing scan rate.

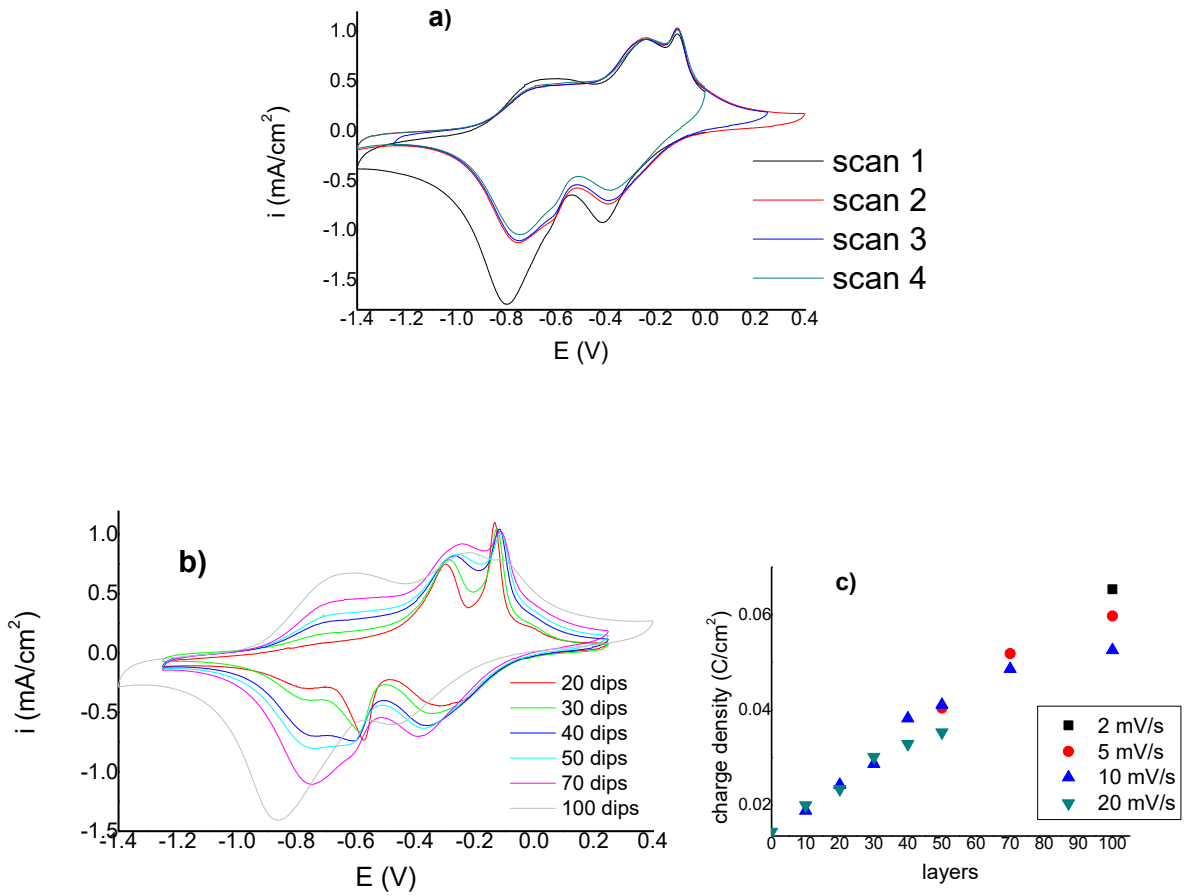

Figure 4.4 CV measurements using LbL Modification Version b, the electrolyte (1 M) KCl/H_2O, using CPE method 3 as explained above (4.3.6). a) (deferent scan number) at 70 cycles, scan rate 10 mV/s. b) CV measurements (4th scan) of the LbL modified electrode at a scan rate of 10 mV/s and increasing modification numbers. c) Observed charge density vs. layers at different scan rates, the surface of electrode 0.9 cm^2

The P9/GO and PSS were used in the LbL method. In this system, PSS acts as a counter ion for the polyviologen. Normally, when P9 is electrochemically reduced, the counter ion leaves the electrode layer because the charge of polyviologen has been compensated by the electron. With PSS, it is different because PSS cannot leave the electrode layer. Instead, a cation will enter the electrode layer to compensate for the charge of PSS when P9 is reduced. To investigate the influence of different cations in the electrolyte, the electrodes were prepared with 100 dip-coating cycles and CV measurements were performed with different cations while keeping the same anion (Br^-). Figure 4.5, part a) shows that a large cation (TBA^+) shows lower capacity compared to small cations (Li^+, K^+). Figure 4.5, part b) shows the lower capacity is ever more evident at a high scan rate. This is a sign that the performance of electrodes is dominated by cation movement.

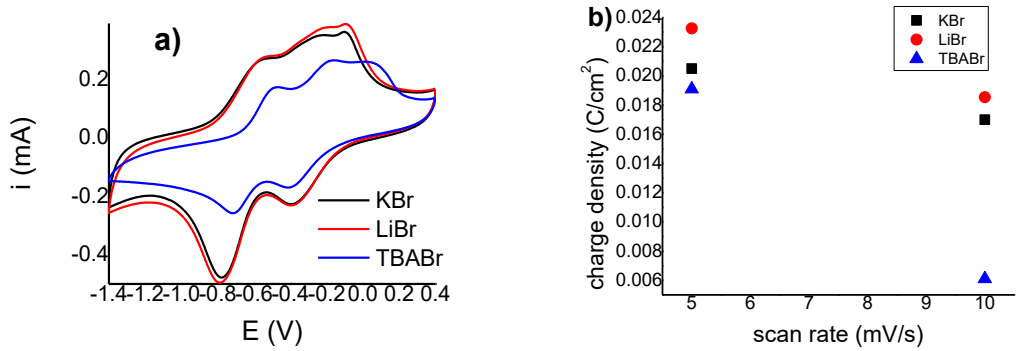

Figure 4.5 The P9 Characterisation using LbL Modification Version b, the influence of electrolytes with constant anion and varying cations (0.5 M / H_2O) at 100 cycles using CPE method 3 as explained above (4.3.6). a) CV measurements (4^{th} scan), scan rate 10 mV/s. b) Observed charge density vs. scan rate in different cation, the surface of electrode 0.9 cm^2

To investigate the influence of pre-modification of the CPE substrate on the film development, a comparison of capacity was performed between blank CPE, CPE modified with GO, and CPE modified with GO followed by reduction to rGO as prepared according to the method (4.2.6, 1,2 and 3). Figure 4.6, part a) mainly shows that the peak shapes are independent of CPE modification but the capacity is different. The plot of capacity vs scan rate in Figure 4.6, part b) for different CPE modifications shows that the modification with GO without reduction yields the highest capacity. In case of GO, it introduces negative charge on CPE surface, which improves the first layer of P9. Principally, Figure 4.6 shows that the capacity is affected by the interaction of electrode surface and also demonstrates the influence of the structure of the film, which affects the thickness of the films.

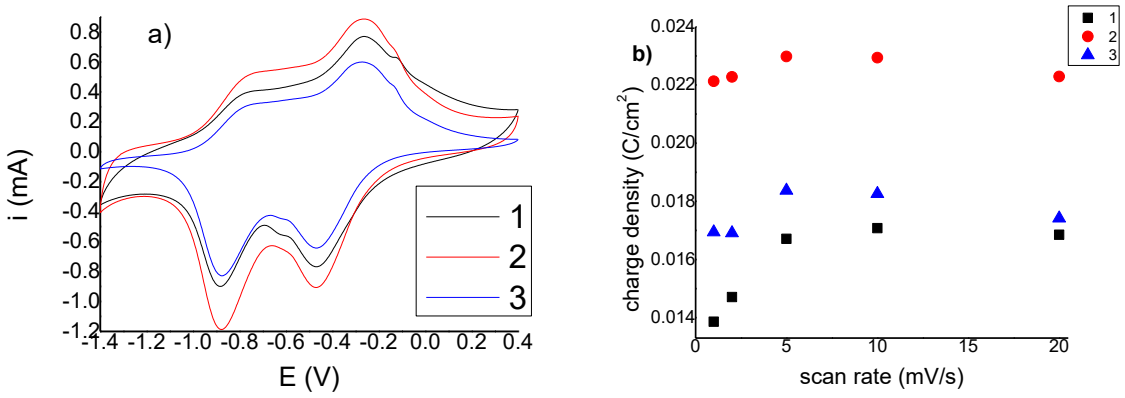

Figure 4.6 The P9 Characterisation using LbL modification version b, the influence of electrode type in a constant electrolyte (0.5 M LiCl/ H_2O) at 30 cycles using CPE as explain above (4.3.6). a) CV measurements (scan number 10), scan rate 20 mV/s. b) Observed charge density vs. scan rate, the surface of electrode 1.05 cm^2

The Quartz Crystal Microbalance (QCM) measurement was used to monitor the weight increase during the dip-coating cycles. Therefore, the frequency of quartz was measured after 5, 10, 15, and 20 dip-coating cycles. Figure 4.7 shows the frequency decrease for increasing dip-coating cycles. From the slope got a frequency decrease of 123 Hz per cycle, which can be converted to a mass change. Using C_f for the electrode (144 Hz μg^{-1} cm^2), the total relevant mass change (Δm) of the sample was (0.854 $\mu g.cm^{-2}$) according to Eq. 4.1.

This value can be compared to the total mass of (P9:GO:PSS)@Au. On the electrode, the composite ratio of P9:GO:PSS is roughly 3:1:6. Therefore, the mass corresponding to the polymer is 0.256 $\mu g.cm^{-2}$ (30 % of the total weight).

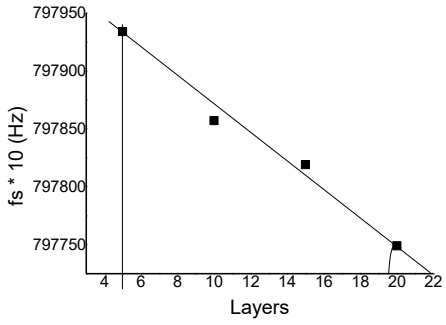

Figure 4.7 The QCM observed resonant frequency vs. layers, using LbL modification version b (4-step coating), using a gold electrode as explain above (4.2.7)

4.4 Summary

This chapter involves the study of the process of layer by layer (LbL), including preparation of redox-active electrode layers by the dip-coating process by repetitive dipping between a polyviologen and garaphene oxide (GO) solution. Cyclic voltammetry (CV) measurement showed that after 15 cycles the capacity does not increase anymore, because the attachment of polymeric chains in the LbL process depends on the conformation of polymer chains in the LbL multi-structure and not on the morphology and size of the substance used. Then, using a polyviologen/GO complex as cationic species and poly(sodium p-styerenesulfonate) (PSS) as anionic species, the capacity increased even up to 100 dip-coating cycles. PSS in the layer acts as a counter ion for polyviologen. Therefore, when viologen is reduced, the charge of PSS is compensated by cations of the electrolyte. Pretreatment of the substrate carbon plate electrode (CPE) with GO resulted in higher capacity because GO introduces negative charges which are favourable for cation (polyviologen) absorption in the first layer.

Using the quartz crystal microbalance (QCM) technique the layer growth was investigated and yielded a mass gain of 0.854 $\mu g.cm^{-2}$ per layer with a polymer content of presumably 0.256 $\mu g.cm^{-2}$. Based on our results, the LbL technique is useful for the preparation of electrodes for battery application. This process greatly helps to homogenize the layers with unstable polymers with GO. On the other hand, better results can be generated in the future after controlling some important factors that influence the structure of the film, like air and humidity, which is affecting the drying rate for the films. Notably, this method is not only limited to the mentioned polymer, but can be expanded to a wide variety of cationic redox polymers, but the disadvantages for this method, using a long time is a problem and disadvantage factor still limits the development of this technique.

Chapter 5
Summary & Outlook

Chapter 5 **Summary and Outlook**

Recently, one of the most important scientific challenge is a better future life for scientists are progressing the ability to efficiently harvest, store and utilize energy with good effectiveness. Since we are encounter significant environmental pollution and depletion of energy resources. In this context, striking developments in electronics including wearable and portable devices and electric vehicles, are being recognized. Thus, energy storage systems are high in demand for the use of these advanced electronics. Among the polymer-based energy storage materials, redox-active polymers are desirable due to high energy storage, also they have excellent features compared with metal-based energy storage materials. Targeting for high energy and power density batteries, chemists are focus on the development of organic molecules including lightweight with multiple redox centers and excellent conductivity. So far numerous materials with different structures have been developed such as conducting polymers, conjugated carbonyls, phenothiazine, thianthrene and organic free radicals. Among them, viologens have great attention due to their structural diversity, excellent theoretical capacity and redox properties. The photophysical and electronic properties of viologens can be easily tuned by induction of heteroatoms, bridging π linkers into the framework or changing substituents on the nitrogen core (alkylation or arylation).

In this thesis, I have synthesized three homo polymers, which are comprising different anoidic and cathodic subunits namely, P1 (viologen + alkyl moiety), P2 (viologen + aryl moiety), P5 (imide moiety), also synthesized five co-polymer namely, P3 (viologen + 4-methoxytriphenylamine), P4 (viologen + cyano-triphenylamine), P6 (viologen + ferrocene), P7 (viologen + triphenylamine) and P8 (viologen + porphyrin). In addition, two genetration (G1 and G2) dentrimers were synthesized.

The characterization of the polymers were performed with cyclic voltammetry (CV), NMR, IR, Thermogravimetric analysis (TGA) and differential scanning calorimetry (DSC). These polymers show greater solubility and exhibited better performance than small molecules. However, these polymers are usually bulk solids, which resulted inadequate utilization of active sites slow ion transport also insulating polymers skeleton may drive to poor conductivity. Thus, redox-active viologen subunits are incorporated with graphene oxide (GO). For instance, the electrochemical performance of polymers were studied based on CV such as activity with and without (GO), the capacity is increased at combined polymer with GO, by changing the

thickness (2.2 – 250 µg). For instance, incorporation of the alkyl group with viologen increases the current by increasing the thickness of polymer with GO. Further to improve the electrochemical stability of the conductive polymers, we have incorporated with reduced graphene oxide (rGO), which is well-known to enhance the desired chemical and physical of redox polymers. This yielded excellent capacity with polymer P3 and P4. However, incorporation of rGO and GO is limited with polymer solubility in aqueous solution. In contrast, dendrimer comprising polymers shows lower solubility in aqueous solution thus, enhance electrochemical and photochemical stability. Also, capacity is increased with thickness up to 7.5 µg. Despite that, a major limitation is observed with dendrimer containing polymers kinetics of charge transfer. The capacity of all polymers and dendrimers is enhanced when combine with GO and rGO. The Coloumbic efficiency of all synthesized polymer remains below 100%, the polymer P1 and P3 shows excellent Coloumbic efficiency as 94% and 90%, respectively. Best of my knowledge these compounds are novel battery materials, thus electrochemical performance is not reported. Therefore, we have compared previously published almost similar compounds, considering different anode and cathode, cell type and thickness scalability the obtained Coloumbic efficiency value are good agreement with previously reported literature values (Coloumbic efficiency 80%)[10b, 13, 85].

To improve the sensitivity of electrochemical analysis drop-casting was demonstrated as a method of producing a film. In this method, a drop of liquid containing a suspension of the polymer of interest is deposited on the surface of the electrode. To improve layer quality, the electrode was prepared by a layer-by-layer (LbL) technique. For example, a linear polyviologen (P9) layer is deposited on the electrode and subsequently GO solution is deposited. Resulting, electrode shows a higher capacity of up to 15 cycles (see Figure 4.3). However, the viologen peaks were not nicely separated.

Alternatively, poly(sodium *p*-styerenesulfonate) (PSS) was used and acts as a counter ion for the viologen. This causes cations in the electrolyte to move instead of anions when the viologen is reduced. This was observed by changing the electrolyte salt. Also, polymer P9 is stable and capacity increases even up to 100 cycles and displays the increase of conductivity by increasing thickness. However, the viologen peaks are not well separated anymore at 100 cycles. The dip-coating process greatly helps to homogenize the layers that are unstable polymers with GO. Notably, this method is not limited to the mentioned polymer, but can be expanded to a wide variety of cationic redox polymers.

Since the variety of redox-active organic monomers is very large, it would be interesting to prepare more polymers with improved electrochemical performance. Especially concerning the solubility of cathode materials under positive polarization. Further, exchanging graphene oxide for other carbon-based materials with negative surface charge, e.g. carbon nanotubes as a conductive filler. Other electrode preparation processes could be investigated, e.g. electrodeposition, spray coating or printing. This might improve electrochemical performance and would be more suitable for potential mass production. Density functional theory (DFT) can be used to predict the electropolymerisation reaction by calculating unpaired electron π-spin density associate of monomeric radical cation in the direction of assess coupling positions in the resultant conductive polymers.

References

[1] J. Xu, R. D. Deshpande, J. Pan, Y.-T. Cheng, V. S. Battaglia, *J. Electrochem. Soc.* **2015**, *162*, A2026-A2035.

[2] T. Georgi-Maschler, B. Friedrich, R. Weyhe, H. Heegn, M. Rutz, *J. Power Sources* **2012**, *207*, 173-182.

[3] D. J. Kim, D.-J. Yoo, M. T. Otley, A. Prokofjevs, C. Pezzato, M. Owczarek, S. J. Lee, J. W. Choi, J. F. Stoddart, *Nat. Energy* **2019**, *4*, 51-59.

[4] M. S. Whittingham, *J. Electroanal. Chem.* **1981**, *118*, 229-239.

[5] A. K. Padhi, K. S. Nanjundaswamy, J. B. Goodenough, *J. Electrochem. Soc.* **1997**, *144*, 1188-1194.

[6] S. Muench, A. Wild, C. Friebe, B. Häupler, T. Janoschka, U. S. Schubert, *Chem. Rev.* **2016**, *116*, 9438-9484.

[7] Z. Song, H. Zhan, Y. Zhou, *Angew. Chem. Int. Ed.* **2010**, *49*, 8444-8448.

[8] W. Choi, D. Harada, K. Oyaizu, H. Nishide, *J. Am. Chem. Soc.* **2011**, *133*, 19839-19843.

[9] F. Wan, J. Zhu, S. Huang, Z. Niu, *Batter. Supercaps* **2020**, *3*, 323-330.

[10] a) W. Li, J. R. Dahn, D. S. Wainwright, *Science* **1994**, *264*, 1115-1118; b) S. M. B. Mousavi, PhD thesis, Universität Osnabrück (Germany), **2016**; c) M. Morita, M. Ishikawa, Y. Matsuda, *Lithium Ion Batteries*, Kodansha Ltd., Tokyo, **1998**, pp. 156-180.

[11] a) Y. Ding, Y. Zhao, Y. Li, J. B. Goodenough, G. Yu, *Energy Environ. Sci.* **2017**, *10*, 491-497; b) Y. Ding, Y. Zhao, G. Yu, *Nano Lett.* **2015**, *15*, 4108-4113.

[12] B. Hwang, M.-S. Park, K. Kim, *ChemSusChem* **2015**, *8*, 310-314.

[13] S. M. Beladi-Mousavi, S. Sadaf, A.-K. Hennecke, J. Klein, A. M. Mahmood, C. Rüttiger, M. Gallei, F. Fu, E. Fouquet, J. Ruiz, D. Astruc, L. Walder, *Angew. Chem. Int. Ed.* **2021**, *60*, 13554-13558.

[14] R. A. Marcus, *J.Chem. Phys.* **1957**, *26*, 867-871.

[15] J. Kim, J. H. Kim, K. Ariga, *Joule* **2017**, *1*, 739-768.

[16] Z. Song, H. Zhou, *Energy Environ. Sci.* **2013**, *6*, 2280-2301.

[17] J. Song, J. Kim, T. Kang, D. Kim, *Sci. Rep.* **2017**, *7*, 42521.

[18] K. Kamata, T. Kawai, T. Iyoda, *Langmuir* **2001**, *17*, 155-163.

[19] a) T. B. Schon, B. T. McAllister, P.-F. Li, D. S. Seferos, *Chem. Soc. Rev.* **2016**, *45*, 6345-6404; b) Q. Zhao, A. K. Whittaker, X. S. Zhao, *Materials* **2018**, *11*, 2567.

[20] C. M. Julien, A. Mauger, K. Zaghib, H. Groult, *Inorganics* **2014**, *2*.

[21] Y. Liang, Z. Tao, J. Chen, *Adv. Energy Mater.* **2012**, *2*, 742-769.

[22] F. Perrozzi, S. Prezioso, L. Ottaviano, *J. Phys. Condens. Matter* **2014**, *27*, 013002.

[23] S. Stankovich, D. Dikin, G. Dommett, K. Kohlhaas, E. Zimney, E. Stach, R. Piner, S. Nguyen, R. Ruoff, *Nature* **2006**, *442*, 282-286.

[24] X. Zhang, D. Zhang, Y. Chen, X. Sun, Y. Ma, *Chin. sci. bull.* **2012**, *57*, 3045-3050.

[25] a) D. R. Dreyer, S. Park, C. Bielawski, R. Ruoff, *Chem. Soc. Rev.* **2010**, *39 1*, 228-240; b) S. Tkachev, E. Buslaeva, A. Naumkin, S. Kotova, I. Laure, S. Gubin, *Inorg. Mater.* **2012**, *48*.

[26] S. Ray, *Applications of Graphene and Graphene-Oxide Based Nanomaterials,* Elsevier Inc., Oxford, 2015, pp. 39-55.

[27] H. A. Becerril, J. Mao, Z. Liu, R. M. Stoltenberg, Z. Bao, Y. Chen, *ACS Nano* **2008**, *2*, 463-470.

[28] R. K. Layek, A. K. Nandi, *Polymer* **2013**, *54*, 5087-5103.

[29] a) L. Sun, *Chin. J. Chem. Eng.* **2019**, *27*, 2251-2260; b) S. Padmajan Sasikala, J. Lim, I. H. Kim, H. J. Jung, T. Yun, T. H. Han, S. O. Kim, *Chem. Soc. Rev.* **2018**, *47*, 6013-6045.

[30] C.-Y. Hsu, V. S. Vasantha, P.-Y. Chen, K.-C. Ho, *Sens. Actuators B Chem.* **2009**, *137*, 313-319.
[31] G. Mezei, Z. Balogh, A. Magyarkuti, A. Halbritter, *J. Phys. Chem. Lett.* **2020**, *11*, 8053-8059.
[32] T. Nakahira, M. Graetzel, *J Phys Chem* **1984**, *88*, 4006-4010.
[33] N. Jordão, L. Cabrita, F. Pina, L. C. Branco, *Chem. Eur. J.* **2014**, *20*, 3982-3988.
[34] L. Chen, H. Willcock, C. J. Wedge, F. Hartl, H. M. Colquhoun, B. W. Greenland, *Org. Biomol. Chem.* **2016**, *14*, 980-988.
[35] J. S. Moore, S. I. Stupp, *Macromolecules* **1986**, *19*, 1815-1824.
[36] W. E. Geiger, *Organometallics* **2007**, *26*, 5738-5765.
[37] a) A. S. Georgopoulou, D. M. P. Mingos, A. J. P. White, D. J. Williams, B. R. Horrocks, A. Houlton, *J. Chem. Soc., Dalton Trans.* **2000**, 2969-2974; b) A. Iordache, M. Oltean, A. Milet, F. Thomas, B. Baptiste, E. Saint-Aman, C. Bucher, *J. Am. Chem. Soc.* **2012**, *134*, 2653-2671; c) S. Bastin, N. Delebecque, F. Agbossou, J. Brocard, L. Pélinski, *Tetrahedron Asymmetry* **1999**, *10*, 1647-1651; d) C. Lang, D. Voll, A. J. Inglis, N. Dingenouts, A. S. Goldmann, L. Barner, C. Barner-Kowollik, *Macromol. Chem. Phys.* **2011**, *212*, 831-839.
[38] a) H. Tahara, R. Baba, K. Iwanaga, T. Sagara, H. Murakami, *Chem. Commun.* **2017**, *53*, 2455-2458; b) X. Liu, Q. Ling, L. Zhao, G. Qiu, Y. Wang, L. Song, Y. Zhang, J. Ruiz, D. Astruc, H. Gu, *Macromol. Rapid Commun.* **2017**, *38*, 1700448; c) K. M. Abraham, M. Alamgir, *J. Electrochem. Soc.* **1990**, *137*, 1657-1658; d) K. M. Abraham, D. M. Pasquariello, E. B. Willstaedt, *J. Electrochem. Soc.* **1990**, *137*, 1856-1857; e) H. Tahara, K. Uranaka, M. Hirano, T. Ikeda, T. Sagara, H. Murakami, *ACS Appl. Mater. Interfaces* **2019**, *11*, 1-6.
[39] V. M. Hultgren, A. W. A. Mariotti, A. M. Bond, A. G. Wedd, *Anal. Chem.* **2002**, *74*, 3151-3156.
[40] a) M. Nanasawa, M. Miwa, M. Hirai, T. Kuwabara, *J. Org. Chem.* **2000**, *65*, 593-595; b) L. He, S. Liu, L. Chen, X. Dai, J. Li, M. Zhang, F. Ma, C. Zhang, Z. Yang, R. Zhou, Z. Chai, S. Wang, *Chem. Sci.* **2019**, *10*, 4293-4305; c) F. Biedermann, O. A. Scherman, *J. Phys. Chem. B* **2012**, *116*, 2842-2849; d) S. M. Beladi-Mousavi, S. Sadaf, A. M. Mahmood, L. Walder, *ACS Nano* **2017**, *11*, 8730-8740; e) S. Asaftei, E. De Clercq, *J. Med. Chem.* **2010**, *53*, 3480-3488.
[41] a) T. Kuorosawa, C.-C. Chueh, C.-L. Liu, T. Higashihara, M. Ueda, W.-C. Chen, *Macromolecules* **2010**, *43*, 1236-1244; b) Q. Zhang, X. Tian, G. Hu, P. Shi, J. Wu, S. Li, H. Zhou, B.-K. Jin, J. Yang, S. Zhang, Y. Tian, *Biochemistry* **2015**, *54*, 2177-2180.
[42] W.-Y. Lee, T. Kurosawa, S.-T. Lin, T. Higashihara, M. Ueda, W.-C. Chen, *Chem. Mater.* **2011**, *23*, 4487-4497.
[43] a) H. Wen, H. Niu, B. Li, X. Ma, X. Bai, Y. Zhang, W. Wang, *Synth. Met.* **2015**, *202*, 89-97; b) M. L. Petrus, R. K. M. Bouwer, U. Lafont, D. H. K. Murthy, R. J. P. Kist, M. L. Böhm, Y. Olivier, T. J. Savenije, L. D. A. Siebbeles, N. C. Greenham, T. J. Dingemans, *Polym. Chem.* **2013**, *4*, 4182-4191.
[44] A. Sonoda, I. Moritani, *J. Organomet. Chem.* **1971**, *26*, 133-140.
[45] a) M. Lee, U. H. Choi, R. H. Colby, H. W. Gibson, *Macromol. Chem. Phys.* **2015**, *216*, 344-349; b) P. K. Bhowmik, H. Han, J. J. Cebe, R. A. Burchett, A. M. Sarker, *J. Polym. Sci. Pol. Chem.* **2002**, *40*, 659-674.
[46] M. L. Keshtov, Y. A. Udum, L. Toppare, V. S. Kochurov, A. R. Khokhlov, *Mater. Chem. Phys.* **2013**, *139*, 936-943.
[47] C.-J. Chen, H.-J. Yen, W.-C. Chen, G.-S. Liou, *J. Mater. Chem.* **2012**, *22*, 14085-14093.
[48] N. Hadjichristidis, M. Pitsikalis, S. Pispas, H. Iatrou, *Chem. Rev.* **2001**, *101*, 3747-3792.

[49] M. Kathiresan, L. Walder, *Macromolecules* **2010**, *43*, 9248-9256.
[50] B. K. Nanjwade, H. M. Bechra, G. K. Derkar, F. V. Manvi, V. K. Nanjwade, *Eur. J. Pharm. Sci.* **2009**, *38*, 185-196.
[51] S. M. Grayson, J. M. J. Fréchet, *Chem. Rev.* **2001**, *101*, 3819-3868.
[52] a) A. A. Chis, C. Dobrea, C. Morgovan, A. M. Arseniu, L. L. Rus, A. Butuca, A. M. Juncan, M. Totan, A. L. Vonica-Tincu, G. Cormos, A. C. Muntean, M. L. Muresan, F. G. Gligor, A. Frum, *Molecules* **2020**, *25*, 3982; b) C. Sandoval-Yañez, C. Castro Rodriguez, *Materials* **2020**, *13*, 570.
[53] J. B. Wolinsky, M. W. Grinstaff, *Adv. Drug Deliv. Rev.* **2008**, *60*, 1037-1055.
[54] P. Singh, *J. Exp. Nanosci.* **2015**, *10*, 429-437.
[55] P. Bhattacharya, E. N. Nasybulin, M. H. Engelhard, L. Kovarik, M. E. Bowden, X. S. Li, D. J. Gaspar, W. Xu, J.-G. Zhang, *Adv. Funct. Mater.* **2014**, *24*, 7510-7519.
[56] a) W. Liu, J. Jiang, K. R. Yang, Y. Mi, P. Kumaravadivel, Y. Zhong, Q. Fan, Z. Weng, Z. Wu, J. J. Cha, H. Zhou, V. S. Batista, G. W. Brudvig, H. Wang, *Proc. Natl. Acad. Sci.* **2017**, *114*, 3578-3583; b) S. Sen, R. B. Jayappa, H. Zhu, M. Forsyth, A. J. Bhattacharyya, *Chem. Sci.* **2016**, *7*, 3390-3398.
[57] T. Lebherz, D. L. Weldin, A. Hintennach, M. R. Buchmeiser, *Macromol. Chem. Phys.* **2020**, *221*, 1900436.
[58] T. Barrett, G. Ravizzini, P. L. Choyke, H. Kobayashi, *IEEE Eng Med Biol Mag* **2009**, *28*, 12-22.
[59] G. R. Newkome, C. D. Shreiner, *Polymer* **2008**, *49*, 1-173.
[60] Y. Zheng, S. Li, Z. Weng, C. Gao, *Chem. Soc. Rev.* **2015**, *44*, 4091-4130.
[61] M. Jikei, M.-a. Kakimoto, *Prog. Polym. Sci.* **2001**, *26*, 1233-1285.
[62] Y. Lu, T. Nemoto, M. Tosaka, S. Yamago, *Nat. Commun.* **2017**, *8*, 1863.
[63] C. O. Sánchez, E. Schott, X. Zárate, D. MacLeod-Carey, P. Sobarzo, N. Gatica, *Polym. Bull.* **2015**, *72*, 897-913.
[64] Y. Li, Y. Zhang, H. Niu, C. Wang, C. Qin, X. Bai, W. Wang, *New J. Chem.* **2016**, *40*, 5245-5254.
[65] L. Ji, Y. Dai, S. Yan, X. Lv, C. Su, L. Xu, Y. Lv, M. Ouyang, Z. Chen, C. Zhang, *Sci. Rep.* **2016**, *6*, 30068.
[66] K. Hatakeyama-Sato, T. Nagano, S. Noguchi, Y. Sugai, J. Du, H. Nishide, K. Oyaizu, *ACS Appl. Polym. Mater.* **2019**, *1*, 188-196.
[67] N. Blouin, A. Michaud, M. Leclerc, *Adv. Mater.* **2007**, *19*, 2295-2300.
[68] Y. Wei, X. Li, Z. Xu, H. Sun, Y. Zheng, L. Peng, Z. Liu, C. Gao, M. Gao, *Polym. Chem.* **2015**, *6*, 973-982.
[69] M. Zhang, S. Yu, Y. Mai, S. Zhang, Y. Zhou, *Chem. Commun.* **2019**, *55*, 6715-6718.
[70] K. Yamamoto, D. Suemasa, K. Masuda, K. Aita, T. Endo, *ACS Appl. Mater. Interfaces* **2018**, *10*, 6346-6353.
[71] S. Heinen, PhD thesis, Universität Osnabrück (Osnabrück, Germany), **1999**.
[72] J. Li, A.-M. Lepadatu, Y. Zhu, M. Ciobanu, Y. Wang, S. C. Asaftei, D. Oupický, *Bioconjugate Chem.* **2014**, *25*, 907-917.
[73] X. Zhang, C.-B. Nie, T.-Y. Zhou, Q.-Y. Qi, J. Fu, X.-Z. Wang, L. Dai, Y. Chen, X. Zhao, *Polym. Chem.* **2015**, *6*, 1923-1927.
[74] Y. Lvov, G. Decher, H. Moehwald, *Langmuir* **1993**, *9*, 481-486.
[75] X. Liu, B. Dai, L. Zhou, J. Sun, *J. Mater. Chem.* **2009**, *19*, 497-504.
[76] I. Choi, R. Suntivich, F. A. Plamper, C. V. Synatschke, A. H. E. Müller, V. V. Tsukruk, *J. Am. Chem. Soc.* **2011**, *133*, 9592-9606.
[77] K. Ariga, J. P. Hill, Q. Ji, *Phys. Chem. Chem. Phys.* **2007**, *9*, 2319-2340.
[78] N. Fukao, K.-H. Kyung, K. Fujimoto, S. Shiratori, *Macromolecules* **2011**, *44*, 2964-2969.

[79] T. Taniguchi, K.-H. Kyung, S. Shiratori, *RSC Adv.* **2015**, *5*, 107488-107496.
[80] F. Jin, M.-L. Zheng, M.-L. Zhang, Z.-S. Zhao, X.-M. Duan, *RSC Adv.* **2014**, *4*, 33206-33214.
[81] T. J. Halthur, P. M. Claesson, U. M. Elofsson, *Langmuir* **2006**, *22*, 11065-11071.
[82] G. Sauerbrey, *Z. Phys.* **1959**, *155*, 206-222.
[83] S. W. Ali, S. Rajendran, M. Joshi, *Polym. Polym. Compos.* **2010**, *18*, 237-249.
[84] Y. Kim, Y. Kim, J. H. Kim, *Nanomaterials* **2020**, *10*, 2211.
[85] N. Goujon, N. Casado, N. Patil, R. Marcilla, D. Mecerreyes, *Prog. Polym. Sci.* **2021**, *122*, 101449.

Abbreviation

Anal. Calc.	Analytical Calculator	Ar	Argon Gas
CC	Current Collector	cm	Centimeter
CV	Cyclic Voltammetry	DCM	Dichloromethane
DMAc	Dimethylacetamide	DME	1,2-Dimethoxyethane
DMF	Dimethyl Formamide	DMSO	Dimethyl Sulfoxide
E	Potential	EC	Ethylene Carbonate
ET	Electron Transfer	EtOAc	Ethyl Acetate
EtOH	Ethanol	ESSs	Energy Storage Systems
FTO	Fluorine Doped Tin Oxide	GC	Glassy Carbon
GO	Graphene Oxide	h	Hour
HOMO	Highest Occupied Molecular Orbital		
HV	High Vacuum	i	Current
I	4,4'-Bipyridine		
II	1,1'-Bis-(2,4-dinitrophenyl)-4,4'-bipyridinium Dichloride		
ITO	Indium Tin Oxide	KCl	Potassium Chloride
Kg	Kilogram	LbL	Layer-by-Layer
LIB	Lithium Ion Battery	$LiClO_4$	Lithium Perchlorate
$LiN(CF_3SO_2)_2$	Lithium Bis(trifluromethanesulfonyl) Imide		
LiTFSI	Lithium Bis(trifluoromethanesulfonyl) Imide		
LP	Linear Polymer		
LUMO	Lowest Unoccupied Molecular Orbital		
mAh	Milliampere Hour	MeCN	Acetonitril
$MeNO_2$	Nitromethane	MeOH	Methanol
Na_2SO_4	Sodium Sulfate		
NH_4PF_6	Ammonium Hexafluorophosphate		
NMP	*N*-Methyl-2-pyrrolidon	OBs	Organic Batteries
P	Polymer	PC	Propylene Carbonate
PI	Polyimide		
PSS	Poly(Sodium p-Styerenesulfonate)	PV	Poly Viologen
PyE	1,2-Bis(4-pyridyl)ethane	QCM	Quartz Crystal Microbalance
rGO	Reduced Graphene Oxide	r.t	Room Temperature

S	Sulfure		
TBABF4	Tetrabutylammonium Tetrafluoroborate		
TBABr	Tetrabutylammonium Bromide		
$TBAPF_6$	Tetrabutylammonium Hexafluorophosphate		
$TBAClO_4$	Tetrabutylammonium Perchlorate		
$TEABF_4$	Tetraethylammonium Tetrafluoroborate		
THF	Tetrahydrofuran	V	Voltage
Wh	Watt Hour		

Curriculum Vitae

1. Personal Data:

Surname:	Mahmood
Forename:	Arsalan Mado
Gender:	Male
Marital Status:	Married
Place and Date of Birth:	Mosul, 01.03.1982
Citizenship:	Iraqian
Address:	Franz-Wieber-Str. 12 49084 Osnabrück, Germany
Mobile Phone:	0049-17647141866
E-mail:	amahmood@uni-osnabrueck.de Arsalan.mado@uod.ac

2. Educational Background:

1988 - 1994	Hammoraby Primary School, Shekhan, Mosul, Iraq
1995 - 1997	Shekhan Intermediate School, Shekhan, Mosul, Iraq
1997 - 2000	AYN-SAFNY High School, Shekhan, Mosul, Iraq

3. Academic Background:

2000 - 2005	Bachelor of Education (B.Sc.) in Chemistry, College of Education, Mosul University, Mosul, Iraq
2007 – 2010	Master of Science (M.Sc.) in chemistry, College Education, Duhok University, Duhok, Iraq. The title " Main Chemical Components of the Essential Oils Obtained from Some Aroma Plants in Duhok Region-Kurdistan"

4. Work Experience:

12.2005 - 05.2007	Assistant researcher at Department of Chemistry, College of Science, Duhok University, Iraq.
05.2010 - 04.2015	Assistant Lecturer of Chemistry at Department of Chemistry, College of Science, University of Duhok, Kurdistan Region, Iraq.
08.2010 - 02.2015	Reporter in Department of Chemistry, Faculty of Science, University of Duhok, Kurdistan Region, Iraq.
10.2015 - now	PhD Student in "Fachbereich Biologie / Chemie Institut für Chemie neuer Materialien", University of Osnabrück, Germany. Title "Synthesis and Energy Storage Performance of Novel Redox-Active Polymers"

5. Languages:

English; good in speaking and writing, **Kurdish**; mother tongue, **Arabic**; excellent in speaking and writing, **German**; weak.

6. Technical Skills:

Spectroscopic measurements using UV Visible spectrophotometers, Gel Chromatography. Analytical separation techniques like; solvent extraction, column chromatography, gas-liquid chromatography (GC), thin-layer chromatography (TLC), High pressure Liquid Chromatography (HPLC), Cyclic Voltammetry (CV) and H1NMR spectroscopy.

7. Computer:

MS Word, MS Excel, MS PowerPoint, Windows XP, Chemoffice, ChemSketch, Arguslab, EndNote, Origin 8G & Internet skills.

8. Driving license:

German/ Class B

Declaration

I hereby declare that this thesis is the summary of my Ph.D. work and has not been submitted to any other university. All the sources and materials used in this thesis are duly acknowledged and cited.

Osnabrück, March, 2022

Mahmood, Arsalan Mado